Development of cold-water coral mounds in the southern Alboran Sea (Western Mediterranean Sea) since the last interglacial

Dissertation for the Doctoral Degree

in Natural Sciences

Dr. rer. nat.

in the Faculty of Geosciences

at the University of Bremen

submitted by

Haozhuang Wang

Bremen, December, 2019

Gutachter

Herr Prof. Dr. Dierk Hebbeln

Herr Prof. Dr. Wolf-Christian Dullo

Datum des Promotionskolloquiums

28, Januar 2020

GLOMAR marum Universität Bremen

Versicherung an Eides Statt / Affirmation in lieu of an oath

gem. § 5 Abs. 5 der Promotionsordnung vom 18.06.2018 / according to § 5 (5) of the Doctoral Degree Rules and Regulations of 18 June, 2018

Ich / I, _____

(Vorname / First Name, Name / Name, Anschrift / Address, ggf. Matr.-Nr. / student ID no., if applicable)

versichere an Eides Statt durch meine Unterschrift, dass ich die vorliegende Dissertation selbständig und ohne fremde Hilfe angefertigt und alle Stellen, die ich wörtlich dem Sinne nach aus Veröffentlichungen entnommen habe, als solche kenntlich gemacht habe, mich auch keiner anderen als der angegebenen Literatur oder sonstiger Hilfsmittel bedient habe und die zu Prüfungszwecken beigelegte elektronische Version (PDF) der Dissertation mit der abgegebenen gedruckten Version identisch ist. / *With my signature I affirm in lieu of an oath that I prepared the submitted dissertation independently and without illicit assistance from third parties, that I appropriately referenced any text or content from other sources, that I used only literature and resources listed in the dissertation, and that the electronic (PDF) and printed versions of the dissertation are identical.*

Ich versichere an Eides Statt, dass ich die vorgenannten Angaben nach bestem Wissen und Gewissen gemacht habe und dass die Angaben der Wahrheit entsprechen und ich nichts verschwiegen habe. / *I affirm in lieu of an oath that the information provided herein to the best of my knowledge is true and complete.*

Die Strafbarkeit einer falschen eidesstattlichen Versicherung ist mir bekannt, namentlich die Strafandrohung gemäß § 156 StGB bis zu drei Jahren Freiheitsstrafe oder Geldstrafe bei vorsätzlicher Begehung der Tat bzw. gemäß § 161 Abs. 1 StGB bis zu einem Jahr Freiheitsstrafe oder Geldstrafe bei fahrlässiger Begehung. / *I am aware that a false affidavit is a criminal offence which is punishable by law in accordance with § 156 of the German Criminal Code (StGB) with up to three years imprisonment or a fine in case of intention, or in accordance with § 161 (1) of the German Criminal Code with up to one year imprisonment or a fine in case of negligence.*

_____   _____

Ort / *Place*,   Datum / *Date*   Unterschrift / *Signature*

Abstract

Cold-water coral (CWC) mounds are widespread morphologies at the sea floor that formed due to the sustained growth of CWCs over geological time scales (thousands to tens of thousands of years). These seabed structures occur along the continental margins of the Atlantic Ocean and its marginal seas. They provide important paleo-archives for the reconstruction of the long-term development of CWCs and coral mounds. In spite of intense studies during the past decades, our knowledge about coral mound formation, and above all, the associated sedimentary processes is still limited.

In the Mediterranean Sea, numerous CWC mounds have been discovered. In the southern Alboran Sea, a coral mound hotspot in the Mediterranean Sea, mounds occur in the so-called East and West Melilla CWC mound provinces (EMCP and WMCP, respectively). In particular, the EMCP can be subdivided into four sub-clusters, each marked by specific mound morphologies and dimensions. The temporal development of coral mounds in the northern and the westernmost sub-clusters of the EMCP has already been investigated, while little is known about their history in the central and southern sub-clusters of the EMCP, as well as in the entire WMCP. Furthermore, the temporal range covered by previous studies was limited to the last ~15 kyrs, i.e. the period since the last deglaciation, having left the older history of coral mound development in the Alboran Sea completely in the dark.

Within this context, this thesis focuses on CWC mound development in the southern Alboran Sea and the driving environmental factors favoring coral mound formation. All investigations are based on comparisons between sediment cores retrieved from the coral mounds (coral bearing; on-mound cores) and from the adjacent seafloor (coral-barren; off-mound cores).

To unravel the sedimentary processes controlling mound formation, two sediment cores (one on- and one off-mound core) from the EMCP have been analyzed for their grain size distributions and sediment compositions. The results show that sediments on the coral mound are finer than the sediment deposited simultaneously on the adjacent seafloor, suggesting a comparably calmer hydrodynamic regime on the mound. Most likely, the coral frameworks reduce the current velocity, enabling the deposition of current-transported fine sediments and preventing these sediments from resuspension. High accumulation rates of siliciclastic sediments (>300 g cm^{-2} kyr^{-1}) among the corals on the mound co-occur with reduced sedimentation at the adjacent sea floor pointing to a focused deposition of available sediments on the mounds. Such a preferred deposition of the sediments on the mound requires strong hydrodynamics transporting the material laterally until it is deposited among the coral frameworks. The energy needed for sustained sediment transport towards the mound is most likely provided by internal waves/tides. Finally, these sediments fill the accommodation space provided by the coral framework and contribute to strikingly high mound aggradation rates (ARs), which in this case in the EMCP reach values up to 589 cm kyr^{-1}.

Uranium-series dating of coral fragments from the unexplored sub-clusters of the EMCP revealed three age clusters, ranging from 112.5-110.6 kyr BP (Marine Isotope Stage (MIS) 5d; southern sub-cluster), 78.1-71.6 kyr BP (MIS 5a), and 13.9-11.7 kyr BP (the last deglaciation; both central sub-cluster of the EMCP). The two coral age cluster in MIS 5d and 5a are the first coral mound formation phases older than the last deglaciation described from the entire Mediterranean Sea. The respective mound ARs for all three mound-aggradation phases range between 67 and 240 cm kyr^{-1}. These three phases coincided with strong bottom hydrodynamics triggered by internal wave propagation at the water mass interface between the Levantine Intermediate Water (LIW) and the Modified Atlantic Water (MAW). The provided additional energy contributed significantly to the lateral food supply to the sessile CWCs, thus, favoring coral growth and sediment delivery, finally resulting in enhanced coral mound formation. The occurrence of the LIW-MAW interface at the water depth level of the coral mounds in the study area was restricted to those periods when the sea level was 20-90 m below present. Therefore, sea level appears to be the dominant pacemaker of coral mound formation in the southern Alboran Sea without acting directly on the CWC or the mounds.

The first U-series datings of coral fragments reported from the WMCP reveal two phases of enhanced mound aggradation (with average ARs of 75-176 cm kyr^{-1}) comprising the periods 14.1-12.9 kyr BP and 11.5-7.6 kyr BP, corresponding to the Bølling-Allerød interstadial and to the Early to Mid-Holocene, respectively. During the Younger Dryas and the Mid to Late-Holocene, coral mound formation was reduced as shown by low mound AR of <40 cm kyr^{-1} (on average). The fast mound formation coincided with high vertical food supply and strong bottom water hydrodynamics supporting the lateral food supply to the CWC. Also in the WMCP, these high energetic bottom water conditions most likely derived from internal waves occurring along the LIW-MAW interface. In analogue to the EMCP, it is proposed that coral mound formation in the WMCP mainly resulted from the high food availability to the corals due to the lateral delivery of food particles to these suspension feeders by internal waves generated strong bottom water hydrodynamics.

In summary, the three case studies here highlight the key role of internal waves for coral mound formation in the southern Alboran Sea since the last interglacial. The strong bottom water hydrodynamics generated by internal waves, on one hand deliver sufficient food particles to the corals for their sustained growth, and on the other hand provide a strong surplus of sediment to be baffled by the coral framework and, thus, contributing to the aggradation of coral mounds.

Kurzfassung

Kaltwasserkorallenhügel sind weitverbreitete morphologische Strukturen am Meeresboden, die über geologische Zeiträume (Tausende bis Zehntausende von Jahren) aufgrund anhaltenden Wachstums von Kaltwasserkorallen (CWC) gebildet werden. Korallenhügel findet man besonders häufig entlang der Kontinentalränder des Atlantischen Ozeans und seiner Randmeere. Sie bilden wichtige Paläoarchive für die Rekonstruktion der langfristigen Entwicklung von Kaltwasserkorallen (CWCs). Trotz zahlreicher Studien in den vergangenen Dekaden ist das Wissen über ihre Entstehung und vor allem über die damit verbundenen sedimentären Prozesse nach wie vor sehr begrenzt.

Im Mittelmeer sind zahlreiche Korallenhügel entdeckt worden. In der südlichen Alborán See, einem ‚Hotspot' für Korallenhügel, treten sie in zwei Provinzen, den sogenannten Ost und West Melilla CWC-Hügelprovinzen (EMCP und WMCP) auf. Die EMCP kann weiter in vier Teilbereiche untergliedert werden, in denen die Korallenhügel jeweils unterschiedliche Morphologien und Dimensionen aufweisen. Die zeitliche Entwicklung der Korallenhügeln in den nördlichen und westlichsten Bereichen der EMCP wurde bereits in früheren Studien untersucht, während zur Entwicklung von Korallenhügeln in den zentralen und südlichen Bereichen der EMCP sowie in der gesamten WMCP bisher kaum etwas bekannt ist. Darüber hinaus ist der zeitliche Rahmen, den frühere Studien abgedeckt haben, auf die letzten ca. 15,000 Jahre, also die Zeit seit der letzten Abschmelzphase, begrenzt, wodurch die frühere Entwicklung der Korallenhügel in der Alboran See bisher noch unbekannt war.

In diesem Kontext konzentriert sich diese Doktorarbeit auf die zeitliche Entwicklung von CWC-Hügeln und die zugrunde liegenden Umweltfaktoren, die die Hügelbildung begünstigten. Alle Untersuchungen basieren auf Vergleichen zwischen Sedimentkernen, die von den Korallenhügeln (Korallen-führende On-Mound-Kerne) und dem angrenzenden Meeresboden (Korallen-freie Off-Mound-Kerne) gewonnen wurden.

Um die sedimentären Prozesse während der Hügelbildung zu entschlüsseln, wurden zwei Sedimentkerne (On-Mound-Kern und Off-Mound-Kern) aus der EMCP bzgl. der Korngrößenverteilung und der Sedimentzusammensetzung analysiert. Die Ergebnisse zeigen, dass die Sedimente auf dem Korallenhügel generell feiner sind als die Sedimente, die sich gleichzeitig auf dem angrenzenden Meeresboden abgelagert haben, was auf ein vergleichsweise ruhigeres hydrodynamisches Regime auf dem Hügel hindeutet. Wahrscheinlich reduziert das Korallengerüst die lokalen Strömungsgeschwindigkeiten, wodurch die Ablagerung von suspendiertem Feinmaterial begünstigt und die Resuspension des Sediments verhindert wird. Hohen Akkumulationsraten von siliziklastischen Sedimenten von >300 g cm^{-2} kyr^{-1} zwischen den Korallen auf dem Korallenhügel treten zeitgleich mit reduzierten Sedimentationsraten auf dem umgebenden Meeresboden auf, was auf eine fokussierte Ablagerung der verfügbaren Sedimente auf den Hügeln hinweist. Solch eine

bevorzugte Ablagerung der Sedimente auf dem Hügel bedarf einer ausgeprägten Hydrodynamik, die die Sedimente lateral transportiert bis sie zwischen den Korallengerüsten abgelagert werden. Die Energie, die für diesen nachhaltigen Sedimenttransport zu den Hügeln benötigt wird, wird wahrscheinlich durch interne Wellen und Tiden bereitgestellt. Diese Sedimente füllten den vom Korallengerüst generierten Ablagerungsraum und tragen somit zu den bemerkenswert hohen Aggradationsraten (ARs) bei, die in diesem Fall in der EMCP bis zu 589 cm kyr^{-1} erreichen können.

Uranreihen-Datierungen von Korallenfragmenten aus den noch nicht erforschten Teilbereichen der EMCP ergaben drei Alterscluster im Bereich von 114,5 bis 110,6 kyr BP (Marines Isotopen Stadium (MIS) 5d; südlicher Teilbereich), 78,1 bis 71,6 kyr BP (MIS 5a) und 13,9 bis 11,7 kyr BP (letzte Abschmelzphase; beide zentraler Teilbereich des EMCP). Die zwei Korallenalterscluster aus dem MIS 5d und 5a sind die ersten Korallenhügel-Bildungsphasen, die bisher aus dem Mittelmeer beschrieben wurden, die älter sind als die letzte Abschmelzphase. Die jeweiligen Mound-ARs für die drei Bildungsphasen variieren zwischen 67 und 240 cm kyr^{-1}. Alle drei Phasen fielen zeitlich mit einer verstärkten Hydrodynamik des Bodenwassers zusammen, die auf die Ausbreitung interner Wellen an der Wassermassengrenzfläche zwischen dem Levantine Intermediate Water (LIW) und dem Modified Atlantic Water (MAW) zurückzuführen ist. Die zusätzliche Energie trug deutlich zu einer erhöhten lateralen Nahrungszufuhr zu den sessilen Korallen bei und unterstützte damit sowohl das Korallenwachstum als auch die laterale Sedimentzufuhr, was letztendlich in einem erhöhten Korallenhügelwachstum resultierte. Das Vorkommen der LIW-MAW-Grenzfläche in der Wassertiefe der Korallenhügeln im Untersuchungsgebiet war auf Phasen beschränkt, in denen der Meeresspiegel 20 bis 90 m unter dem heutigen Wert lag. Somit erscheint der Meeresspiegel der dominante Schrittmacher der Korallenhügelbildung in der südlichen Alborán See zu sein, ohne direkt auf die Korallen oder die Korallenhügel einzuwirken.

Die ersten Uranzerfallsreihendatierungen von Korallenfragmenten aus der WMCP zeigen zwei Häufungen von Altern, die die Zeiträume von 14.1-12.9 kyr BP und von 11.5-7.6 kyr BP umfassen und somit dem Bølling-Allerød Interstadial und dem frühen bis mittleren Holozän entsprechen. Während dieser Zeiten lag das maximale Hügelwachstum im Durchschnitt zwischen 75 und 176 cm kyr^{-1}. Während der Jüngeren Dryaszeit und des mittleren bis späten Holozäns war die Korallenhügelbildung reduziert, wie die niedrigen AR von durchschnittlich <40 cm kyr^{-1} zeigen. Die schnelle Hügelbildung ging mit einer hohen vertikalen Nahrungsversorgung und einer starken Bodenwasserhydrodynamik einher, wobei letztere die laterale Nahrungsversorgung für die Korallen unterstützte. Auch in der WMCP sind diese hochenergetischen Bodenwasserbedingungen höchstwahrscheinlich auf die Bildung interner Wellen an der LIW-MAW Wassermassengrenzfläche zurückzuführen. In Analogie zur EMCP wird angenommen, dass die Bildung der Korallenhügel in der WMCP hauptsächlich auf die hohe Nahrungsverfügbarkeit für die Korallen zurückzuführen ist, die durch eine laterale Anlieferung von Nahrungspartikeln durch interne Wellen angetrieben wurde.

Zusammenfassend belegen diese drei Fallstudien die Schlüsselrolle der internen Wellen bei der Bildung von Korallenhügeln in der südlichen Alborán See seit dem letzten Interglazial. Die starke Hydrodynamik des Bodenwassers, die durch interne Wellen erzeugt wird, liefert den Korallen einerseits genügend Nahrungspartikel für ihr anhaltendes Wachstum, andererseits verbessert sie die Zufuhr von Sedimenten zu den Korallenhügeln, welche zwischen den Korallengerüsten zur Ablagerung kommen. Beides trägt maßgeblich zum Wachstum der Korallenhügel bei.

Acknowledgements

The past four years have witnessed my devotion, perseverance, creativity, love and patience on my PhD. Along the way, I noticed dramatic changes in myself, the way I think, the lifestyle I like. There are many people I would like to express my acknowledgement, who helped me a lot to complete the whole work and embrace the changes.

I would like to thank my parents and my young brother, and my relatives in China for their trust and support on my decision to stay years outside China. Their unconditional love and understanding backs me to forward.

I would like to thank Prof. Dierk Hebbeln, who offered me the great opportunity to pursue my PhD degree at MARUM, University of Bremen, Germany. Great thanks to Dierk Hebbeln for guiding me into the amazing deep-sea world, for providing me various opportunities to communicate with other researchers all over the world.

During the past four years, I am lucky to be supervised by Prof. Dierk Hebbeln, and co-supervised by Dr. Claudia Wienberg, and Dr. Jürgen Titschack. Particularly for their great patience, and careful guidance in every step of scientific research, providing me a lot of constructive instructions, suggestions and comments, helping me to progress dramatically. Also, I am grateful to Dr. Matthias Zabel for his time and devotion in my thesis committee meetings, fruitful discussions and advices.

Thanks to the working group AG Hebbeln, for the comfortable and lovely atmosphere. For laughing times that we spent together during the coffee break, lunch, and all the activities in our spare times. Thanks to Carmen Friese, Dharma Reyes Macaya, Leonardo Tamborrino, Cornelia Kwiatkowski, Florian Boxberg, Sandy Boehnert, Gema Martinez Méndez, Martina Hollstein, Martin Bartels, Muhammad Yusuf Awaluddin, Jens Weiser, Yanming Ruan, Adhitya Kusuma Wardana, Claudia Wienberg, Jürgen Titschack, Dierk Hebbeln, Mayhar Mohtadi, Stephan Steinke, Tina Klose, Lydie Dupont, Jutta Bülten, Dana Pittauer, Rodrigo da Costa Portilho Ramos, Chelsea Korpanty, Christina Gnade, Jasmin Fahrenholz and Sinah Teumer, for the great time we spent together. Special thanks to my lovely friends and officemates: Dr. Carmen Friese, Dharma Reyes Macaya, Hadar Elyashiv, Sandy Boehnert, and Leonardo Tamborrino for their shared times in the same office and happiness together for different activities in Bremen.

Many thanks to all the colleagues from the Bremen International Graduate School for Marine Sciences (GLOMAR) for their kind help in the administrative affairs.

Thanks to the help from the technicians for the help in the lab work, including: Dr. Henning Kuhnert, Birgit Meyer-Schack, Vera Lukies, Dr. Vera Barbara Bender, Volker Diekamp, Dr. Holger Kuhlmann, Martin Krogmann.

Table of Contents

Chapter 1

Introduction

1.1 Cold-water corals and coral mounds

Framework-forming scleractinian cold-water corals (CWCs) are distributed worldwide. In particular, the two most common species, *Lophelia pertusa* and *Madrepora oculata*, are considered as ecosystem engineers since their frameworks form CWC reefs and provide habitats for various deep-sea faunas (Freiwald and Roberts, 2006; Roberts et al., 2009). For example, investigations in the NE Atlantic revealed more than 1300 species in *L. pertusa* reefs, which is comparable to numbers found in tropical coral reefs (Roberts et al., 2006), making the cold-water coral reefs to 'deep-sea oases'.
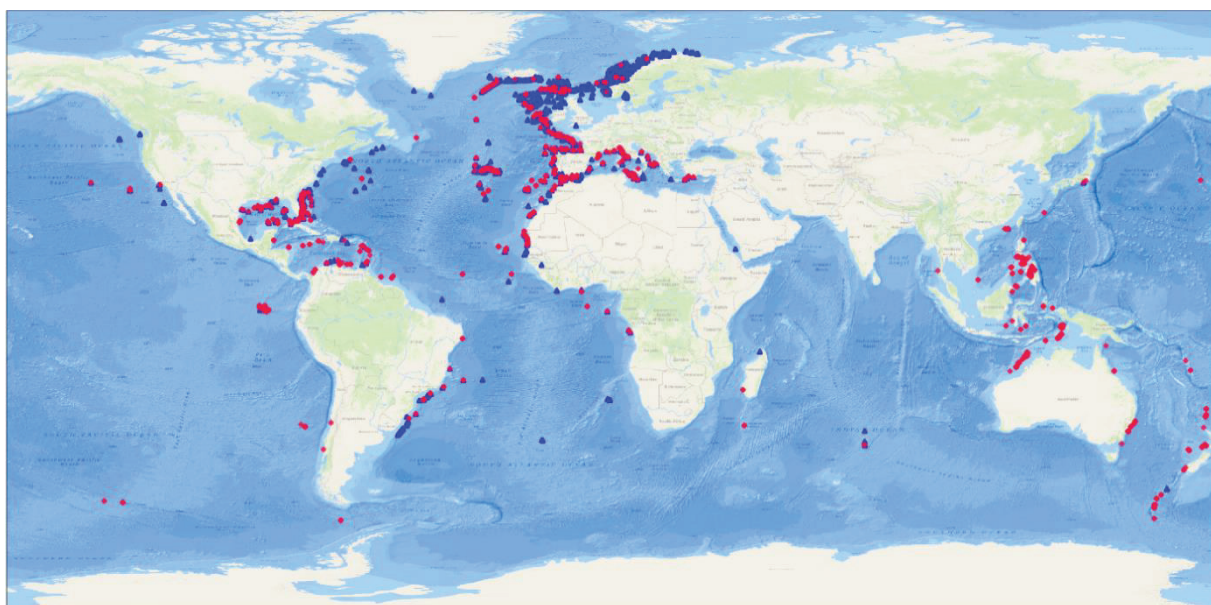
Figure. 1-1. Global distribution of the scleractinian cold-water corals (CWCs) *Lophelia pertusa* (blue filled triangles) and *Madrepora oculata* (red filled dots). The two species show cosmopolitan distribution pattern. The high density of the two species in the NE Atlantic is due to the fact that most of the investigations of the CWCs have been carried out in the NE Atlantic. Data from Freiwald A, Rogers A, Hall-Spencer J, Guinotte JM, AJ Davies, Yesson C, Martin CS, Weatherdon LV (2017).

CWCs are different from the tropical corals. They live in the deep ocean predominantly below the euphotic zone, in water masses with specific chemical and physical properties. Studies conducted in the Atlantic revealed living CWCs predominantly within waters with temperatures of 4-12 °C and salinities of 32-38, as well as dissolved oxygen contents below 6.5 ml l^{-1} (Freiwald, 2002; Schroeder, 2002; Davies et al., 2008; Brooke and Ross, 2014; Ramos et al., 2017; Wienberg et al., 2018; Hanz et al., 2019). In addition, Dullo et al. (2008) found that in the NE Atlantic CWC prefer a density range of 27.35-27.65 kg m^{-3}. Above all, high food availability preconditions coral proliferation and long-term development. Since these deep ocean faunas mostly live below the photic zone and, thus, comprise only non-symbiotic species (Roberts et al., 2009), they use their tentacles to catch food particles

(Mortensen, 2001), including phytoplankton, zooplankton, phyto-detritus, and organic matter (e.g., Duineveld et al., 2007; Kiriakoulakis et al., 2007; Dodds et al., 2009; Mueller et al., 2014). The food is transported to the corals through strong hydrodynamics derived from various processes, e.g., internal tides/waves, local down welling and mixing processes (e.g., White et al., 2005; Thiem et al., 2006; e.g., Davies et al., 2009; Mienis et al., 2009a; Wagner et al., 2011; Mienis et al., 2012; Hebbeln et al., 2014).
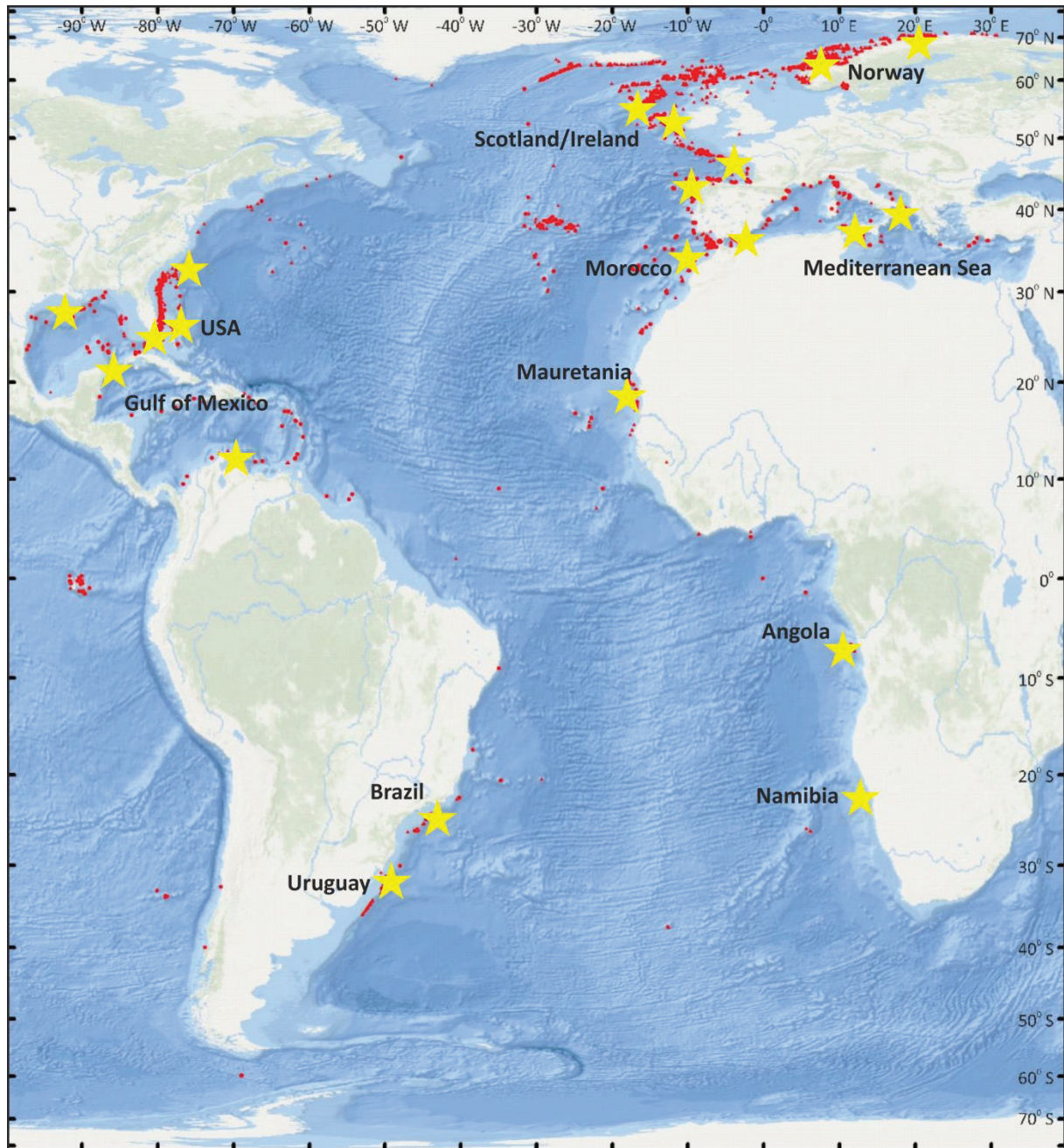
Figure. 1-2. Distribution of cold-water corals (*Lophelia pertusa* and *Madrepora oculata*; red dots) and coral mounds (yellow stars) in the Atlantic and adjacent seas, including the Gulf of Mexico and the Mediterranean Sea. Up to present, CWC mounds are mainly discovered along the continental margins in water depths of 200-1100 m in the Atlantic (Wienberg and Titschack et al., 2017). The data are taken from Hebbeln and Samankassou (2015) and references therein and from recent work done off Angola (Hanz et al. 2019) and Namibia (Tamborrino et al. 2019).

2

A peculiar feature of these reef-forming CWCs is their ability to form coral mounds over geological timescales. Coral mounds are very important seabed structures at continental margins due to their wide distribution and various appearances (dimensions and morphologies). In the north Atlantic, these biogenic structures are widespread along the continental slopes mainly in water depths of 200-1000 m (Wienberg and Titschack, 2017). These mounds can be arranged into mound clusters also known as CWC mound provinces. Within such a mound province, tens to hundreds (or even thousands) of individual mounds cover up to tens of square kilometers (Wheeler et al., 2007; Hebbeln et al., 2014; Ramos et al., 2017; Lo Iacono et al., 2018; Hebbeln et al., 2019). Mostly, coral mounds within the mound provinces appear as mound belts extending parallel to the isobaths of continental slope, e.g., off Ireland (Beyer et al., 2003), off NW Morocco (Hebbeln et al., 2019), and off Mauritania (Wienberg et al., 2018), as well as in the southern Alboran Sea (Hebbeln, 2019). A closer look at the coral mounds reveals that their appearance is high variably. Up to now, coral mounds are discovered to have oval to arcuate or conical, elongated or ridge-like shapes (e.g., Correa et al., 2012a; Hebbeln et al., 2019). Their height varies between several to hundreds of meters above the seafloor. For the elongated or ridge-like mounds, their extensions are up to tens of kilometers (e.g., De Mol et al., 2002; Mienis et al., 2006). Even within the same mound province the appearance of coral mounds can be highly variable (e.g., Wienberg et al., 2018; Hebbeln 2019).

In addition, coral mounds are important paleo-archives enabling the reconstruction of coral growth and mound formation, as well as of paleoceanography, on geological time scales. It is based on the fact that these mounds consist mainly of CWC fragments, hemipelagic sediment and remains of coral associated fauna (e.g., Dorschel et al., 2007b; Mienis et al., 2009b), with coral contents of 0 to ~50% (weight content) (e.g., Dorschel et al., 2007b; Titschack et al., 2009). Given their wide distribution and high carbonate content, these unique architectures are likely an important carbonate reservoir on local or even regional scales (e.g., Dorschel et al., 2007b; Titschack et al., 2016).

1.2 Cold-water coral mounds in the southern Alboran Sea, Mediterranean Sea

In the Mediterranean Sea, most coral mounds have been discovered in the southern Alboran Sea, where they are arranged into two mound provinces occurring west and east of the Spanish enclave Melilla. The respective mound provinces are named the Eest and the Wast Melilla CWC mound provinces (EMCP and WMCP, respectively; Lo Iacono et al., 2014; Hebbeln, 2019). in the EMCP, coral mounds have impressive diverse morphologies and dimensions (Hebbeln, 2019). In general, the coral mounds are arranged into three mound clusters from north to south. In the northern sub-cluster of the EMCP, mounds are developed into ridge-like structures (Brittlestar Ridges, I, II, III). In the central sub-cluster, arcuate mounds are discovered. In the southern sub/cluster of the EMCP, coral mounds show elongated shapes and are partly buried. In general, these coral mounds have heights of 10-150 m above the sea floor (Hebbeln, 2019; for detailed mound description, please refer to sub-chapter 2.2).

Besides, investigations in the EMCP found numerous small coral colonies on top of the Brittlestar Ridges and some of the smaller mounds in the central sub-cluster of the EMCP. The dominant species are *L. pertusa*, *M. oculata* and sporadic live *Dendrophyllia cornigera* (Hebbeln et al., 2009). Different from the coral mound in the EMCP, a total of 108 were recognised in the WMCP. These mounds are oval-conical-shaped structures with heights of 0-48 m above the sea floor with rather similar morphologies and dimensions (Lo Iacono et al., 2014). At the mound surface, no living corals were found (Hebbeln et al., 2015).

Sediment core records from the EMCP have shown that coral mounds experienced pronounced aggradation during the Bølloid-Allerød (B/A) interstadial and the Early Holocene, with associated mound AR of >2 m kyr^{-1} during these two periods. During the Younger Dryas (YD), however, coral mound formation is highly reduced with mound AR of 30-50 cm kyr^{-1}. Mound aggradation in the EMCP is controlled by different environmental factors, such as surface and export productivity, bottom water hydrodynamics and oxygen content in the water. These conditions seem to be steered by the water column structure in the study area (Fink et al., 2013; Stalder et al., 2015; 2018). In contrast, still little is known about past coral growth and mound formation in the WMCP. With seismic data form the area, Lo Iacono et al., (2014) revealed that coral mounds in the WMCP initiated simultaneously. Due to the sea-level rise, changing hydrodynamics and sedimentation rate along continental slope gradually buried coral mounds in the WMCP (Lo Iacono et al., 2014). However, hitherto no sediment core records from the WMCP were available.

1.3 Open questions about coral mound formation in the Alboran Sea

Attempts made to unravel the coral mound development in the northern sub-cluster of the EMCP with major focus on the growth history of corals. However, the associated sedimentary process is still unknown. Given the high content and especially the high accumulation rate of hemipelagic sediments within/on the mounds, there must be very peculiar sedimentary processes involved, which are still not well understood yet. It is assumed that a key role is played by the coral frameworks. By reducing the local current velocity and by generating coral-derived ecological accommodation space, fine sediments deposition may be triggered (known as the baffling effect). Since the growth rate of CWCs (5-33 mm year^{-1}) is far greater than the sedimentation rate along continental slopes (in the order of tens centimenters per thousand years) (Hebbeln et al., 2016; and references therein), filling the fast increasing accommodation space within the coral framework needs another sediment source in addition to the vertical particle flux. This is most likely provided by the lateral flux of suspended sediments under enhanced hydrodynamics, which in turn are baffled by the coral framework. However, this assumption has not been substantiated by data yet.

Another interesting aspect is the various coral mound dimensions and morphologies in the EMCP which has not been explored yet. It most likely reflects different hydrodynamic regimes during mound

formation (Hebbeln, 2019). Nevertheless, the knowledge about mound formation in this area is limited to the northern and westernmost sub-clusters of the EMCP (Fink et al., 2013; Stalder et al., 2015; 2018). Nothing is known so far about mound formation in the central and southern sub-clusters of the EMCP.

In contrast to the EMCP, where there are already some information about the mound formation exist. Nothing comparable has been done so far for the WMCP, which lacks the presence of presently living CWCs. Thus, several questions arise about the CWC growth and mound development in the southern Alboran Sea:

a) What are the processes controlling mound formation? How did the huge amounts of terrigenous sediments reach the mounds? What is the role of baffling effect of the coral-framework on sediment deposition?

b) When were the coral mounds in the central and southern sub-clusters of the EMCP formed? Was the timing different from that of the other sub-clusters of the EMCP? If yes, what caused the difference?

c) When were the coral mounds in the WMCP formed? What is the main factor driving mound formation in this area? What are the differences in the mound formation history between the WMCP and the EMCP?

To answer these questions, three studies were designed and conducted as reported in the following chapters. In the first study, two sediment cores (on- and off-mound cores) from the EMCP that already provided a record on mound development since the last deglaciation were used (Fink et al., 2013). In this project, each core is used to reconstruct changes of the hydrodynamic conditions and associated sedimentary process during mound formation for the respective setting. Comparisons between the two cores provide evidence for how changing hydrodynamics controlled mound formation as well as common seafloor deposition. For the second project, sediment cores from coral mounds in the central and southern sub-clusters of the EMCP were exploited to obtain information about coral mound formation in the respective areas. An off-mound core from the northern sub-cluster of the EMCP was used to trace change of paleoenvironmental conditions. Comparisons between the mound formation and paleoceanography records from these cores allowed to put mound formation in a paleo-environmental context. For the third project, four sediment cores from two sub-clusters of the WMCP (on-mound cores) were collected to unravel the mound development in this area. Another sediment core was collected from the seafloor adjacent to the coral mounds (off-mound core) to reconstruct the ambient paleoceanographic conditions. By comparing the records from the on- and the off-mound cores, we are able to decipher the development of coral mound and the associated paleo-environmental factors in the WMCP. Further comparisons of coral mound formation between the WMCP and the EMCP provide information on mound development in the wider southern Alboran Sea.

1.4 Thesis outline, overview and authors' contributions

The thesis is organized in a cumulative form. In Chapter 4, sediment deposition and associated hydrodynamics during mound formation is analyzed. In Chapter 5, coral mound formation in the central and southern sub-clusters of the EMCP is discussed. In Chapter 6, coral mound development in the WMCP, southern Alboran Sea since the last deglaciation is introduced. The three manuscripts are in preparation for submission to international journals or were published. All the work are prepared and written in collaboration with scientists from various fields. Below, an outline for each manuscript and the contribution of authors is given. In the final chapter, a summary and outlook for further research are given.

Manuscript I (Chapter 4):

Cold-water coral mound formation: the importance of ecological accommodation space and sediment supply

Haozhuang Wang, Jürgen Titschack, Claudia Wienberg, Dierk Hebbeln

In preparation for: *Sedimentology*

This study aims to reconstruct the sedimentary process during the mound formation, which is assumed to result from the interplay of fast growing corals and strong hydrodynamics controls the coral mound aggradation mainly through the baffling effect of the coral framework. Grain-size distribution of siliciclastic sediments from both, the on- and the off-mound cores were used to trace the change of hydrodynamics in the respective settings. Comparisons of the grain-size distributions of the two cores during the mound formation allow tracing the impact of the baffling effect. By quantifying the sediment accumulation from the coral mound and from the adjacent seafloor, we identified the processes controlling sediment transport to and deposition on the coral mound.

Dierk Hebbeln and Jürgen Titschack designed the study. With the guidance of Jürgen Titschack, Haozhuang Wang, Pia Triebeneck, and Nathalie Deichholz sampled and measured the grain size of the siliciclastic sediments. Haozhuang Wang sampled and measured the dry bulk density of the sediment under the guidance of Jürgen Titschack. Haozhuang Wang prepared the samples for the measurement of total carbon and total inorganic carbon. Haozhuang Wang interpreted the data and wrote the manuscript with constructive discussions with Jürgen Titschack, Claudia Wienberg and Dierk Hebbeln.

Manuscript II (Chapter 5):

Sea level change-related formation of cold-water coral mounds since the last interglacial in the southern Alboran Sea

Haozhuang Wang, Dierk Hebbeln, Jürgen Titschack, Claudia Wienberg

In preparation for: *Quaternary Science Reviews*

The aim of this study is to decipher the coral mound development in the central and southern sub-cluster of the EMCP, southern Alboran Sea. To achieve this goal, two sediment cores were retrieved from coral mounds in these two sub-clusters. Coral fragments from these cores were selected for dating to obtain information on past mound aggradation, which could be documented as far back as the last interglacial. In addition, an off-mound sediment core retrieved from the northern sub-cluster of the EMCP was used for reconstructing the paleoceanographic setting. Comparisons between the coral mound formation and the paleo-environmental conditions allow to identify the key factors controlling mound formation in the central and southern sub-cluster of the EMCP and to put these observations into a larger, EMCP-wide perspective.

Haozhuang Wang, Dierk Hebbeln, Claudia Wienberg and Jürgen Titschack designed the study. The sample preparation for U/Th dating was done by Haozhuang Wang under the supervision of Dierk Hebbeln and Claudia Wienberg. Haozhuang Wang prepared the stable oxygen and carbon isotope measurements on benthic foraminifera under the guidance of Claudia Wienberg and Dierk Hebbeln. The grain-size measurement was done by Haozhuang Wang under the guidance of Jürgen Titschack. Haozhuang Wang interpreted the results and wrote the manuscript with fruitful contributions with Claudia Wienberg, Dierk Hebbeln and Jürgen Titschack.

Manuscript III (Chapter 6):

Cold-water coral mounds in the southern Alboran Sea (western Mediterranean Sea): Internal waves as an important driver for mound formation since the last deglaciation

Haozhuang Wang, Claudio Lo Iacono, Claudia Wienberg, Jürgen Titschack, Dierk Hebbeln

Published in *Marine Geology*, doi: https://doi.org/10.1016/j.margeo.2019.02.007

This study aims to decipher the development of CWC mounds in the WMCP, southern Alboran Sea. One set of sediment cores that collected from various coral mounds were used to reconstruct coral mound development by U/Th dating of coral fragments. Another sediment core collected from the seafloor close to the coral mounds was utilized to unravel the change of environmental conditions in the WMCP, particularly for the period of mound formation. Comparisons between coral mound

formation and the associated environmental conditions allow to identify key factors driving mound formation in the WMCP.

Chapter 2

Regional setting and cold-water coral mound provinces in the southern Alboran Sea

2.1 Alboran Sea

The Alboran Sea forms the westernmost part of the Mediterranean Sea, connecting the Mediterranean Sea and the Atlantic Ocean. It is bordered by Spain to the north and Morocco to the south. The Alboran Sea is characterized by complex topographies, which consists of three main basins: West, East and South Alboran Basin (WAB, EAB and SAB, respectively; see Fig. 2-1). Particularly, the SAB is separated from the other basins by the topography highs i.e. Alboran Ridge (Muñoz et al., 2008; Palomino et al., 2015) (Fig. 2-1).
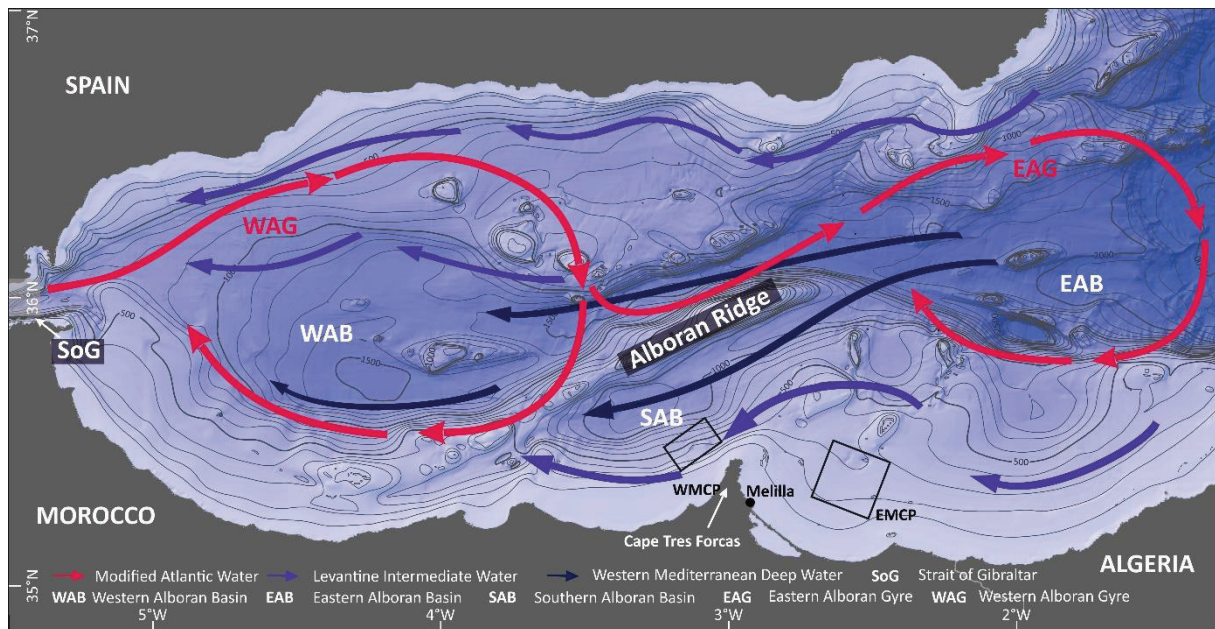
Figure. 2-1. Bathymetry map of the Alboran Sea, western Mediterranean Sea (Map: Marine Information Service (2016); EMODnet Digital Bathymetry, http://doi.org/10.12770/c7b53704-999d-4721-b1a3-04ec60c87238). Displayed is the major circulation in the Alboran Sea. The West and East Melilla cold-water coral mound provinces (WMCP and EMCP), respectively are indicated.

Circulation in the Alboran Sea is characterized by three dominant water masses. Atlantic Water flows into the Alboran Sea through the Strait of Gibraltar, mainly at water depths of 0-200 m. The eastward-flowing Atlantic Water mixes with the Mediterranean surface waters, forming the Modified Atlantic Water (MAW). The MAW forms two gyres in the Alboran Sea, the quasi-permanent West and the unstable East Alboran Gyre (WAG and EAG), respectively (Heburn and La Violette, 1990). In the NW WAG, the inflow AW forms an upwelling area; whereas a frontal zone forms in the eastern boundary of the EAG due to the interaction between the MAW and the Mediterranean surface waters. These two areas are featured in high productivity in the Alboran Sea (e.g., Prieur and Sournia, 1994; Sarhan et al., 2000; Ruiz et al., 2001).

9

The intermediate water in the Alboran Sea, from upper part to lower part, consists of Winter Intermediate Water (WIW, originated from the Eastern Mediterranean Sea), Levantine Intermediate Water (LIW, formed in the Levantine Sea), and the Tyrrhenian Dense Water (TDW, formed in the Tyrrhenian Sea). As the WIW and the TDW are rarely recognized due to the mixing of the three water masses, the whole intermediate water is known as the LIW (Millot, 2009). The West Mediterranean Deep Water (WMDW), formed in the Gulf of Lions in the Western Mediterranean Sea, fills the deepest part of the Alboran Sea. It flows under the LIW at water depths of >600 m (Millot, 2009).

The sediments in the Alboran Sea mainly consist of siliciclastic material, originated predominantly from riverine and aeolian inputs. Apart from this, coastal erosion also contributes to the sedimentation (Moreno et al., 2005; Lobo et al., 2006; Jimenez-Espejo et al., 2008). In the southern Alboran Sea, the Moroccan Moulouya River is the main river flowing into the sea. Its discharge reaches highest volumes during the autum-summer period (Snoussi et al., 2002).

2.2 Cold-water coral mound provinces in the Alboran Sea

In the southern Alboran Sea, coral mounds are arranged into two mound provinces. They are located east of Melilla and west of Cape Tres Forcas and, and named as the East and the West Melilla CWC mound provinces (EMCP and WMCP), respectively (Fig. 2-1). In the EMCP, coral mounds are arranged into three clusters, stretching over ~25 km from north to south (Hebbeln, 2019). In the norther sub-cluster of the EMCP, zigzag-shaped ridge-like mounds were discovered attached to southern flank of the volcanic Banc de Provençaux (Fig. 2-2). The three ridges are named as Brittlestar Ridges (BR) I, II and III from east to the west. They occur at water depths of 475-375 m and reach 50-150 m high above the seafloor, stretching from 3 km to nearly 20 km in length. The BR I and II are in S-SE and SW orientation, respectively. The BR III shows
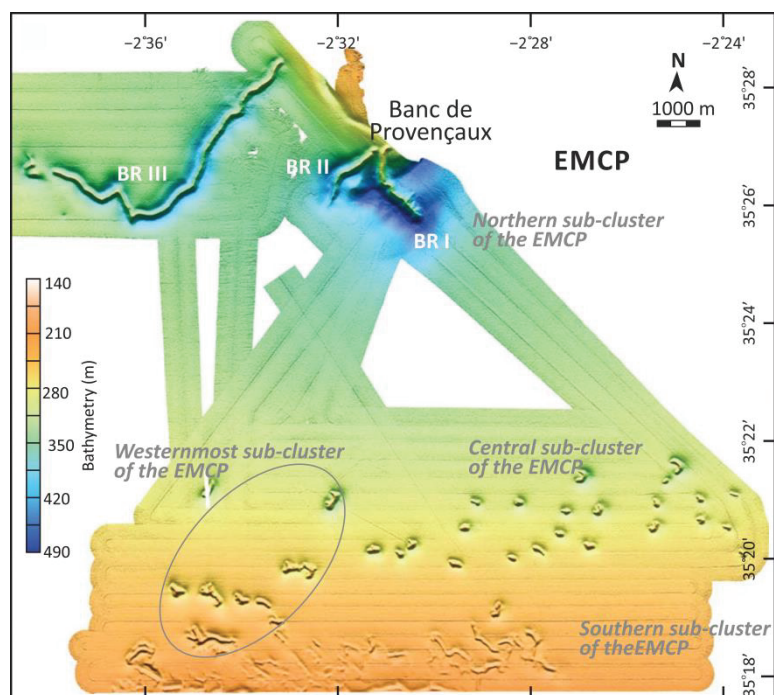
Figure. 2-2. Bathymetric map of the East Melilla cold-water coral mound province (EMCP), southern Alboran Sea (modified from Hebbeln, 2019).

peculiar features with abrupt change in its orientation. Its main orientation is SW, which turns to WNW at the western part of the ridge (Fig. 2-2). In the central sub-cluster of the EMCP, coral mounds

show oval to arcuate shapes. They occur at water depths of 230-320 m, showing longest axes of up to few hundreds of metres. Their heights vary between 20 and 40 m above the sea floor, displaying high flank gradients with angles of >30°. The shapes of these mounds show a gradual change from oval to ridge-like in E-W direction (Fig. 2-2). In the southern sub-cluster of the EMCP, coral mounds were found at water depths of 200-240 m. These are ridge-like mounds, winding mostly in E-W direction. These structures reach ~10 m above the sea floor, with lengths of up to 5 km along NW-SE direction. Towards the south, the coral ridges become gradually buried by fine sediments. In addition, the central and southern sub-clusters of the EMCP converge in the westernmost of the EMCP at water depths of ~230 m. Ridge-like mounds in this area stretch in NW-SE direction (Fig. 2-2; Hebbeln , 2019).

In the WMCP, 103 oval shaped coral mounds reaching heights of 1-48 m above the surrounding seafloor were recognized in water depths of 298-590 m (Lo Iacono et al., 2014(Fig. 2-3). They are separated into two mound clusters, with the major mound cluster in the east and a secondary cluster in the west. The main mound cluster comprises 81 individual mounds mainly showing a SSW-NNE extension. These mounds have heights of 8-42 m above the seafloor, and diameters of 49-476 m. Their flanks display gradients between 8° and 10°. The secondary mound cluster consists of 22 individual mounds,
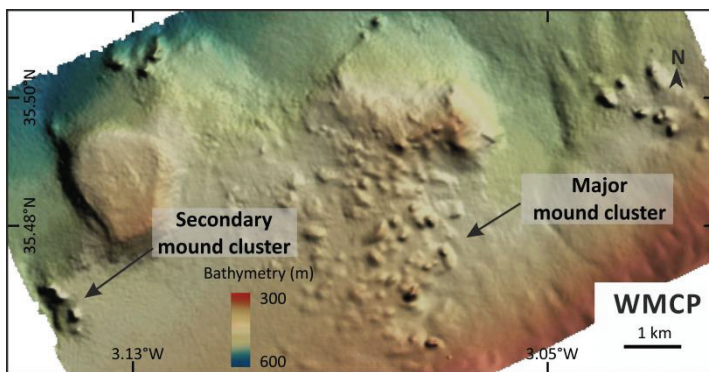
**Figure. 2-3**. Bathymetric map of the West Melilla cold-water coral mound province (WMCP), southern Alboran Sea (modified from Lo Iacono et al., 2014).

which show predominantly in NNW-SSW extensions. They are relatively large, displaying a mean height of 21 m. In the WMCP, no living CWCs were observed (Fig. 2-3; Lo Iacono et al., 2014).

Chapter 3

Materials and Methods

For this study, a total number of eleven gravity cores retrieved from the southern Alboran Sea were used. For the manuscript I, one on-mound core GeoB13729-1 obtained from the Brittlestar Ridge I in the EMCP, and one off-mound core retrieved from the adjacent seafloor were exploited. Manuscript II dealt with two on-mound cores GeoB18105-1 and GeoB18120-1 collected from the central and southern sub-cluster of the EMCP, respectively, supplemented by one off-mound core, MD-13-3457, taken from the seafloor in the northern EMCP. For manuscript III, four on-mound cores, MD13-3451, MD13-3452, GeoB18127-1 and GeoB18130-1, collected from various coral mounds in the WMCP have been selected. The off-mound core GeoB18131-1 was retrieved from the adjacent seafloor. (Fig. 3-1).

These sediment cores were obtained during three cruises. The cores GeoB13729-1 and GeoB13731-1 were obtained during the expedition POS 385 with the RV Poseidon (Hebbeln et al., 2009). The MD cores (MD13-3451, MD13-3452 and MD13-3457) were obtained during the cruise MD194 "Gateway" Eurofleets with the RV Marion Dufresne (Van Rooij et al., 2013). Four GeoB cores (GeoB18105-1, GeoB18120-1, GeoB18127-1, and GeoB18130-1) were collected during the cruise MSM 36 "MoccoMeBo" with the RV Maria S. Merian (Hebbeln et al., 2015).. The on- and off-mound cores have recoveries of 148-1016 cm and 431-2031 cm in length, respectively (Table 3-1).
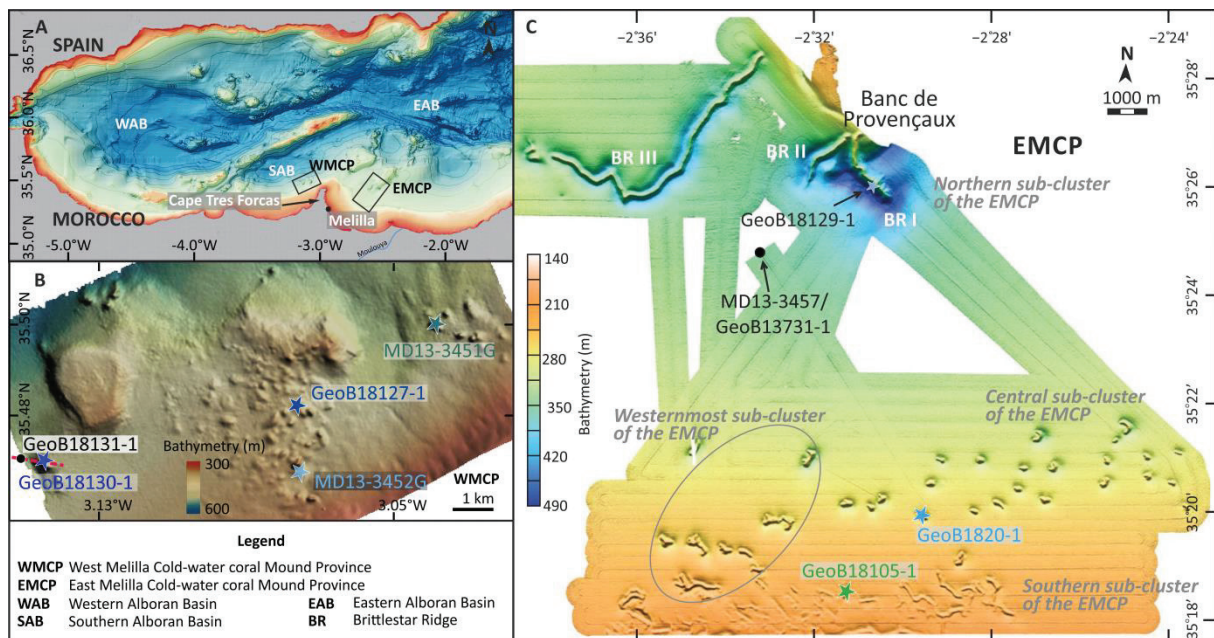
Figure. 3-1 A: Schematic map of the cold-water coral mound provinces in the southern Alboran Sea. The West and East Melilla cold-water coral mound provinces (WMCP and EMCP) are indicated. B_ Sampling sites in the WMCP. C: Sampling sites in the EMCP. The on- and off-mound cores in (B) and (C) are represented by filled stars and dots, respectively. The individual figures are modified from Lo Iacono et al., (2014); Hebbeln, (2019) and Wang et al., (2019).

The on-mound cores were first frozen for 24 hours at -20 °C before splitting in order to keep the structure of the cores intact. A giant diamond saw was used for core splitting. A conventional procedure was used for splitting the the off-mound cores.

Table 3-1. Metadata of gravity cores collected from the southern Alboran Sea, western Mediterranean Sea. WD: water depth; R: recovery.

Manuscript	Cruise	Core Type	Core ID	Latitude [N]	Longitude [W]	WD [m]	R [cm]
I	POS-385	Off-mound	GeoB13731-1	35°24.80′	2°33.22′	362	447
	POS-385	On-mound	GeoB13729-1	35°26.07′	2°30.83′	442	447
II	MSM-36	On-mound	GeoB18105-1	35°18.44′	2°31.32′	224	571
	MSM-36	On-mound	GeoB18120-1	35°19.88′	2°29.60′	249	1016
	MD194	Off-mound	MD13-3457	35°24.80′	2°33.22′	345	2031
III	MD194	On-mound	MD13-3451G	35°29.996′	3°02.398′	370	522
	MD194	On-mound	MD13-3452G	35°28.128′	3°04.661′	305	558
	MSM-36	On-mound	GeoB18127-1	35°28.969′	3°04.641′	365	563
	MSM-36	On-mound	GeoB18130-1	35°28.099′	3°08.747′	379	148
	MSM-36	Off-mound	GeoB18131-1	35°28.093′	3°09.301′	457	851

3.1 On-mound core analyses

3.1.1 Sediment composition

Sediments from coral mounds mainly comprise CWC fragments, hemipelagic sediment, and remains of coral associated fauna (mostly carbonate) (e.g., Titschack et al., 2009; 2015). The hemipelagic sediments mainly consist of siliciclastics, carbonate and organic carbon, as well as biogenic opal. Notably, Mediterranean Sea sediments are characterized by low biogenic opal contents (e.g., Masqué et al., 2003). In this context, CWC content, siliciclastic sediment, carbonate and organic carbon was determined for the coral mound sediments.

CWC content

CWC content (vol.%) was determined based on the approach by Titschack et al. (2016). For detailed information on the data processing please refer to sub-chapter 3.1.3. The weight of CWC in sediment was obtained by multiply the CWC content (vol.%) and its density (2.66 g cm^{-3}; Dorschel et al., 2007).

Dry bulk density

For assessing the dry bulk density the wet mass, the dry mass and the dry volume of the sediment need to be determined (Blum, 1997). In this thesis, the dry bulk density of core GeoB13729-1 was measured in 10-cm resolution, in the Geotechnic Laboratory at MARUM, University of Bremen, Germany. Firstly, ~8 cm^3 of sediment were wet weighted and then dried in a convection oven at constant temperatures of 110-120 °C for 24 hours to remove the interstitial water and interlayer water from clay. Then, the dried sediments were dry weighted and measured following the protocol by Blum (1997). A Pentapyc 5200e gas pycnometer (Quantachrome instruments) was used for the measurement of volume. The calculation of the dry bulk density follows the method from Blum (1997).

Total carbon (TC) and total organic carbon (TOC)

Organic carbon in marine sediments is predominantly derived from the surface ocean productivity, where it is produced by photosynthesis of primary producers. A minor proportion of organic matter can originate from the terrigenous environment (Opsahl and Benner, 1997). Most of these organic materials is decomposed in the ocean. Only a small fraction reaches the seafloor and is preserved within the sediments.

In this thesis, core GeoB13729-1 was analyzed for TC and TOC at 10-cm resolution in University of Bremen, Germany. The sediment was freeze-dried and grounded into two subsamples weighting approximately 50 mg each. For the TC measurement, one subsample was combusted within a crucible at 2300 °C in a constant oxygen stream. The obtained CO_2 was used to calculate the TC. For the TOC determination, 12.5% HCl was added to remove the total inorganic carbon (TIC). Afterwards, the subsample was combusted in the same way as for the TC measurement. The $CaCO_3$ content was obtained by subtracting the TOC from TC using the following equation:

$$CaCO_3 \ (wt.\%) = (TC-TOC) \ (wt.\%) \times M_{CaCO3}/M_C.$$

M_{CaCO3}: Molecular weight of calcium carbonate (100 g mol^{-1})

M_C: Molecular weight of carbon (12 g mol^{-1})

3.1.2 Grain size measurements

In the deep ocean, variations in the sediment grain-size distribution mostly reflect variations in bottom current velocities affecting the deposition as well as the re-mobilization of particles (McCave and Swift, 1976). This effect is strongest in the fine fraction of siliciclastic sediments between 10 and 63 µm, known as sortable silt (e.g., McCave and Hall, 2006; McCave et al., 2017), as siliciclastic sediments in this size fraction are non-cohesive and, thus, very sensitive to changes in current velocity. Siliciclastic sediments therefore are widely utilized to trace hydrodynamics. A simple measure for

changes in the grain-size distribution of siliciclastic sediments is the mean grain-size that often can be used to infer about current strength variability. In the Alboran Sea, the mean grain-size change has been used as a proxy of current strength variation over geological time scales (e.g., Fink et al., 2013).

In this thesis, siliciclastic sediments from on-mound core GeoB13729-1 were used for the grain-size analyses. Prior to the analysis, the terrigenous sediment fraction was isolated by boiling about 2 g of bulk sediments, with 10 ml of H_2O_2 (30%; until the reaction stopped), 10 ml of HCl (10%; 1 min) and 6 g NaOH pellets (10 min) to remove the organic carbon, calcium carbonate and biogenic opal, respectively. The samples were diluted (dilution factor: >25) after each step, and finally boiled with tetra-sodium diphosphate decahydrate ($Na_4P_2O_7 * 10H_2O$) for 3 minutes to destroy aggregates (see also McGregor et al., 2009). The measurement was performed with a Beckman Coulter Laser Diffraction Particle Size Analyzer LS 13320, at the Particle-Size Laboratory at MARUM, University of Bremen, Germany. Deionized, degassed and filtered water (filtered with mesh size: 0.2 μm), was used during the entire process to reduce the potential influence of air bubbles or particles within the water. The obtained results provide the grain-size distribution of an individual sample from 0.04 μm to 2000 μm in 116 size classes. The calculation of the particle sizes relies on the Fraunhofer diffraction theory and the Polarization Intensity Differential Scattering (PIDS) for particles from 0.4 to 2000 μm and from 0.04 to 0.4 μm, respectively. The reproducibility is checked regularly by replicate analyses of three internal glass-bead standards and is found to be better than ±0.7 μm for the mean and ±0.6 μm for the median particle size (1σ). The average standard deviation integrated over all size classes is better than ±4 vol.% (note that the standard deviation of the individual size classes is not distributed uniformly). All provided statistic values are based on a geometric statistic.

3.1.3 Core description

Here, visual and computed tomography (CT) based core descriptions were applied for the on-mound cores. For cores GeoB18105-1, GeoB18120-1, MD13-341-1 and MD13-3452-1, the CWC content and preservation was described based on visual core description (2D) of the cutting surface. Coral content (surface (Surf.)%) is estimated based on coral coverage of the cutting surface. Coral fragments with lengths of >5 cm are defined as large clasts, of 1-2 cm length as medium clasts, and of <1 cm length as coral rubble. For the cores GeoB18127-1 and GoB18130-1, CT-based core description (3D) was used to assess CWC preservation, which is determined by CWC content (volume (vol.) %), CWC clast size and orientation.

The CT-based core descriptions depend on an orthoslice of the sediment in X-Y-Z orientation. It shows the attenuation of X-ray beams (unit: Hounsfield unit (HU)), which differs between different materials with varying densities. The X-ray beam attenuation provides the baseline to distinguish between different sediment compositions in the core. These on-mound cores were CT scanned with a Toshiba Aquilion 64 computer tomography at the hospital Klinikum Bremen-Mitte, Bremen, Germany.

The data processing was done by using the Zuse Institute Berlin edition of Amira software (version 2015.37; Stalling et al., 2005; http://amira.zib.de).

Prior to the data analyses, the core liner rims were deleted from the data set with the *Segmentation* editor and the *Arithmetic* module. Afterwards, different sections were merged for the cores GeoB18127-1 and GeoB18130-1 with the *Merge* module. Secondly, CWC fragments larger than 1 mm were segmented from matrix sediment with the *MultiThresholding* module. Likewise, coral content (vol.%) is quantified through *MaterialStatistics* module. To obtain the CWC clast size and orientation, coral fragments were firstly separated from each other with the *ContourTreeSegmentation* module, and then were parameterized with the *ShapeAnalysis* module. The coral clast size and orientation were measured with the *GrainSizeDistribution* and *GrainAngelDistribution* modules, respectively. Finally, the image of coral clasts throughout the whole core was provided using the *SurfaceGen* and *SurfaceView* modules. For the details of data processing, please refer to the supplementary material of Chapter 4.

3.1.4 Radiocarbon dating

The accelerator mass spectrometry (AMS) radiocarbon (^{14}C) dating is widely used in paleoceanographic research throughout the world. Its application in corals is based on the ^{14}C equilibrium between seawater and corals during calcification of coral skeletons.

In nature, there are two major stable carbon isotopes, ^{12}C and ^{13}C, consisting of 98.89% and 1.11% respectively (Faure, 1986). The radioactive isotope, ^{14}C, originates from the transformation of nitrogen atoms triggered by cosmic radiation upon entering the upper layers of the atmosphere. In the following, the resulting ^{14}C atoms are quickly diffused in the lower layer of the atmosphere and oxidized to ^{14}CO$_2$, entering the carbon cycle. In seawater, dissolved ^{14}CO$_2$ is incorporated into carbonates, such as foraminiferal shells or coral skeletons (e.g., Hughen, 2007). Once these organisms die, the ^{14}C absorption by the organism ends, the ^{14}C amount in the carbonate gradually decreases by radioactive decay (5568 ± 30 years; Libby, 1955). Therefore, by measuring the ^{14}C content (relative to the ^{12}C content) in the samples, the time since the death of the organism, i.e., radiocarbon age, can be estimated.

However, several factors may lead to a deviation of the obtained radiocarbon age from the true age. One factor are changing ^{14}C concentrations in space and time, causing systematic variations compared to ages obtained by other methods, for example, dendrchronology. Another important factor derives from the reservoir effects, namely the ^{14}C age difference between different water masses reflecting the time that passed since these waters were isolated from the atmosphere. Consequently, the ^{14}C concentrations of deep ocean can be reduced, thus, resulting in too old ^{14}C ages that preserved in carbonate shells produced by deep ocean benthic organisms (Bard, 1988). On a global scale, the mean

reservoir age for surface ocean waters, to which continuously older waters are admixed by upwelling and mixing, is approximately 400 years (Reimer et al., 2013). On local scale, the reservoir effect also deviates from the global mean, known as ΔR, which, in cases, might need to be considered. Therefore, the obtained ^{14}C age need to be converted to calendar ages using a calibration curve (e.g., Reimer et al., 2013; and references therein) and a reservoir age correction.

Ubiquitous application of ^{14}C dating calls for a global standard for different labs to make the results, from varied labs in the world comparable. Since 1970s, obtained ^{14}C ages meeting these standards are provided as *conventional radiocarbon ages*. The standards include: i> 'Libby half-life' is assumed as the half-life of ^{14}C (5568 ± 30 years; Libby, 1955); ii> the National Bureau of Standards (NBS) oxalic standard is used as the radiocarbon standard; iii> the year of 1950 AD is applied as a reference given the ^{14}C increase due to the atomic bomb since 1950s. All ages are reported as the year before present (BP = 1950 AD).

In this thesis, twelve CWC fragments (*L. pertusa* and *M. oculata*) were sampled from the on-mound cores MD13-3451G and MD13-3452G for AMS ^{14}C dating. The analyses were performed at the Poznan Radiocarbon Laboratory, Poznan, Poland. Before the analyses, all the samples were chemically cleaned with hydrogen peroxide. The obtained ages were corrected for ^{13}C and a mean ocean reservoir age of 400 years. All the ages have been converted to calendar years using the MARINE 13 calibration curve (Reimer et al., 2013) of the web-based CALIB 7.10 software (Stuiver and Reimer, 1993; http://calib.org/calib/calib.html). Consequently, all ages are reported as calendar years BP.

3.1.5 Uranium-Thorium dating

Uranium-series dating is a widely used method to date aragonitic marine carbonate as produced by cold-water corals because i>.U is incorporated by cold-water corals from seawater without fractionation, the initial isotope activity must be approximate to seawater, ii>. U/Th dating provides ages covering a large time interval (from several years to 800,000 years) usually sufficient to cover the time span preserved in sediment cores taken from CWC mounds.

The U/Th dating is based on the decay chain of uranium from ^{238}U to ^{230}Th (Fig. 3-2). In natural systems, ^{238}U has long half-lives of 0.7 billion years, which is much longer than its daughter products ^{234}U (~245,000 years) and ^{230}Th (~75,000 years) (Jaffey et al., 1971; Cheng et al., 2000b). Among the thorium isotopes, ^{232}Th is the most abundant in nature (~100%), and its half-life is 14 billion years, much longer than its daughters (Holden, 1989). In a closed decay system, therefore, the daughter isotopes (^{230}Th and ^{234}U) mainly originate from the natural decay of their parent U isotopes. Under secular equilibrium, namely the quantity of a radioactive isotope is constant due to its same rate of

production and decay, the activity of daughter isotope (^{234}U and ^{230}Th) should equal the activity of their parent isotopes over millions of years.

For U/Th dating, the initial ^{230}Th in carbonate is zero since the secondary carbonate does not incorporate ^{230}Th. Because the half-life of ^{238}U is more than one magnitude larger than the half-life of the ^{234}U and ^{230}Th (Fig. 3-2), if the decay system is closed, the development of ^{234}U/^{238}U and ^{230}Th/^{234}U, therefore can be described by the following equations according to Ivanovis and Harmon (1992).

$$(^{230}Th/^{238}U)\ (t)= [1 - \exp(-\lambda_{230}\ t)] + [(^{234}U/^{238}U)\ (t)-1]\ [\lambda_{230}/(\lambda_{230} - \lambda_{234})\ [1 - \exp-(\lambda_{230} - \lambda_{234})t]$$

Figure. 3-2. Decay chain of U isotopes displaying the isotopes used in uranium series dating in the thesis (grey shaded squares). Half-life periods of these elements are given in h: hour; d: day; yr: year.
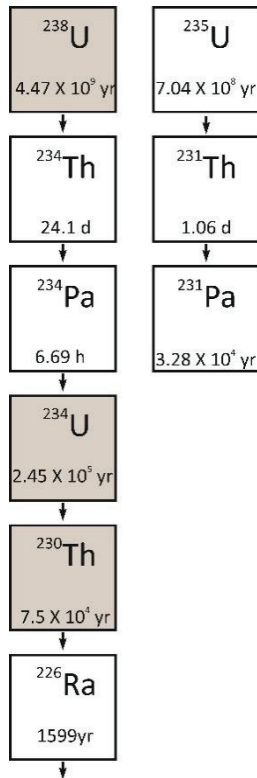
The (^{234}U/^{238}U) (t) is the measured (^{234}U/^{238}U) activity ratio, λ is the decay constant, t is the decay time.

The equation is based on the present activity ratios (^{234}U/^{238}U, and ^{230}Th/^{238}U) of the coral, and thus can be used for age determination. The t is determined graphically or numerically. For the corresponding error of the age, it is obtainable with numerical methods.

Notably, the obtained age can also be biased because the decay system is open and/or the initial ^{230}Th is not zero. It is mainly caused by the transportation of ^{234}U, which is absorbed on particles and transported via minerals. Such scenario is mostly discovered during sea-level low stands. i.e. glacial periods. With low sea levels during the cold periods, exposed nearshore areas are exposed to weathering processes, causing excess delivery of ^{234}U to the ocean waters. This U excess tends to cause ^{230}Th growth of the host material, thereby exceeding the ^{238}U derived from ^{230}Th. Therefore, the U/Th coral ages are deviated. Accordingly, coral age reliability can be checked by assessing the validity of the closed decay system.

Common practice to show the ^{234}U/^{238}U ratio is in the δ notation. The δ^{234}U (unit: ‰) represents the deviation of ^{234}U/^{238}U ratio from the ratio under secular equilibrium.

$$\delta^{234}U = \frac{(^{238}U/^{234}U)_{sample} - (^{238}U/^{234}U)_{secular\ equilibrium}}{(^{238}U/^{234}U)_{secular\ equilibrium}} \times 1000$$

As mentioned above, initial δ^{234}U of corals is in the range of marine waters (Cheng et al., 2000b). During interglacial periods, the δ^{234}U of ocean water is in the range of 146 ± 10 ‰ (Esat and Yokoyama, 2006; Andersen et al., 2010). In contrast, the δ^{234}U of sea water is in the range of 149 ± 10 ‰ during the glacial period (Esat and Yokoyama, 2006). These δ^{234}U values of seawater determine the initial δ^{234}U of corals. If the δ^{234}U are within the range of seawater δ^{234}U during different periods, the corresponding coral ages thus are considered as reliable.

In this thesis, the CWC fragments (including *L. pertusa* and *M. oculata*) were collected from the on-mound cores GeoB18127-1, GeoB18130-1, GeoB18120-1 and GeoB18105-1 for U/Th dating. Prior the dating, all the coral fragments were mechanically cleaned following the method described by Frank et al. (2004). U-series isotope were measured with a Thermo Fisher iCAP-QS inductively coupled plasma mass spectrometer (ICP-MS) at the Institute of Environmental Physic, Heidelberg University, Germany. The international uranium standard material HU1 was used for reproductivity assessment (Cheng et al., 2000b; Frank et al., 2004; Wefing et al., 2017). All the obtained coral ages were reported as kilo years (kyr) before present (BP; Present = 1950 CE). Mound AR was calculated using the linear interpolation of dated core depths for each core.

3.2 Off-mound core analyses

3.2.1 Sediment composition

As mentioned in sub-chapter 3.1.1, hemipelagic sediments from the Mediterranean Sea mainly consists of siliciclastic material, carbonate and organic carbon (e.g., Masque et al., 2003). In this context, the content of each of these fractions was measured.

Dry bulk density

In the thesis, the off-mound core GeoB13731-1 was used for the dry bulk density measurement. The sampling resolution of the core was 5 cm. The whole measurement was conducted in the Geotechnic Laboratory at MARUM, University of Bremen, Germany. For the detailed procedure, please refer to sub-chapter 3.1.1.

Total carbon and total organic carbon

Here, the off-mound core GeoB13731-1 was used to determine the contents of TC and TOC. The sampling resolution was 5 cm, and the measurement was performed at the University of Bremen, Germany. For the detailed procedure, please refer to sub-chapter 3.1.1.

3.2.2 Grain size measurements

The off-mound cores GeoB13731-1, GeoB18131-1, and MD13-3457 were used for grain size measurement. The measurements were performed on the terrigenous sediment fraction only following the procedure outlined in sub-chapter 3.1.2. For cores GeoB13731-1 GeoB18131-1, and MD13-3457, the sampling resolution was 10-cm, 5-cm, and 10-cm, respectively. In addition, for core GeoB13731-1

the sampling resolution was increased to 2 cm between 318-330 cm core depths. The grain-size data (10-cm resolution) from core GeoB13731-1 were obtained by Fink et al., (2013).

3.2.3 Radiocarbon dating

In the thesis, age models of the off-mound cores GeoB13731-1, GeoB18131-1 and MD13-3457 were developed based on the AMS ^{14}C dating and on the oxygen isotope chronology. For the AMS ^{14}C dating, a total of twenty-one samples of mixed planktonic foraminifera were collected for dating, with seven samples from the core GeoB13731-1, six samples from core GeoB18131-1 and eight samples from core MD13-3457. For cores GeoB18131-1 and MD13-3457, >8 mg of carbonate from mixed planktonic foraminifera >150 µm were analyzed at the Poznan Radiocarbon Laboratory, Poznan, Poland. For core GeoB13731-1, mixed planktonic foraminifera were dated at the Keck Carbon Cycle AMS Facility of the Earth System Science Department, University of California, Irvine, USA. The AMS ^{14}C datings from core GeoB13731-1 were already published by Fink et al., (2013). All the obtained ages were corrected and converted to calendar years as described in the sub-chapter 3.1.5.

3.2.4 Stable oxygen and carbon isotopes of benthic foraminifera

Isotope stratigraphy

The use of stable oxygen isotopes of benthic foraminifera for age model reconstruction is based on the fact that: i> stable oxygen isotopes of benthic foraminifera, particularly the epifaunal species, are in equilibrium with the stable oxygen isotope composition of the bottom water; ii> deep water stable oxygen isotopes are mainly driven by changes in the global ice volume and, thus, allow for establishing a relative chronology based on the well-established deep marine oxygen isotope record (Lisecki and Raymo, 2005).

In nature, the two most common oxygen isotopes, ^{16}O and ^{18}O, comprise 99.63% and 0.20% of all oxygen, respectively (Faure, 1986). To express more accurately the abundance of rare isotopes, the ratio of the rare isotope to the common isotope ($^{18}O/^{16}O$) is introduced. Furthermore, to show the difference between the sample and the standard, the stable oxygen isotope composition is expressed as delta (δ) value:

$$\delta^{18}O = \frac{(^{18}O/^{16}O)_{sample} - (^{18}O/^{16}O)_{standard}}{(^{18}O/^{16}O)_{standard}} \times 1000$$

The seawater $\delta^{18}O$ (unit: ‰) varies both within the change of global ocean $\delta^{18}O$ and local $\delta^{18}O$. During the late Cenozoic, global ocean $\delta^{18}O$ variability predominantly originates from global ice volume changes. The ^{16}O evaporates more easily and is thus enriched in clouds and water vapors than the ^{18}O, whereas the latter is more readily to condense and remove from the clouds and water vapors. With

increasing latitude and altitude, i.e., the decreasing temperature, the $\delta^{18}O$ of snowfall in the high latitude and altitude area is strongly depleted. During the glacial periods, maximum volume of ice sheets on land stored low $\delta^{18}O$ waters, causing relatively high mean $\delta^{18}O$ of the oceans in the world. Unlike the glacial periods, less volume of ice sheets on land during the interglacial periods, tends to reduce mean $\delta^{18}O$ of the global oceans. In addition, the seawater $\delta^{18}O$ is also influenced by local processes, for example the local evaporation-precipitation balance, input of freshwater, advection or upwelling. However, these changes mainly influence the surface and sub-surface seawater $\delta^{18}O$ and are documented in the $\delta^{18}O$ of planktonic foraminifera shells. The above outlined ice-volume change induced global mean $\delta^{18}O$ variation will be reflected by the benthic foraminifera $\delta^{18}O$ (Ravelo and Hillaire-Marcel, 2007).

Circulation tracer

The use of stable carbon isotopes of shells of benthic foraminifera, particularly for epifaunal species, to trace the water masses also is based on the isotope equilibrium between the foraminifera shell and the bottom waters (Mackensen and Schmiedl, 2019). In nature, the two most prominent stable carbon isotopes, ^{12}C and ^{13}C, account for 98.89% and 1.11% of all carbon isotopes, respectively (Faure, 1986). In analogue to stable oxygen isotopes, $\delta^{13}C$ (unit: ‰) also is defined as:

$$\delta^{13}C = \frac{(^{13}C/^{12}C)_{sample} - (^{13}C/^{12}C)_{standard}}{(^{13}C/^{12}C)_{standard}} \times 1000$$

Over geological time scales, global mean $\delta^{13}C$ of dissolved inorganic carbon (DIC) in seawater is controlled by the carbon cycle, particularly the carbon partition between the ocean, atmosphere and land biosphere reservoirs. During warm climate periods, a larger terrestrial biosphere, typically enriched in ^{12}C, leads to an enhanced ^{12}C-storage on land (Bender, 1971). As a result, the ocean and atmosphere become relatively enriched in ^{13}C (e.g., Kroopnick, 1985; Boyle, 1997). Unlike the interglacial periods, the global mean $\delta^{13}C_{DIC}$ during the glacial periods is depleted, due to the low ^{12}C-storate on land resulting from the reduced terrestrial biosphere. In addition, the $\delta^{13}C_{DIC}$ of seawater is further influenced by local changes between the photosynthesis and respiration, the mixing of water masses and the water source. (Ravelo and Hillaire-Marcel, 2007; and references therein).

In the deep ocean, seawater $\delta^{13}C_{DIC}$ variations mainly reflect changes in water mass provenance, local mixing, and export productivity (Ravelo and Hillaire-Marcel, 2007; and references therein). High export productivity tends to cause the depletion of ^{13}C in the bottom water triggered by the release of ^{12}C-enriched CO_2 by respiration of organic matter at the seafloor. The ^{12}C-enriched organic matter is formed at the sea surface by the preference uptake of ^{12}C by primary producers (e.g., Degens, 1969). Along the pathway of circulation, the waters gradually become $\delta^{13}C$ depleted due to the continuing respiration of organic matter (e.g., Rohling and Cooke, 1999). Such changes in $\delta^{13}C_{DIC}$ will be documented in the $\delta^{13}C$ of epifaunal benthic foraminifera shells.

In this thesis, the $\delta^{13}C$ of epifaunal benthic foraminifera is used like a tracer of water mass circulation in the Alboran Sea. It is based on the fact that the impact of export productivity on the $\delta^{13}C$ of benthic foraminifera is light under strong thermohaline circulation during the last 150 kyr (Toucanne et al., 2012). The $\delta^{13}C$ of benthic foraminifera, therefore, most likely reflects the change of the dominant water mass in the study area.

Here, epifaunal benthic foraminifera (>150 µm) from cores GeoB13731-1 (*Cibicoides kullenbergi*), GeoB18131-1 (mixed *Cibicoides mundulus* and *Cibicoides pachyderma*) and MD13-3457 (*Cibicoides mundulus*) was used for the $\delta^{18}O$ and $\delta^{13}C$ measurements, with sampling resolutions of 5 cm. In addition, to exclude any foraminiferal vital effect on the record of core GeoB18131-1, for another 16 samples $\delta^{18}O$ and $\delta^{13}C$ of 10 individuals of two foraminifera species, *Cibicoides pachyderma* and *Cibicoides mundulus*, were measured separately.

The analyses were performed with a Finnigan MAT 252/251 gas isotope ratio mass spectrometer connected to Kiel I/II automated carbonate preparation device, at the MARUM, University of Bremen. Under a constant temperature of 75 °C, the measurements were conducted on the CO_2 generated by phosphoric acid treatment. The ground Solnhofen limestone was used as internal standard that has been calibrated against Vienna Pee Dee Belemnite (V-PDB) with the NBS 18, 19 and 20 standard. For the core GeoB18131-1, the analytical standard deviation for the $\delta^{18}O$ and $\delta^{13}C$ was ±0.04‰ and ±0.03‰, respectively. The $\delta^{18}O$ and $\delta^{13}C$ anomalies between *Cibicoides pachyderma* and *Cibicoides mundulus* have mean values of 0.04‰ and -0.04‰, respectively, with a standard deviation of <0.25 for both. For the core Geob13731-1, the analytical standard deviation for the $\delta^{18}O$ and $\delta^{13}C$ was ±0.07‰. For the core MD13-3457, the analytical standard deviation for the $\delta^{18}O$ and $\delta^{13}C$ were ±0.09‰ and ±0.04‰, respectively. The data from core GeoB13731-1 were obtained from Fink et al., (2013).

3.2.5 X-ray fluorescence scanning

The chemical composition of sediment cores by X-ray fluorescence (XRF) scanning is widely used in marine science to provide non-destructive, high resolution, and semi-quantitative records (e.g., Thomas Richter et al., 2006). Briefly, with the incoming X-ray radiation, electrons from inner shell of an atom are ejected. Afterwards, this vacancy is filled by electrons from the outer shells of the atom. During this process, the energy difference between these shells is emitted as fluorescence radiation, which is specific for each element. The intensity of the radiation is proportional to the amount of corresponding element.

In this study, the off-mound core MD13-3457 was used for XRF scanning to obtain the intensities of elements: Ca and Fe and Mn in 2 cm resolution. Prior the XRF scanning, the split core surface was first covered with a 4 micron thin SPEXCerti Prep Ultralene1 foil to avoid contamination of the XRF measurement unit and desiccation of the sediment. The measurement was conducted with XRF Core

Scanner II (AVAATECH Serial No. 12) at the MARUM, University of Bremen. The XRF Core Scanner data were collected in two runs using generator settings of 10 kV (for Al,Si, S, K, Ca, Ti, Mn, Fe) and 30kV (for Br, Sr, Rb, Zr), currents of 0.2 mA and 1 mA, and sampling times of 20 seconds directly at the split core surface. The here reported data have been acquired by a Canberra X-PIPS Silicon Drift Detector (SDD; Model SXD 15C-150-500) with 150 eV X-ray resolution, the Canberra Digital Spectrum Analyzer DAS 1000, and an Oxford Instruments 50 W XTF5011 X-Ray tube with rhodium (Rh) target material. Raw data spectra were processed by the analysis of X-ray spectra by Iterative Least square software (WIN AXIL) package from Canberra Eurisys.

In the Alboran Sea, where biogenic opal production is low, the carbonate content in sediment mainly originates from the foraminifera and coccolithophores, and can be used as a proxy of ocean productivity (Rühlemann et al., 1999). The Fe in the sediment mainly derives from terrigenous input. Therefore, the Ca/(Ca+Fe) ratio can be used to trace the change of sediment supply between the marine and land, and further providing the variation of ocean surface productivity. The Mn is a redox-sensitive element, which exists as insoluble oxi-hydroxides when the dissolved oxygen content in the waters is high, resulting high Mn content in the sediment and vice versa (e.g., Calvert and Pedersen, 2007; Martinez-Ruiz et al., 2015). In this study, the Mn content (%, relative to the total counts in 15 points running average) is used to reflect the change of dissolved oxygen content in the water.

3.2.6 Benthic foraminifera accumulation rate

The benthic foraminifera accumulation rate (BFAR) is widely used as an export productivity proxy (e.g., Berger, 1992) based on the observation that population density of deep-sea fauna correlates well with the food availability (e.g., Fontanier et al., 2002). Herguera and Berger (1991) revealed that the BFAR positively correlates with the total organic matter sinking to the seafloor, particularly in oxygenated sediments (Herguera, 2000). It is notable that the BFAR also can be influenced by taphonomic processes (Murray, 2006). Nonetheless, our records show continuous occurrences of gastropods in all layers of the sediment, clearly suggesting that dissolution is not a major factor influencing the BFAR record.

In this thesis, off-mound core GeoB18131-1 was used for the BFAR analyses at core depths of 0-368 cm. In detail, the sampling resolutions were 10 cm in the uppermost 158 cm of the core and 5 cm at core depths of 158-368 cm. The benthic foraminfiera counting was performed at MARUM, University of Bremen, Germany. Firstly, the bulk samples were wet sieved and only the fraction >150 μm was used for counting benthic foraminifera. Samples were split until they contained approximately 300 individuals of benthic foraminfera and then counted (Patterson and Fishbein, 1989). Finally, the obtained results were corrected for the splits. BFAR (unit: X 10^3 individuals cm^{-2}kyr^{-1}) calculation follows the equation from Ehrmann and Thiede (1985).

$$BFAR = SR \times DBD \times foram/1000$$

BFAR: benthic foraminifer accumulation rate;

SR: Sedimentation Rate (unit: cm kyr^{-1});

DBD: Dry bulk sediment density (unit: g cm^{-3});

foram: number of foraminifers per gram in the dry bulk sample (unit: individuals g^{-1}).

Chapter 4

Cold-water coral mound formation: the importance of ecological accommodation space and sediment supply

Haozhuang Wang[a], Jürgen Titschack [a, b], Claudia Wienberg [a], Dierk Hebbeln [a]

a Center for Marine Environmental Sciences (MARUM), Bremen University, Leobener Strasse 2, 28359 Bremen, Germany

b Senckenberg am Meer (SAM), Marine Research Department, Südstrand 40, 26382 Wilhelmshaven, Germany

Abstract

Cold-water coral (CWC) mounds are widely distributed along the continental margins of the Atlantic Ocean and its marginal seas. Their formation results from the interplay between the sustained growth of framework-forming CWCs and the concurrent deposition of sediments within the branched coral framework that stabilizes the biogenic construction allowing for enhanced mound aggradation. While much effort has been conducted to reconstruct the temporal development of CWC mounds in various areas, little is known about the sedimentary processes supporting the formation of CWC mounds. Therefore, we aimed to reconstruct changes in sediment transport and deposition by comparing two sediment cores collected from a CWC mound and from the adjacent seafloor (on- and off-mound cores). The cores originate from the southern Alboran Sea, where the most recent CWC mound formation period corresponded to the Early Holocene (~11.2-9.8 kyr BP). During this time interval, siliciclastic sediments deposited on-mound are finer (mode: 7 Φ) than those simultaneously deposited on the adjacent seafloor (mode: 4 Φ), a difference that remained constant over the entire mound formation period. The coarse sediments deposited in the off-mound setting overall indicate highly turbulent conditions prevailing in the area. The concurrent deposition of fine sediments on mound was only possible with the re-establishment of dense coral frameworks that effectively baffled suspended sediments from the near-bottom waters by significantly reducing the current velocity and further provided a low-energy accommodation space for the deposition of these sediments, also preventing their re-suspension. The extremely high on-mound accumulation rate of siliciclastic (matrix) sediments (~323 g cm^{-2} kyr^{-1}), being around 30 times higher than on the adjacent seafloor, is related to an internal waves-induced increased lateral delivery of sediments, which rapidly filled the accommodation space provided by the coral framework and significantly contributed to the very high

mound aggradation rates (ARs) of up to 589 cm kyr^{-1}. Based on our results, we provided a conceptual model highlighting the crucial role of sediment supply and CWC-derived ecological accommodation space for coral mound formation.

4.1 Introduction

Cold-water coral (CWC) mounds occur commonly along the upper and mid continental slopes (200 - 1000 m water depths) in the Atlantic Ocean and the adjacent Mediterranean Sea and Gulf of Mexico (Roberts et al., 2006; Wheeler et al., 2007; Hebbeln et al., 2014; Hebbeln and Samankassou, 2015; Wienberg and Titschack, 2017; Lo Iacono et al., 2018). They rise up to several tens and even hundreds of meters above the seafloor (e.g., Mienis et al., 2007) and occur in clusters or provinces often comprising hundreds of individual mounds (e.g., Colman et al., 2005; Grasmueck et al., 2006; Wheeler et al., 2007; Hebbeln et al., 2014; 2019; Tamborrino et al., 2019). CWC mounds are formed by the complex interplay between the sustained growth of framework-forming CWCs and the concurrent deposition of sediments within the branched coral framework (Roberts et al., 2009). Therefore, coral mound deposits consist mainly of CWC fragments and (hemi-)pelagic sediments, with minor contributions from coral-associated benthic species, such as mollusks, bryozoans and echinoderms (e.g., Wheeler et al., 2005; de Haas et al., 2009). A suit of environmental parameters controls the proliferation of CWCs, including temperature, salinity, dissolved oxygen concentrations, pH, water density, etc. (e.g., Freiwald, 2002; Davies et al., 2008; Dullo et al., 2008; Davies and Guinotte, 2011). High food availability represents another crucial factor controlling the flourishment of these suspension feeders in the deep ocean (e.g., Thiem et al., 2006 and references therein), which is determined by enhanced surface production and strong bottom hydrodynamics. In particular, internal waves/tides occurring at the boundary of water masses significantly enhance the turbulence mixing at mid-depths (Pomar et al. 2012) and support the proliferation of CWCs as they enrich (nepheloid layers) and laterally transport food particles to the corals (e.g., Thiem et al., 2006; Orejas et al., 2009; White and Dorschel, 2010; López Correa et al., 2012; Hebbeln et al., 2014; Matos et al., 2015; Collart et al., 2018).

However, besides sustained coral growth steered by distinct environmental conditions, the supply and on-mound deposition of sediments is a further prerequisite for the formation of coral mounds, expressed by ~50% of (hemi-)pelagic sediments contributing to the total coral mound deposits (e.g., Dorschel et al., 2007b; Titschack et al., 2009; 2015; 2016). While the supply of sufficient sediments is controlled by the regional hydrodynamics, the local deposition of the delivered sediments is significantly influenced by the CWC frameworks that affects the velocity of bottom currents (baffling effect; Dorschel et al., 2007a; e.g., Guihen et al., 2013), and further provides accommodation space for the deposition of the current-transported sediments. However, the associated sedimentary processes involved in coral mound formation are still underexplored. Even though, the baffling effect of framework-forming CWCs has been conservatively discussed by several studies (e.g., Huvenne et al., 2009b; Titschack et al., 2009; 2015; Victorero et al., 2016), very little is known on how and to what extent the coral frameworks influence the local hydrodynamic regime and control grain-size distribution and accumulation rates of sediments deposited on-mound, which in turn contributes to the aggradation of the coral mound.

In this study, we aimed to decipher the interaction between the coral framework and the hydrodynamic and sedimentary processes to reconstruct how this impacted CWC mound formation. To achieve this goal, we selected two sediment cores, one retrieved from a coral mound (on-mound core) recording a pronounced CWC mound formation period with partly high aggradation rates (AR) and a second one collected from the adjacent the seafloor recording concurrent sedimentation in the off-mound area (age models and environmental proxy data of both cores were already published by Fink et al. (2013). By comparing the grain-size distribution, composition and accumulation rate of siliciclastic sediments of both cores, we gained new insight into differences of the hydrodynamics prevailing in the on- and off-mound settings. Moreover, by relating these data to varying mound ARs, which represent different phases of mound formation that are displayed by variations in the coral preservation patterns (from corals preserved in living position to coral rubble deposits; see also Titschack et al., 2016), we were able to assess the influence of the coral framework on the local bottom currents and to quantify the baffling capacity of the coral framework (defined by the baffling effect and the CWC provided accommodation space) during CWC mound formation.
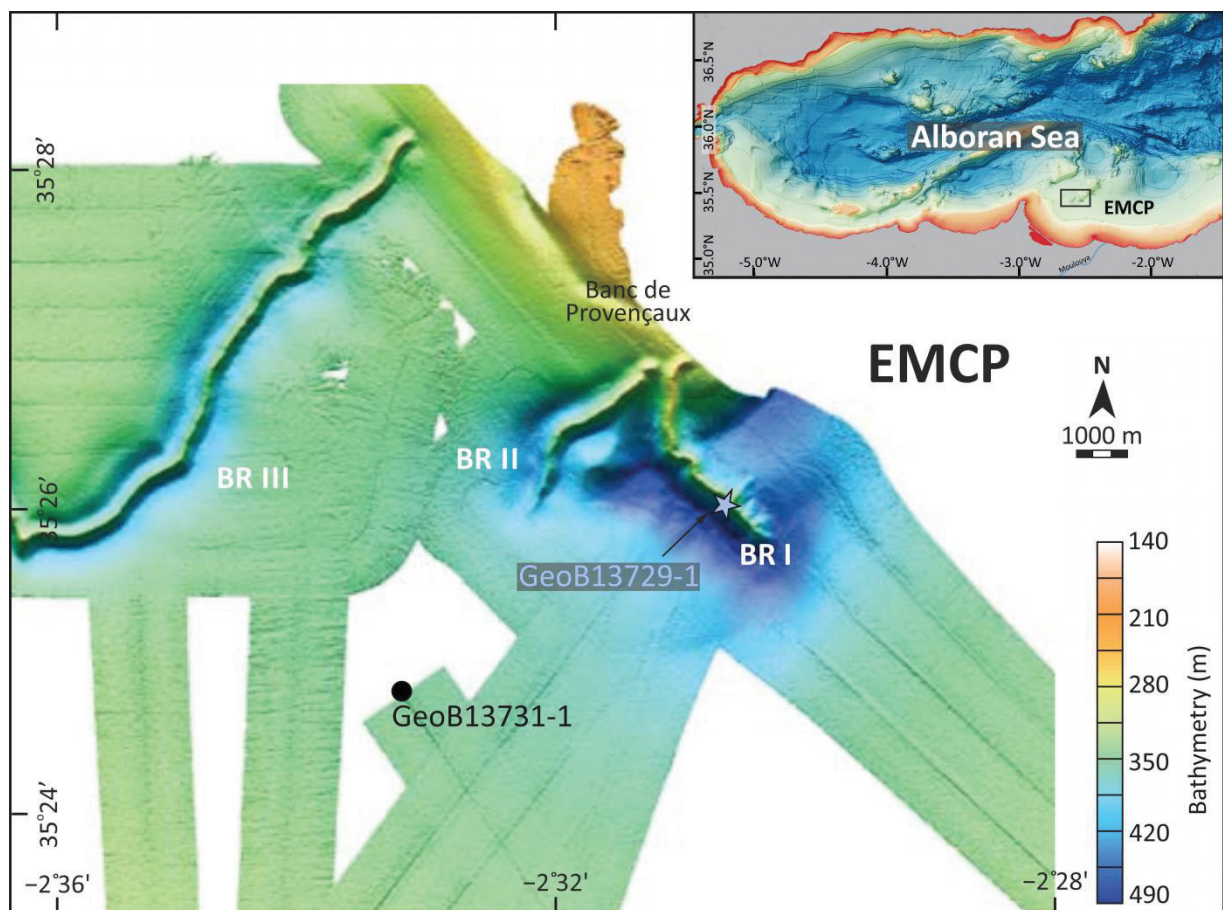

Figure. 4-1. Bathymetry map of the East Melilla cold-water coral mound province (EMCP) in the southern Alboran Sea (see overview map for location) showing the core locations (off-mound: GeoB13731-1, on-mound: GeoB13729-1). BR: Brittlestar ridge. Map modified from Hebbeln , (2019).

4.2 Material and method

Two gravity cores were investigated, which were retrieved from the East Melilla coral mound province (EMCP) in the southern Alboran Sea during the RV Poseidon cruise POS 385 (Hebbeln et al., 2009). The on-mound core GeoB13729-1 was collected from the upper flank of the Brittlestar Ridge I (Fig. 4-1), a steep and elongated north-southeast trending coral ridge rising 50-150 m above the surrounding sea floor (for further details see Hebbeln, 2019). The on-mound core has a recovery of 447 cm (Table 4-1) and contains CWC fragments of various preservation states throughout the core (see Titschack et al., 2016). Five AMS ^{14}C dates obtained from the CWC fragments revealed a pronounced mound formation period corresponding to the Early Holocene (11.2-9.8 kyr BP; published by Fink et al. 2013). The off-mound core GeoB13731-1 was collected from the seafloor about 4 km southeast of the Brittlestar Ridge I and has a recovery of 431 cm (Table 4-1). The age model established for this core, based on seven AMS ^{14}C datings of mixing planktonic foraminifers and a linear interpolation between them, showed that the core sediments were deposited during the last ~23 kyr (published by Fink et al. 2013). For this study, the AMS 14C ages of both cores were re-calibrated and converted into calendar years with the Marine13 calibration curve (Reimer et al., 2013) using the software CALIB 7.10 (Stuiver and Reimer, 1993; http://calib.org/calib/calib.html) (Table 4-2). Based on the re-calibrated AMS ^{14}C ages, sedimentation rates (SRs) for the off-mound core and mound ARs for the on-mound core were (re-)calculated (Table 4-2).

Table 4-1. Metadata of gravity cores collected in the EMCP (southern Alboran Sea) during the cruise POS 385 with the German RV Poseidon in 2009 (Hebbeln et al., 2009).

Core Type	Core ID	Latitude [N]	Longitude [W]	Area	Water depth [m]	Recovery [cm]
Off-mound	GeoB13731-1	35°24.80′	2°33.22′	Off-mound	362	431
On-mound	GeoB13729-1	35°26.07′	2°30.83′	Brittlestar Ridge I	442	447

4.2.1 Grain-size analyses

For the off-mound core GeoB13731-1, grain-size distribution data of the siliciclastic sediment fraction were already published by Fink et al. (2013). The sampling resolution was 10 cm and analyses were performed with a Beckman Coulter LS200 with 92 size classes ranging between 0.4 and 2000 µm (for further details see Fink et al. 2013). For this study, additional samples were collected from the off-mound core in 2-cm-resolution from the core depth interval 318-338 cm, which according to the existing age model temporally corresponded to the Early Holocene mound formation period (11.2-9.8 kyr BP) archived in the on-mound core GeoB13729-1 (Fink et al. 2013). Further samples were collected in 10-cm-resolution from the matrix sediments of the entire on-mound core. For all sediment samples (off- and on-mound cores), the biogenic components (organic carbon, carbonate and opal fraction) were removed prior to the grain-size analyses following the procedure of McGregor et al. (2009). During the entire preparation, deionized, degassed and filtered water (mesh size of 0.2 µm)

was used to reduce the potential influence of air bubbles or particles in the water. The new set of sediment samples were measured in the Particle-Size laboratory at MARUM (University of Bremen, Germany) using a Beckman Coulter LS13320 with 116 size classes ranging from 0.04 to 2000 μm. As all samples exhibited contents of <5 vol.% in the size fraction between 0.04 and 2000 μm, this fraction was considered as negligible and removed. The remaining grain-size distribution was renormalized to the fraction of 0.4-2000 μm to allow a direct comparison with the formerly published grain-size distribution data obtained with the LS200. The statistic values are based on a geometric statistic.

4.2.2 Dry bulk density measurement

Sediment dry bulk density (DBD) measurements were conducted in 10-cm-resolution for the cores GeoB13731-1 and GeoB13729-1. Approximately 8 cm3 sediment was wet weighted and subsequently dried for 24 hours within a convection oven at temperatures of 100-110°C. After cooling to room temperature in a desiccator, sediment volumes were measured with a Pentapyc 5200e gas pycnometer (Quantachrome instruments). The measurements were performed in the Geotechnic Laboratory at MARUM, University or Bremen, Germany. The DBD were determined by following the ODP methodology of Blum (1997).

4.2.3 Total carbon and total organic carbon measurement

Total carbon (TC) and total organic carbon (TOC) were analysed in 10 and 5 cm resolution for the cores GeoB13731-1 and GeoB13729-1, respectively. Prior to the analyses, freeze-dried sediment was first grounded, and then divided into two subsamples of approximately 50 mg each to determine the TC and TOC.

For the TOC measurement, the total inorganic carbon (TIC) was removed with 12.5% HCl prior to the analysis. Both subsamples (for TC and TOC) were measured with a Leo CS 200 at the Department of Geosciences, University of Bremen, Germany. The TIC content (weight content, wt.%) was calculated by subtraction of TOC from TC following the equation:

$$CaCO_3 \text{ (wt.\%)} = (TC-TOC) \text{ (wt.\%)} \times M_{CaCO_3}/M_C.$$

M_{CaCO_3}: Molecular weight of calcium carbonate (100 g/mol)

M_C: Molecular weight of carbon (12 g/mol)

4.2.4 Calculation of sediment composition and associated accumulation rate

The main difference of sediment composition between the on- and the off-mound cores are the corals within the on-mound core. Accordingly, the calculation given below contains the corals. For the off-mound core, the coral content is taken as zero for all equations.

The sediment weight was obtained by summing the weights of matrix sediments and the corals.

$$Ws = \rho_{matrix} \times (100 - C_{Coral}) + \rho_{coral} \times C_{Coral}$$

Whereas the ρ_{matrix} is the density of matrix sediment [unit: g cm^{-3}], ρ_{coral} (2.66 g cm^{-3}) is the density of CWC skeletons (see Dorschel et al., 2007). CCoral represents the coral content [vol.%] that was obtained from CT analyses (data published in Titschack et al., 2016).

The contribution of each sediment fraction to the total sediment was obtained by the equation:

$$W_{Com} = (Ws - \rho_{coral} \times C_{Coral}) \times C_{Com} / 100$$

C_{Com} is the content of the respective sediment fractions within the matrix sediment [wt.%] and W_{Com} is its content [wt.%] in the total sediment.

Accumulation rates of the different sediment fractions were calculated by multiplying the weight of each sediment fraction with the respective SR (for the off-mound core) or the AR (for the on-mound core):

$$Acc_{Com} = W_{Com} \times SR \text{ or } W_{Com} \times AR$$

The herein Acc_{Com} is the accumulation rate of different sediment fractions. The calculations of sediment fractions and associated accumulation rate follow the method published by Titschack et al. (2009) with minor adaptions.

Table 4-2. ASM ^{14}C dates obtained from mixed planktonic foraminifiera and cold-water coral fragments (*Lophelia pertusa*) from the off-mound core GeoB13731-1 and the on-mound core GeoB13729-1, respectively. The ages were corrected for ^{13}C and a reservoir age of 400 years. The AMS ^{14}C ages were converted into calendar age with the CALIB 7.10 (Stuiver and Reimer, 1993; http://calib.org/calib/calib.html), using the MARINE-13 curve (Reimer et al., 2013). Sediment rate (SR) and coral mound aggradation rate (AR) are calculated based on a linear interpolation of the ages.

Core ID (GeoB-)	Core Depth [cm]	Lab-code UCIAMS-	Conventional Age [kyr] BP]		2σ Range cal. Age [kyr BP, P=AD 1950]		Median Probability Age [kyr BP]	SR/AR [cm kyr^{-1}]
			^{14}C age	± error				
Off-mound 13731-1	8	78807	0.550	0.015	0.125	0.260	0.194	-
	128	78808	2.005	0.015	1.507	1.636	1.565	87.5
	203	78809	4.035	0.015	3.973	4.133	4.054	30.1
	328	78810	9.480	0.020	10.232	10.408	10.316	20.0
	353	78811	11.630	0.025	13.009	13.242	13.130	8.9
	368	78812	14.775	0.035	17.339	17.665	17.517	3.4
	423	788013	19.345	0.050	22.606	22.994	22.806	10.4
On-mound 13729-1	2.5	73570	9.085	0.030	9.657	9.934	9.801	-
	49	73571	9.330	0.025	10.125	10.224	10.177	123.7
	140	73572	9.705	0.025	10.519	10.692	10.606	212.1
	315	73573	9.935	0.030	10.745	11.051	10.903	589.2
	375	73574	10.225	0.030	11.130	11.293	11.210	195.4

4.3. Result

4.3.1 Off-mound core GeoB13731-1

4.3.1.1 Age model and sedimentation rates
The age model of the off-mound core was originally published by Fink et al. (2013), and re-calibrated for this study (Table 4-2). The off-mound core sediments were deposited during the last 22.8 kyr with SR ranging from 3.4 to 87.5 cm kyr^{-1}. The SRs were rather low between 22.8 and 10.3 kyr BP and varied between 3.4 and 10.4 cm kyr^{-1}. During the period of 10.3 - 1.6 kyr BP, the SR increased to values between 20.0 and 30.1 cm kyr^{-1}. Since 1.6 kyr BP, the SR was high with a value of 87.5 cm kyr^{-1} (Table 4-2, Fig. 4-2).

4.3.1.2 Grain size distribution
The grain-size distribution of the siliciclastic sediment fraction showed multi-modal distribution patterns throughout the entire core. From 22.8 to 17.5 kyr BP and ~9.8 to 0.2 kyr BP, a dominant mode at ~8 Φ (4 µm) with contents of 2.3-3.4 vol.%, a medium mode at ~5 Φ (~31 µm) with contents of 1.0-1.9 vol.%, and a minor mode at ~4 Φ (63 µm) with contents of 0.3-1.4 vol.% occurred (Figs. 2, 3). Between 17.5 and 9.8 kyr BP, the grain-size distribution showed a distinctively different pattern with a dominant mode at ~4 Φ (63 µm) with contents between 2.2 and 4.9 vol.%, a medium mode at ~5 Φ (~31 µm) with contents between ~2.0 vol.% and ~2.5 vol.%, and a minor mode at ~7 Φ (8 µm) with contents between 1.1 and 2.2 vol.% (Figs. 4-2, 4-3).

4.3.1.3 Sediment composition
The sediment composition of core GeoB13731-1 is rather homogenous (Fig. 4-2). Siliciclastic sediments are the main component of the core sediments with a content ranging from 58.2 to 73.0 wt.% (average: 63.9 wt.%). The pelagic-derived carbonate content varies between 26.2 and 41.2 wt.% (average: 35.3 wt.%), while the organic carbon content is throughout the core very low (<1.0 wt.%; and therefore not displayable in Fig. 4-2). Between 22.8 and 9.8 kyr BP, the contents of siliciclastic sediment and carbonate showed almost no fluctuations and ranged from 58.2–66.0 wt.% and from 33.3-41.2 wt.%, respectively (Fig. 4-2). Since 9.8 kyr BP, the siliciclastic sediment content slightly increased (59.1–68.7 wt.%) and finally reached its highest content (61.9–73.0 wt.%) between 1.6 and 0.2 kyr BP (Fig. 4-2). On the contrary, the carbonate contents slightly decreased to 30.4–40.3 wt.% between 9.8 and 1.6 kyr BP and to 26.2–37.2 wt.% between 1.6 and 0.2 kyr BP.

4.3.1.4 Accumulation rate of siliciclastic sediment
The accumulation rate of the siliciclastic sediment fraction (Acc$_{Silic}$) showed a trend comparable to the SR (Fig. 4-2) and varied throughout the core between 2.4 and 59.0 g cm^{-2} kyr^{-1}. While between 22.8 and 1.6 kyr BP, the Acc$_{Silic}$ were very low ranging from 2.4 to 18.8 g cm^{-2} kyr^{-1} (average: 11.6 g cm^{-2}

kyr^{-1}), only since 1.6 kyr BP the Acc$_{Silic}$ significantly increased to the range of 47.5-59.0 g cm^{-2} kyr^{-1} (average: 55.2 g cm^{-2} kyr^{-1}).
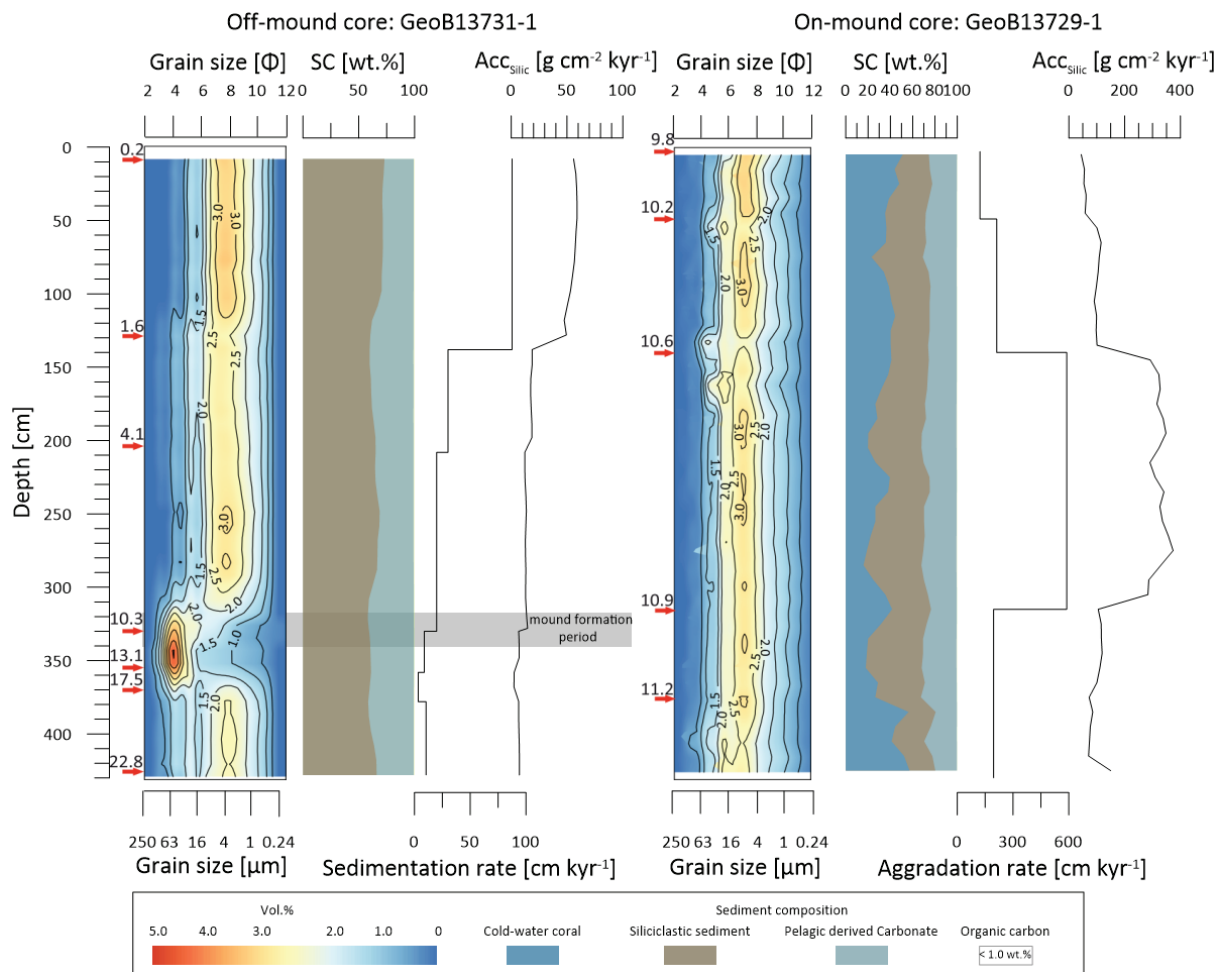
Figure. 4-2. Logs of the off-mound core GeoB13731-1 and the on-mound core GeoB13729-1. Data obtained from the off-mound core (from left to right): ASM ^{14}C datings (indicated by red arrows) obtained from mixed planktonic foraminifera, grain size distribution of siliciclastic sediments, sediment composition (SC), sedimentation rate, accumulation rate of siliciclastic sediments (Acc$_{Silic}$). The off-mound core interval temporally corresponding to the mound formation period archived in the on-mound core is highlighted by a grey bar (for detailed comparison see also Fig. 4-3). Data obtained for the on-mound core (from left to right): AMS ^{14}C datings (indicated by red arrows) obtained from cold-water coral fragments, Acc$_{Silic}$, SC, coral mound aggradation rate, Acc$_{Silic}$. All datings were published by Fink et al. (2013). The content of cold-water corals were published by Titschack et al. (2016).

4.3.2 On-mound core GeoB13729-1

4.3.2.1 Age model and mound aggradation rates

The age model of the on-mound core GeoB13729-1 is based on five AMS ^{14}C coral ages which were originally published by Fink et al. (2013) and re-calibrated for this study (Table 4-2). The ages of dated corals range between 11.2 and 9.8 kyr BP (Table 4-2), while the entire coral-bearing core covers from bottom to core top an (extrapolated) age range from 11.4-9.8 kyr BP. The calculated coral mound AR ranges between ~124 and 589 cm kyr^{-1}. During the period of 11.4-10.9 kyr BP, the mound AR was

195 cm kyr^{-1}, while between 10.9 and 10.6 kyr BP, it increased significantly to 589 cm kyr^{-1}. Between 10.6 and 9.8 kyr BP, the AR dropped again and ranged between 212 and 124 cm kyr^{-1} (Fig. 4-2).

4.3.2.2 Grain size distribution

The grain-size distribution of the siliciclastic fraction was quite homogenous and no systematic variations of the sediment content occurred when compared with the mound AR. In general, the grain sizes showed a multi-modal distribution with a dominant mode at ~7 Φ (8 µm) with contents of ~2.2-3.3 vol.%, two medium modes between 4 and 6 Φ (63 and 16 µm, respectively) with respective contents of 0.3-2.2 vol.% and 1.9-2.7 vol.%, and a minor mode at ~3 Φ (125 µm) with contents of ~0-0.6 vol.% (Figs. 4-2, 4-3).

4.3.2.3 Sediment composition

In contrast to the off-mound core, the sediments of the on-mound core not just comprised siliciclastic sediments, pelagic-derived carbonate and organic carbon, but also carbonate derived from CWCs (and subordinated from other benthic fauna; Fig. 4-2). The carbonate content of the matrix sediment, dominated by the pelagic-derived carbonate, is rather stable, varying between 19.1 and 32.2 wt.% (average: 26.7 wt.%). The organic carbon content is very low (<1.0 wt.%; not displayable in Fig. 4-2) throughout the entire core. The main variations in sediment composition derive from the macroscopic CWC and the siliciclastic sediment contents. The CWC and siliciclastic sediment contents show opposing trends. Between 11.4 and 10.6 kyr BP, the CWC content mostly fluctuated at ~20 wt.%, with high values reaching ~40 wt.% during the period between 11.4-11.2 kyr BP, and at ~10.9 and at ~10.7 kyr BP (Fig. 4-2). The siliciclastic sediment content was overall rather high with >40 wt.%. Only during the time intervals mentioned above, the siliciclastic sediment was <40 wt.% (Fig. 4-2). Between 10.6 and 9.8 kyr BP, the CWC content mostly remained high with values predominantly at ~40 wt.%, whereas the siliciclastic sediment content was relatively low, mainly with values of <40 wt.% (Fig. 4-2).

4.3.2.4 Accumulation rate of siliciclastic sediment

The Acc$_{Silic}$ co-varied with the mound AR and ranged between 44.2 and 373.4 g cm^{-2}kyr^{-1}. During the period of 11.4-10.9 kyr BP, the Acc$_{Silic}$ is in the range of 70.6-149.9 g cm^{-2} kyr^{-1} (average: 99.8 g cm^{-2} kyr^{-1}). Between 10.9 and 10.6 kyr BP, the Acc$_{Silic}$ is high, varying between 283.4 and 373.4 g cm^{-2} kyr^{-1} (average: 323.4 g cm^{-2} kyr^{-1}). During the period of 10.6-9.8 kyr BP, the Acc$_{Silic}$ is relatively low, with values in the range of 44.2-115.7 g cm^{-2} kyr^{-1} (average: 83.5 g cm^{-2} kyr^{-1}; Fig. 4-2).

4.3.3 Difference in grain-size distribution of simultaneously deposited siliciclastic sediment fraction from the on- and off-mound cores

Between 17.5 to 9.8 kyr BP, the siliciclastic sediment fraction within the off-mound core exhibited a significant shift to coarser modes compared to the sediments deposited before and after this period, while the on-mound core displaying the Early Holocene mound formation period (~11.4-9.8 kyr BP) was constantly dominated by fine modes (Fig. 4-2). The difference in grain-size distribution of simultaneously deposited siliciclastic sediment fraction (ΔContent) is examined by subtracting the average sediment content of the off-mound core from that of the on-mound core. The resulting differential diagram exhibits a size-dependent enrichment of the fine fraction (fine silt and clay; ΔContent$_{Fine}$) within coral mound sediments between ~0-1.3 vol.% and a size-dependent depletion of the coarse fraction (coarse silt and sand; ΔContentCoarse) of between -2.7 and ~0 vol.% (Fig. 4-3). The averaged total enhancement of the siliciclastic fine fraction (across all fine size fractions; ΔContent$_{Fine}$) was in the range of 24.4-38.7 vol.% (average: 31.2 vol.%) within the mound, showing no clear correlation with the mound AR (Fig. 4-3).
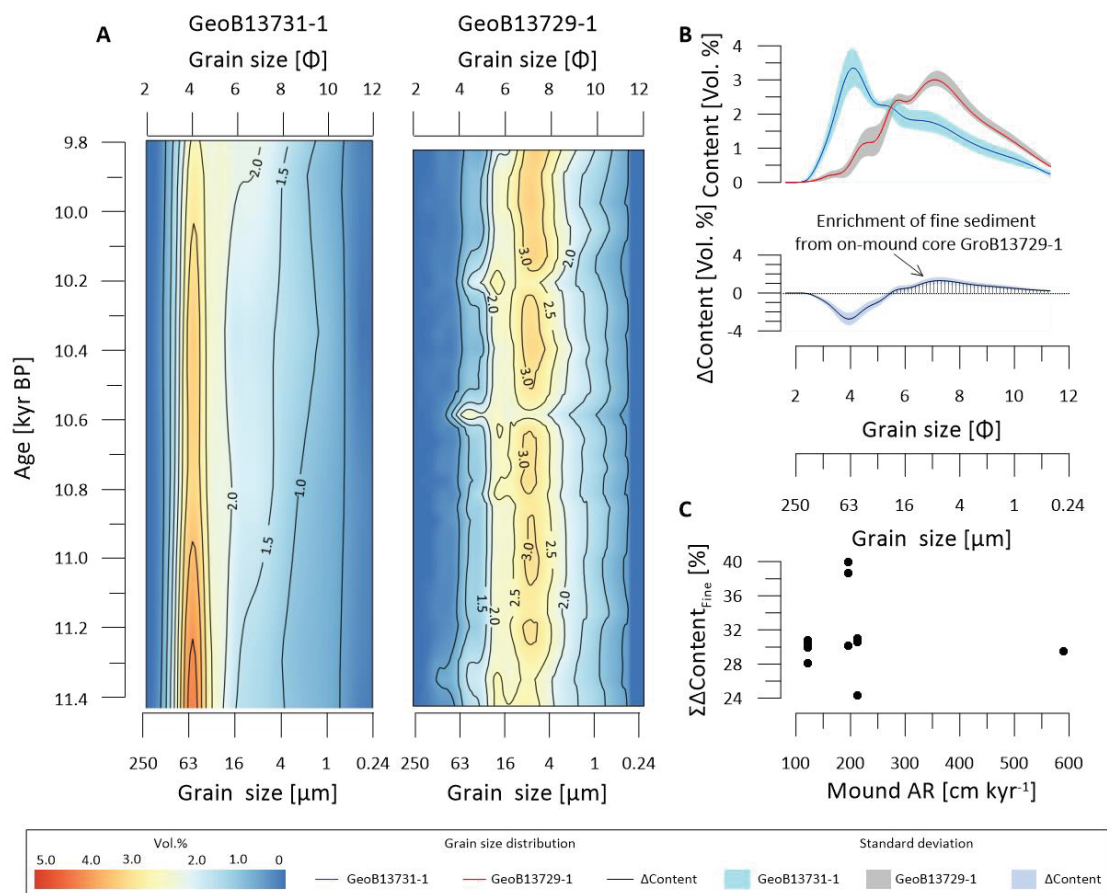
Figure. 4-3. A: Grain-size distribution of the siliciclastic sediment fraction obtained from the off-mound core GeoB13731-1 and the on-mound core GeoB13729-1. B: The averaged grain-size distribution of the two cores. The difference in grain-size distribution between the on- and the off-mound cores (ΔContent) was obtained by subtracting the off-mound core from the on-mound core grain-size distribution. The dashed area represents the averaged total enhancement of the siliciclastic fine fraction ($\Sigma\Delta$Content$_{Fine}$). C: Scatter plot of the $\Sigma\Delta$Content$_{Fine}$ versus mound aggradation rate (AR).

4.4. Discussion

Coral mound formation is the result of a complex interplay between coral growth and sediment deposition with various hydrodynamic, sedimentological and biological processes being involved (Fig. 4-4; Roberts et al., 2009; Hebbeln et al., 2016; Wienberg and Titschack, 2017). While the proliferation of corals is mainly controlled by high food availability and strong bottom currents (e.g., Thiem et al., 2006; Davies et al., 2009; Mienis et al., 2012; De Clippele et al., 2017), the sediment deposition on a coral mound depends on sediment supply and on large- to small-scale hydrodynamics (e.g., Mienis et al., 2006; Dorschel et al., 2007a; 2009b; Foubert et al., 2011; Wheeler et al., 2011; Correa et al., 2012b; Cyr et al., 2016; Victorero et al., 2016). Overall, the sedimentary processes on a coral mound are controlled by (i) the regional hydrodynamic regime (e.g., geostrophic currents, internal waves; large-scale process) and (ii) its interaction with and alteration by the mound (medium-scale process) and (iii) the coral frameworks being distributed on the mound's surface (small-scale process) both functioning as an obstacle in the current (see also De Clippele et al., 2017). Consequently, a comparison of the grain-size distribution of the siliciclastic sediment fraction deposited on a coral mound, resulting from the integrated impact of the medium- to small-scale hydrodynamics within the mound environment, and deposited on the adjacent seafloor, reflecting the large-scale regional hydrodynamic regime, is a promising approach to investigate the integrated influence of the coral mound morphology and the coral frameworks on the mound formation process (Fig. 4-4).

The grain-size distribution of the siliciclastic sediment fraction retrieved from sediments (GeoB13731-1) deposited adjacent to coral mounds in the southern Alboran Sea (EMCP) shows two different patterns. A pronounced shift to coarse sediments with a major mode of ~4 Φ (63 μm) occurred between 17.5 and 9.8 kyr BP, while before and after this time interval, fine sediments with a dominant mode of ~8 Φ (4 μm) prevailed (Fig. 4-2). The shift to coarser sediments suggests a significant strengthening of the bottom currents along the continental slope off north Morocco starting during the last glacial termination and persisting until the Early Holocene (e.g., Fink et al., 2013; Lo Iacono et al., 2014; Stalder et al., 2015; 2018; Wang et al., 2019). This turbulent hydrodynamic regime also supported the most recent major coral mound formation stage in the southern Alboran Sea (in the EMCP and the neighboring West Melilla coral mound province), even though this started with some delay during the Bølling-Allerød and lasted until the Early Holocene (Fink et al., 2013; Stalder et al., 2015, 2018; Wang et al., 2019). It is suggested that mound formation in the southern Alboran Sea became (re-)activated as soon as the mounds got into the influence of internal waves that developed along the pycnocline between the Modified Atlantic Water and the underlying Levantine Intermediate Water and caused a further enhancement of the turbulence at mid-depths as well as an enrichment and increased lateral transport of food particles towards the CWCs (Wang et al. 2019).

In contrast to the off-mound area, the matrix sediments deposited on-mound (GeoB13729-1) during the Early Holocene mound formation period showed a homogenous and significantly different grain-size-distribution pattern with a dominant fine mode at ~7 Φ (8 µm) and a ~31 vol.%-enrichment of the fine fraction relative to the simultaneously deposited off-mound deposits (Fig. 4-3). This fine mode of the siliciclastic fraction suggests rather calm hydrodynamic conditions locally prevailing on-mound that allowed even the fine fraction of the suspended sediments to settle, and is at first glance in conflict with the concurrently deposited coarse off-mound sediments that suggest regionally enhanced current velocities. Additionally, the on-mound deposition of dominantly fine sediments also contradicts with the common sense that positive topographies such a coral mound tend to accelerate bottom current velocities, preventing the fine sediment from deposition (e.g., Cyr et al., 2016).

The paradox between fine sediment deposition on-mound and the strong background hydrodynamics (large-scale hydrodynamic process) as well as the nature of the mound's positive topography (medium-scale hydrodynamic process) highlights the efficiency of the coral framework to baffle fine sediments (small-scale hydrodynamic process) and to act as a sediment trap. The baffling effect is defined as the capability of CWCs with a branching skeleton to considerably reduce the velocity of bypassing bottom waters (e.g., Guihen et al., 2013)that allows the current-transported sediments to settle even under highly turbulent background conditions (e.g., Ginsburg and Lowenstam, 1958; Flügel, 2004; Titschack et al., 2009). In particular, large and densely distributed coral frameworks baffle effectively bypassing sediments by reducing remarkably the current velocity between their branches. The resultant low-energy conditions on-mound even favor the deposition of the fine sediment (Fig. 4-4). This interpretation is supported by flume tank and modeling studies that highlight the remarkable surface roughness of branching corals with large bottom drag coefficients (Monismith, 2007), which significantly slows down bypassing currents, both on colony- and reef-scale (e.g., Chang et al., 2009; Guihen et al., 2013; Johansen, 2014; Lowe and Falter, 2015; Mienis et al., 2019).

The efficient baffling of coral frameworks might even contribute to the fast aggradation of coral mounds. Our records indeed show very high on-mound average Acc_{Silic} (83.5 to 323.4 g $cm^{-2}kyr^{-1}$) during the entire mound formation period, which are about ~8-30 times higher than on the adjacent seafloor (10.8 g $cm^{-2}kyr^{-1}$). With a roughly constant baffling effect as reflected by the $\Sigma\Delta Content_{Fine}$ of ~31%, the extremely high siliciclastic accumulation on coral mounds calls for additional process of sediment delivery to coral mounds. During the mound formation, the occurrence of pycnocline tends to enrich the sediment, extending their residence time (e.g., Pomar et al., 2012). Concurrently, the propagating internal waves at the water mass boundary interact with the slopes causing strong bottom hydrodynamics. Therefore, the suspended and re-suspended sediments are delivered at the pycnocline and repeated flushing to the corals. This process probably strikingly enhanced the sediment delivery to the coral mounds, which is similar to the food delivery (e.g., Davies et al., 2009; Mienis et al., 2009a).
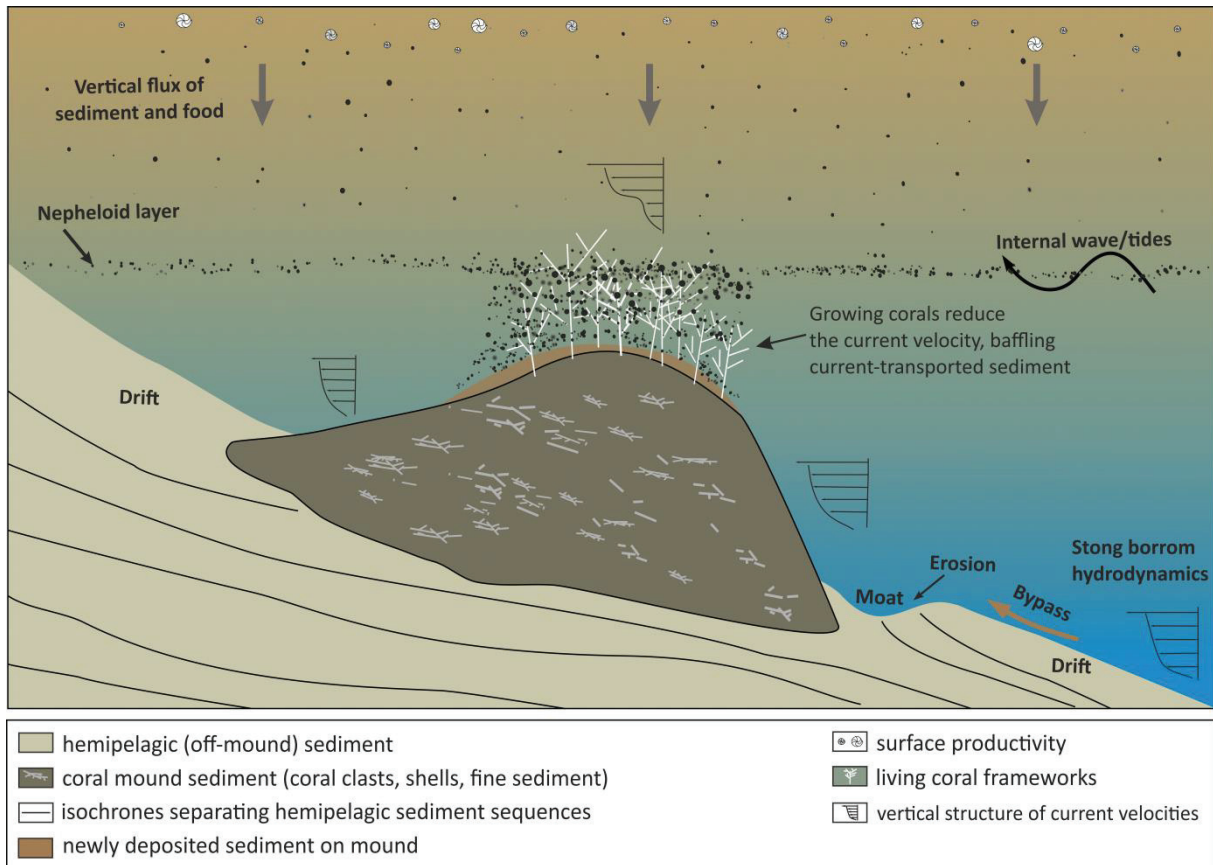
Figure. 4-4. Schematic plot showing the various hydrodynamic, sedimentological and biological processes being involved in cold-water coral mound formation. High primary productivity and strong bottom currents delivering food are a prerequisite for coral growth on top of a mound, while mound formation requires besides coral growth also the supply of sufficient sediments. Internal tides and waves occurring at the pycnocline of two water masses enhance the turbulence and increase the supply of food particles and sediments. Particulate material becomes enriched (forming nepheloid layers) and is laterally flushed through the coral framework, which favors coral growth and hence mound formation. In the off-mound area, strong bottom currents generate a bypass situation and prevent the deposition of (fine) sediments. Concurrently, the positive topography of the coral mound acting as an obstacle in the flow enhances bottom current velocities, which favors erosion at the current-exposed base of the mound resulting in the formation of a moat. On the contrary, due the baffling effect of the coral frameworks thriving on top of the mound, the bottom current velocities become significantly reduced, which allows even fine sediments to settle. In addition, the coral frameworks provide accommodation space for the deposition of sediments.

It might be speculated that the fine sediments deposited on-mound, while lacking in the off-mound area, have also a positive effect on the mound AR. This would implicate that the difference in grain-size distribution between the on- and the off-mound cores (ΔContent), particularly within the fine fraction (6-12 Φ; <16 μm), should positively correlate with the mound AR. However, our data show that the average $\Sigma\Delta$Content$_{Fine}$ (exhibiting values of ~31 vol.%) does not vary significantly (Fig. 4-3). Consequently, the rather stable $\Sigma\Delta$Content$_{Fine}$ clearly indicates that the capacity of the coral framework to baffle fine sediments is consistently high during the entire mound formation period despite varying ARs (124-589 cm kyr^{-1}; Table 4-2). This suggests that even though the baffling effect of coral frameworks represents an important prerequisite for coral mound formation, its impact on changes in mound AR seems to be rather limited, which is to some extent in conflict with former studies who

suggested that the baffling effect of coral framework plays a major role in this respect (e.g., Dorschel et al., 2007a; Titschack et al., 2009; Glogowski et al., 2015; Titschack et al., 2015; Stalder et al., 2018).

In addition, our results clearly demonstrate that also the CWC content of the mound deposits cannot be used to directly assess changes in the AR. At first glance, it might be assumed that high CWC contents reflect high AR. However, our data show that CWC contents are rather low (<40 wt.%) during the phase of fastest mound aggradation (AR: 589 cm kyr^{-1}) and rather high (at ~40 wt.%) when the AR is reduced (<200 cm kyr^{-1}; Fig. 4-2), a pattern that was also found in other studies in the NE Atlantic and Mediterranean Sea (Titschack et al., 2009; 2015; 2016; Wang et al., 2019). This pattern can be explained by the preservation of the coral frameworks, which is clearly controlled by the sediment supply. During times of low sediment supply, the frameworks remain exposed and become subject to strong biodegradation and fragmentation resulting in coral rubble deposits (high coral content), while a high sediment supply causes a fast burial of the (dead portion of the) coral frameworks, preventing biodegradation and preserving the frameworks in life position (low coral content) (Titschack et al., 2015; 2016; Wang et al., 2019). This is further supported by the on-mound AccSilic, which increases concurrently with the AR (Fig. 4-2), emphasizing the importance of high sediment supply for coral preservation, and hence, mound formation.

The baffling capacity of coral frameworks, which is defined as the amount of sediment that can be baffled by branching corals, does not just depend on to what extent the bottom current velocity is reduced under the influence of coral frameworks. Indeed, it is further dependent on the open space generated by the coral frameworks that allow the deposition of the baffled sediments in a sustainable way. Similar to CWC mounds, carbonate factories or depositional environments in shallow-water areas (e.g., rhodolith and maerl beds, shallow-water coral reefs; see Titschack et al., 2016) also influenced by strong hydrodynamics, while in turn biological processes, particularly the growth of the carbonate-producing organisms, alter these hydrodynamics by baffling and generate a low-energy ecological accommodation space for sediment deposition (Al-Awwad and Pomar, 2015; Pomar and Haq, 2016). Therefore, in analogue to the shallow-water carbonate systems, we term the accommodation space on a CWC mound CWC-derived ecological accommodation space (following the terminology of Pomar, 2001a; 2001b; see also Pomar and Kendall, 2008). The CWC-derived ecological accommodation space is predominantly controlled by the growth of the CWCs, thereby large and densely distributed coral frameworks provide much more ecological accommodation space compared to small colonies distributed in a rather scattered manner on the mound's surface (Figs. 4-5A, 4-5C).

Overall, it is anticipated that a high baffling capacity tends to cause more deposition of sediments on-mound as long as enough accommodation space is provided and the sediment supply is high (Fig. 4-5). Therefore, changes in mound AR are mainly controlled by the interplay between sediment supply and the CWC-derived ecological accommodation space defined by the dimension and density of coral

frameworks being present on the mound's surface. Hence, during periods of high sediment supply, large and densely distributed coral frameworks providing large accommodation space result in higher AR compared to small frameworks distributed in a scattered manner, which offer only a limited space for sediment deposition (Figs. 4-5B, 4-5C). On the contrary, a low sediment supply, not being sufficient to fill the CWC-derived large accommodation space, has a significant impact on the preservation of the coral frameworks as they become exposed to enhanced bioerosion. As a result, frameworks become increasingly degraded, resulting in the formation of coral rubble deposits, which on one hand increase the coral content in the final mound deposits, but on the other hand result in low AR (Fig. 4-5A).
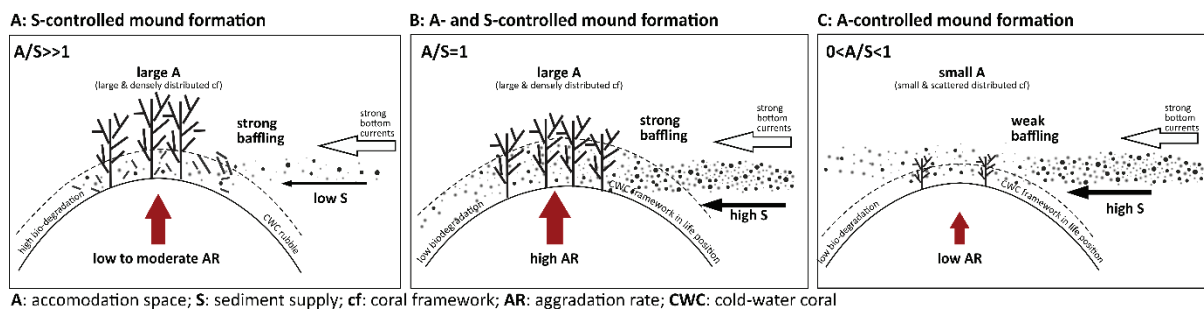

Figure. 4-5. Scheme showing three different scenarios of cold-water coral (CWC) mound formation and associated mound aggradation rates (ARs) resulting from the interplay between sediment supply (S) and the growth of framework-forming CWCs providing ecological accommodation space (A). A: The CWC-derived A exceeds S (A/S>>1). Large and densely distributed coral frameworks (cf) have a strong baffling effect and provide large A. As the S is too low to completely fill the CWC-derived A, the cf become exposed to biodegradation and fragmentation, which causes their collapse and the deposition of coral rubble (high CWC content in mound deposits). The associated AR is low to moderate and mainly controlled by S. B: The CWC-derived A is equal to S (A/S=1). Large and densely distributed cf have a strong baffling effect. Due to a high S, the large A provided by the cf become rapidly filled preventing biodegradation and preserving the cf in life position (low CWC content in mound deposits). The associated AR is high and controlled by A and S. C: The CWC-derived A is outpaced by S (0<A/S<1). Small cf distributed on the mound in a scattered manner provide only small A. The high S causes a complete filling of the CWC-derived A and fast burial of the cf, preventing them from biodegradation (low CWC content in mound deposits). Despite the high S, the associated mound AR is very low as it is mainly controlled by A.

In summary, we highlight in this study that (i) a high coral framework baffling capacity is an important prerequisite for coral mound formation, but that the interplay of (ii) the CWC-derived ecological accommodation space controlled by the height/dimension of the framework and (iii) the sediment supply are the key factors influencing changes in mound AR. Three major scenarios can be differentiated (Fig. 4-5):

i: The CWC-derived ecological accommodation space considerably exceeds the amount of supplied sediments (A/S>>1; Fig. 4-5A). The fast and sustained growth of CWCs forming large, densely distributed frameworks maximizes the baffling effect and the on-mound deposition of current-transported sediments. As the sediment supply is low, a large part of the CWC-derived accommodation space remains unfilled and part of (the dead portion of) the coral frameworks exposed to prolonged biodegradation and fragmentation. This eventually causes the collapse of the coral framework and the deposition of coral rubble, which results in a high coral content within the mound

deposits. The coral mound AR under this scenario is low to moderate and mainly controlled by the sediment supply.

ii: The CWC-derived ecological accommodation space is equal to the amount of supplied sediments (A/S=1; Fig. 4-5B). The fast and sustained growth of corals forming large and densely distributed frameworks maximizes the baffling effect and the on-mound deposition of current-transported sediments. The sediment supply is constantly high and the CWC-derived accommodation space becomes rapidly and completely filled. The coral frameworks become buried preventing them from biodegradation and fragmentation and preserving them in live position, which results in a low coral content within the mound deposits. The coral mound AR is very high (>100 and up to >1000 cm kyr^{-1}) and controlled by both the CWC-derived accommodation space and the sediment supply.

iii: The CWC-derived ecological accommodation space is outpaced by the amount of supplied sediments (0<A/S<1; Fig. 4-5C). The corals are slowly growing and form small frameworks that are distributed in a scattered manner on the mound's surface. The baffling effect is weak and the corals provide a rather small accommodation space. The sediment supply is very high and the coral frameworks become soon buried preventing them from biodegradation and fragmentation, causing (comparable to scenario 1) a low coral content in the mound deposits. However, despite the high sediment supply, the CWC mound AR is very low (<10 cm kyr^{-1}), as under this scenario, mound formation is mainly controlled by the CWC-derived accommodation space.

The linear grow rates of the common mound-forming species *Lophelia pertusa* is 5-34 mm yr^{-1} (Roberts, 2002; Gass and Roberts, 2006) and *Madrepora oculata* is 5-7 mm yr^{-1} (Orejas et al., 2011). These growth rates are much higher than SRs along continental margins, which are in the magnitude of tens of millimeters per thousand years (Hebbeln et al., 2016 and references therein), sediment deposition outpacing the growth of the corals and causing their burial during their prolific life span is rather unlikely – even though frequently mentioned in the literature as potential limiting factor (White et al., 2005; Freiwald et al., 2009; Mienis et al., 2012; Sánchez et al., 2014).

4.5. Conclusion

CWC mounds are formed due to the complex interplay between coral growth and sediment deposition. It is believed that the baffling capacity of coral frameworks, i.e., the amount of sediment that can be deposited on-mound due to their baffling effect and the accommodation space they provide, accounts for high on-mound sediment accumulation and finally causes fast mound aggradation. It on one hand changes the hydrodynamics generating ecological accommodation space for sediment deposition even under the influence of strong bottom hydrodynamics, on the other hand controls the pattern of grain-size distribution.

Our results reveal different patterns of sediment grain-size distribution from the continental slope and coral mounds during mound formation. While in the off-mound area, coarse sediments with major mode of 4 Φ (63 μm) imply highly dynamic conditions, the on-mound deposition of siliciclastic sediments is characterized by fine sediments with mode of 7 Φ (8 μm), suggesting low-energy hydrodynamics. The rather calm hydrodynamics prevailing in the coral mound environment results from the baffling of coral frameworks, which generate ecological accommodation space favoring the deposition of suspending sediment. Thereby, the averaged total enhancement of the siliciclastic sediment in fine fraction ($\Sigma\Delta\text{Content}_{Fine}$) is ~31 vol.% and constant throughout the period of mound formation, indicating that the baffling capacity was most likely maximized. Therefore, the obtained extremely high on-mound accumulation rate of siliciclastic sediment, up to ~323.4 g cm^{-2} kyr^{-1} and about 30-fold greater than that of the adjacent seafloor (average: ~10.8 g cm^{-2}kyr^{-1}), is due to the enhanced horizontal delivery of sediment by internal waves. Concomitantly, the coral content within the on-mound sediment was not positively correlated to the mound AR, highlighting the role of sediment supply in filling the coral-generated ecological accommodation space. In summary, our result suggests that the baffling capacity is prerequisite of coral mound formation, and the coral mound aggradation is mainly controlled by the interplay between coral-derived ecological accommodation space and sediment supply.

Acknowledgement

Chapter 5

Sea level change-related formation of cold-water coral mounds since the last interglacial in the southern Alboran Sea

Haozhuang Wang[a], Dierk Hebbeln [a], Jürgen Titschack [a, b], Claudia Wienberg [a]

a Center for Marine Environmental Sciences (MARUM), Bremen University, Leobener Strasse 2, 28359 Bremen, Germany

b Senckenberg am Meer (SAM), Marine Research Department, Südstrand 40, 26382 Wilhelmshaven, Germany

Abstract

In the Mediterranean Sea, the most impressive cold-water coral (CWC) mounds are found in the southern Alboran Sea, specifically in the East Melilla CWC mound province (EMCP). There, coral mounds are arranged into four sub-clusters displaying specific shapes, with each sub-cluster being aligned with a specific water depth level. So far, coral mound formation only has been investigated for the westernmost and the northern sub-clusters of the EMCP, covering the last 14 kyrs. In this context, here we reconstruct the history of coral mound development in the unexplored central and southern sub-clusters and provide for the first time evidence for coral mound formation in the Mediterranean Sea prior to the last deglaciation. In the central sub-cluster, two age clusters of 78.0-72.2 kyr BP and 13.9-11.7 kyr BP represent remarkable mound formation, with respective mound aggradation rates (AR) of 67 and 216 cm kyr^{-1}. In the southern sub-cluster, U/Th dating of corals document coral growth between 121.8 to 106.3 kyr BP with enhanced mound aggradation of 240 cm kyr^{-1} from 114.5 to 110.6 kyr BP. Coral mound formation corresponds with the presence of strong bottom water hydrodynamics, a common precondition for cold-water coral growth through enhancing the lateral food supply. These enhanced dynamics were most likely caused by internal tides developing along the water mass interface between the Levantine Intermediate Water (LIW) and the Modified Atlantic Water (MAW). Placing the coral mounds within the reach of these internal tides appears to be controlled by the position of the relative sea level, which, thus, exerts a dominant first order control on coral mound formation in the Alboran Sea.

5.1 Introduction

Cold-water coral (CWC) mounds are widely distributed along continental margins (Hebbeln and Samankassou, 2015; Wienberg and Titschack, 2017). Over geological time scales such coral mounds can grow up to several hundred meters in millions of years (Mienis et al., 2006; Kano et al., 2007). These coral mounds predominantly consist of fragments of scleractinian reef-forming CWCs and hemipelagic sediment, with a dominance of the latter component (White et al., 2005; Titschack et al., 2015; Titschack et al., 2016). Therefore, coral mounds, can serve as excellent archives of coral growth and mound formation, as well as of associated paleoceanographic changes.

Past decades have witnessed a great advance in our understanding of CWC mounds. Mostly, they occur as impressive mound clusters (also termed as CWC mound provinces), comprising hundreds of individual mounds covering up to thousands of square kilometers (e.g., Wheeler et al., 2007; Hebbeln et al., 2014; Ramos et al., 2017; Hebbeln et al., 2019). Often, coral mounds are arranged into several belts of mound clusters parallel to the isobaths of the continental slope (e.g., De Mol et al., 2002; Hebbeln et al., 2014; Wienberg et al., 2018; 2019). A closer look at individual mounds revealed different dimensions and morphologies, with the latter ranging from conical, elliptical, elongated to even ridge-like shapes. The conical or elliptical mounds usually have diameters of up to a few kilometers, elongated or ridge-like mounds can reach lengths up to tens of kilometers, and widths of several hundred meters (Wheeler et al., 2007; Hebbeln et al., 2014; Wienberg et al., 2018; Hebbeln et al., 2019). Most likely, variations in mound morphologies result from the different local hydrodynamic regimes (Correa et al., 2012a; Hebbeln et al., 2019).

Since CWCs play a key role in mound formation, most studies exploiting the mound archive mainly focused on the development of the corals in the past. Studies in the North Atlantic and the associated marginal seas revealed that over the last three glacial-interglacial cycles coral growth over are controlled by environmental conditions, with on- and offsets of coral growth having been paced by glacial/interglacial climate variability (e.g., Dorschel et al., 2005; Rüggeberg et al., 2007; Frank et al., 2009; Wienberg et al., 2010; Frank et al., 2011; López Correa et al., 2012; van der Land et al., 2014; Matos et al., 2015; Bonneau et al., 2018). The most important factor driving coral growth and mound formation presently and in the past was food supply to the corals resulting from either enhanced surface ocean productivity for the vertical or strong bottom water hydrodynamics for the lateral food supply or a combination of both (White and Dorschel, 2010; Wienberg et al., 2010; Raddatz et al., 2014; Hebbeln et al., 2016; Matos et al., 2017; Wang et al., 2019). As a key factor enhancing bottom water hydrodynamics and subsequent lateral food supply to the corals, internal waves developing along water mass boundaries have been identified (e.g., Mienis et al., 2007; Orejas et al., 2009; Hebbeln et al., 2014). In addition, in highly productive areas, oxygen minimum zones in the water column can hamper coral growth despite high food availability (Fink et al., 2015; Wienberg et al., 2018; Hanz et al., 2019).

In the Mediterranean Sea, most known coral mounds were discovered in the southern Alboran Sea close the Spanish enclave Melilla (Fig. 5-1; Fink et al., 2013; Lo Iacono et al., 2014). The CWC mounds east of Melilla, i.e., within the East Melilla CWC mound province (EMCP), have been divided by their unique morphologies initially into three sub-clusters, which each one being most likely controlled by local topography and hydrodynamic conditions (Hebbeln et al., 2019) (Fig. 5-1). Former studies on the development of CWC mounds in the EMCP revealed quite similar mound development patterns marked by pronounced mound aggradation during the Bölling-Alleröd (B/A) interstadial and the Early Holocene (interrupted during the late Younger Dryas (YD) triggered by enhanced surface water productivity and energetic bottom water hydrodynamics (Fink et al., 2013; Stalder et al., 2015; Stalder et al., 2018; Wienberg, 2019). Since the Early Holocene, coral growth largely ceased and mound formation stagnated once the area became oligotrophic and the bottom water hydrodynamics weakened (Fink et al., 2013; Stalder et al., 2015; Stalder et al., 2018). Also for the southern Alboran Sea, an important impact of internal waves on CWC development has been suggested (Wang et al., 2019). However, all available studies on mound development within the EMCP are restricted to the northern and westernmost sub-clusters of the EMCP (Fink et al., 2013; Stalder et al., 2015; 2018) raising the question of how coral mounds in the morphologically very distinct central and southern sub-clusters of the EMCP developed.

Therefore, this study aims to reconstruct CWC mound development in these unexplored sub-clusters of the EMCP. Coral fragments from two so-called on-mound sediment cores from mounds in the central and southern sub-clusters have been dated to reveal the history of mound formation. Furthermore, this history has been put into a paleoceanographic context based on data obtained from a coral-barren core taken from the adjacent sea floor (i.e., an off-mound core). The data obtained allow the first assessment of coral growth in the central and southern EMCP and provide the first information about coral mound formation in this region prior to the last deglaciation.

5.2 Regional setting

The Alboran Sea in the westernmost Mediterranean Sea connects the Mediterranean Sea with the Atlantic Ocean. It is a narrow basin bordered by the Iberian Peninsula in the north and by the North African margin in the south (Fig. 5-1).
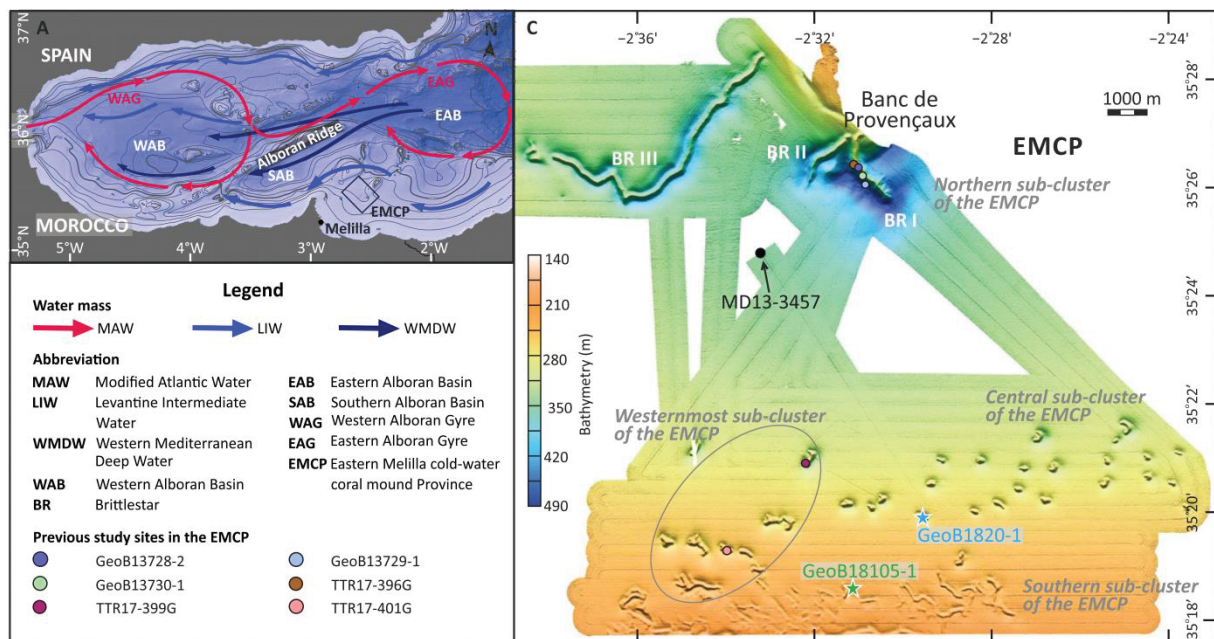
Figure. 5-1. A: Bathymetry map of the Alboran Sea, west Mediterranean Sea, with the modern circulation pattern (Millot, 1999, 2009). EMODnet Digital Bathymetry, http://doi.org/10.12770/c7b53704-999d-4721-bla3-04ec60c87238). B. Schematic map of the East Melilla cold-water coral mound province (EMCP) in the southeastern Alboran Sea (modified from Hebbeln, 2019). Sampling sites are indicated. The on-mound core GeoB18105-1 (green star) was collected from an unnamed ridge-shaped mound from the southernmost EMCP. The core GeoB18120-1 (blue star) was derived from the Mole Mound in the mid EMCP. The off-mound core MD13-3457 (black circle) was collected from the area between the northern and mid EMCP. Sediment core sites used for previous studies from this area (Fink et al., 2013; Stalder et al., 2015; Stalder et al., 2018) are also indicated.

5.2.1 Oceanography in the Alboran Sea

The Alboran Sea is characterized by three dominant water masses. At the surface, the Atlantic Water (AW) flows into the Alboran Sea through the Strait of Gibraltar. The eastward flowing AW meets the Mediterranean surface water and forms the Modified Atlantic Water (MAW) (Millot and Taupier-Letage, 2005). It flows eastward and extends to water depths of 150-200 m. At intermediate depth between 200 m and 600 m, the Levantine Intermediate Water (LIW) flows westward. It originates from the eastern Mediterranean Sea due to the sinking of dense surface waters during cold winters (Millot, 2009). Beneath the LIW, the Western Mediterranean Deep Water (WMDW), formed in the Gulf of Lions, flows westward at water depths of >600 m (Millot, 2009).

At present, the Alboran Sea is the most productive area in the entire Mediterranean Sea (D'Ortenzio and Ribera d'Alcalà 2009). The inflow of AW in the Alboran Sea forms a two-gyre-system, named as the West and East Alboran Gyres (WAG, and EAG), respectively (Arnone et al., 1990) (Fig. 5-1). At the northwestern WAG, coastal upwelling generates a high productive area (e.g., Ruiz et al., 2001). At the northeastern EAG, along the front between the MAW and the Mediterranean surface waters, the Almeria-Oran Zone forms another high productive area, known as the Almeria-Oran Front (AOF;

Lohrenz et al., 1988). In the northern Alboran Sea, internal waves were observed at ~250 m water depth (Van Haren, 2014), which would roughly align with the water mass interface between the LIW and the MAW.

5.2.2 East Melilla cold-water coral mound province

Based on varying mound morphologies and dimensions, Hebbeln (2019) described three E-W-trending belts stretching over ~25 km from the northern to the southern EMCP, with the westernmost central sub-cluster being here treated as an additional fourth sub-cluster distinct from the remaining central sub-cluster (Fig. 5-1). In the northern sub-cluster, zigzag-shaped ridges stretching from 3 km to nearly 20 km in length are discovered attached to the southern flank of volcanic Banc de Provençaux. The three steep ridges are named as Brittlestar I, II and III from the east to the west. These ridges are based at water depths between 475 and 375 m and reach ~50-150 m above the seafloor. More than 25 coral mounds with oval to arcuate shapes occur in water depths of 230-320 m and form the central sub-cluster. The lengths of the mounds amount up to few hundreds of meters, and their heights above the sea floor vary between 20 and 40 m resulting in steep flanks with angles of > 30°. From the east to the west, the mounds in this area gradually change from oval to ridge-like shapes. In the southern sub-cluster, a belt with ridge-like coral mounds was found at water depths of 200-240 m. These ridge-shaped mounds only reach ~10 m above the sea floor, exhibiting winded shapes mostly stretching in E-W direction. The ridges in this region are up to 5 km long. Towards the south, these coral ridges become gradually buried by sediments. In terms of morphology and dimension, coral mounds from the central and southern sub-clusters gradually meet in the west, forming the newly defined westernmost sub-cluster in which the mounds occur in water depths of ~ 230 m, displaying ridge-like shapes, mostly trending in NW-SE direction (Fig.5-1; Hebbeln, 2019).

5.3 Material and methods

Two of the three cores were collected from coral mounds (on-mound cores) in the central and southern sub-clusters of the EMCP, GeoB18120-1 and GeoB18105-1 (RV Maria S. Merian cruise MSM-36 "MoccoMebo"; Hebbeln et al., 2015). The third core, MD13-3457 (RV Marion Dufresne cruise MD194 "Gateway"-Eurofleets; Van Rooij et al., 2013), was collected from the adjacent seafloor (off-mound core) close to the site of short core GeoB13731-1 described by Fink et al. (2013). The on-mound cores GeoB18105-1 (water depth: 224 m) and GeoB18120-1 (water depth: 249 m) have recoveries of 571 and 1016 cm, respectively. The off-mound core MD13-3457 (water depth: 345 m) has a recovery of 2031 cm (Table 5-1).

Table 5-1. Metadata of gravity cores collected in the EMCP (southern Alboran Sea) during the cruise MSM-36 "MoccoMeBo" with the German RV Poseidon in 2015 (Hebbeln et al., 2015) and the cruise MD194 "Gateway"-Eurofleets with the French RV Marion Dufresne in 2013.

Core Type	Core ID	Latitude [N]	Longitude [W]	Water depth [m]	Recovery [cm]
On-mound	GeoB18120-1	35°19.88′	2°29.60′	249	1016
	GeoB18105-1	35°18.44′	2°31.32′	224	571
Off-mound	MD13-3457	35°24.80′	2°33.22′	345	2031

5.3.1 On-mound cores analyses

The on-mound cores mainly consist of coral fragments embedded in hemipelagic sediments. They were firstly frozen for 24 hours. Afterwards, these cores were opened while frozen with a diamond stone saw to keep the internal structures intact.

5.3.1.1 Uranium-thorium (U/Th) dating

Twenty-five coral fragments (*Madrepora oculata* and *Lophelia pertusa*) were selected from the cores GeoB18105-1 (ten samples) and GeoB18120-1 (fifteen samples) for U/Th dating. Prior to the analyses, all coral fragments were mechanically cleaned with an air-pump-saw following the procedure described by Frank et al. (2004). For the dating, a ThermoFisher iCAP-Qs inductively coupled plasma mass spectrometer (ICP-MA) at the Institute of Environmental Physics at Heidelberg University (IUP), Germany, was used. The reproducibility of the measurements was assessed by using the international uranium standard material HU1 (Cheng et al., 2000a; Frank et al., 2004; Wefing et al., 2017). All the ages are reported in kyr BP (Table 5-2). Thereafter, for both cores the mound aggradation rates (ARs) were calculated using linear interpolation between the dated depths (Table 5-2).

5.3.2 Off-mound core analyses

5.3.2.1 Radiocarbon dating

A total of eight samples of mixed planktonic foraminifera were selected for radiocarbon dating. For each sample, more than 15 mg of planktonic foraminifera of > 150 μm were picked for accelerator mass spectrometry (AMS) radiocarbon (^{14}C) dating. The analyses were performed at the Poznan Radiocarbon Laboratory, Poznan, Poland. The obtained data were corrected for ^{13}C and a mean ocean reservoir age of 400 years was used. The ages in calendar years (kiloyears before present, kyr BP, present = 1950 CE) were obtained by converting the data with the MARINE 13 curve (Reimer et al., 2013) using the CALIB 7.10 software (Stuiver and Reimer, 1993; http://calib.org/calib/calib.html).

5.3.2.2 Benthic foraminifera stable oxygen and carbon isotopes

The stable oxygen ($\delta^{18}O$) and carbon ($\delta^{13}C$) isotope composition of the epi-benthic foraminifera *Cibicidoides mundulus* was analyzed on ~10 specimen collected from the > 150 µm fraction in 5-cm downcore resolution with a Finnigan MAT 252 gas isotope ratio mass spectrometer connected to Kiel II automated carbonate preparation device at the MARUM, University of Bremen, Germany. The analyses were based on the CO_2 evolved from the reaction between phosphoric acid and carbonate at a constant temperature of 75 °C. The internal standard was ground Solnhofen limestone, which has been calibrated to the Vienna Pee Dee belemnite (V-PDB) with the NBS 19 standard. The data are reported relative to the V-PDB standard. The standard deviation of the $\delta^{18}O$ and $\delta^{13}C$ analyses is ±0.09‰ and ±0.04‰, respectively. The $\delta^{18}O$ data are used to establish the age model for the off-mound core, and the $\delta^{13}C$ are used as a water mass indicator (e.g., Wang et al. 2019)

5.3.2.3 Grain size measurement

The terrigenous fraction of the sediment was used for grain size measurements, with a sampling resolution of 10 cm. Before the analyses, the biogenic components were removed with 10 ml of H_2O_2 (30%; until the reaction stopped), 10 ml of HCl (10%; 1 min) and 6 g NaOH pellets (10 min) following the method of McGregor et al. (2009). To avoid the potential influence of particles and air bubbles in the water, during the whole process, deionized, degassed and filtered water (filtered with mesh size: 0.2 µm), was utilized. The measurement was performed using a Beckman Coulter Laser Diffraction Particle Size Analyzer LS 13320 at the Particle-Size Laboratory, MARUM, University of Bremen, Germany. For each sample, the grain-size distribution from 0.04 to 2000 µm is provided. The corresponding statistic values are based on a geometric statistic. In this study, we use the mean grain size as a proxy for bottom current velocity as it has been done before in this region (e.g., Fink et al., 2013; Wang et al., 2019).

5.3.2.4 X-ray fluorescence scanning

To obtain information about the elemental composition of the sediment, the off-mound core MD13-3457 was scanned with the XRF Core Scanner II (AVAATECH Serial No. 12) at the MARUM, University of Bremen, in 2 cm resolution. Prior to the scanning, the split core surface was covered with a 4 micron thin SPEXCerti Prep Ultralene1 foil to avoid contamination of the XRF measurement unit and desiccation of the sediment. The XRF Core Scanner data were collected in two runs using generator settings of 10 kV (for Al, Si, S, K, Ca, Ti, Mn, Fe) and 30kV (for Br, Sr, Rb, Zr), currents of 0.2 mA and 1 mA, and sampling times of 20 seconds directly at the split core surface. The here reported data have been acquired by a Canberra X-PIPS Silicon Drift Detector (SDD; Model SXD 15C-150-500) with 150 eV X-ray resolution, the Canberra Digital Spectrum Analyzer DAS 1000, and an Oxford Instruments 50 W XTF5011 X-Ray tube with rhodium (Rh) target material. Raw data spectra were processed by the analysis of X-ray spectra by Iterative Least square software (WIN AXIL)

package from Canberra Eurisys. Here, only the Ca/(Ca+Fe) ratio, as a rough paleoproductivity indicator (e.g., Fink et al., 2013), and the Mn content (% of all counts), as a proxy for the oxidation state at the seabed (e.g., Calvert and Pedersen, 2007; Martinez-Ruiz et al., 2015), are presented.

5.4 Results

5.4.1 On-mound core record

5.4.1.1 Cold-water coral ages and mound aggradation rate since the last interglacial
All U/Th datings reveal initial $\delta^{234}U$ values in the range of 146.8±10‰ close to modern seawater (Table 5-2; Andersen et al., 2010), and, therefore, are considered reliable. For core GeoB18120-1, the obtained fifteen CWC ages range between 78.0 and 4.7 kyr BP, with five ages (78.0-71.5 kyr BP) corresponding to MIS 5a, one age (52.8 kyr BP) to MIS 3, eight ages (13.9-11.7 kyr BP) to the last deglaciation, and one single age (4.7 kyr BP) to the Mid Holocene (Table 5-2; Fig. 5-2). The two MIS 5a ages of 78.0 kyr BP (core depth: 1013 cm and 859.5 cm), and 72.2 kyr BP and 71.5 kyr BP (core depth: 623 cm and 635 cm) are very close to each other. For MIS 3 only one age of 52.8 kyr BP was obtained. The last deglaciation ages cluster in two ranges: 13.9-13.4 kyr BP (core depths: 534-366.5 cm) and 12.5-12.4 kyr BP (core depths: 176.5-114 cm). For each age cluster, the obtained coral ages overlap within their errors or are very close to each other. The resulting average mound ARs for the age clusters amount to 67 cm kyr^{-1} for MIS 5a (AR range: 47-86 cm kyr^{-1}) and to 216 cm kyr^{-1} for the last deglaciation (Fig. 5-2).

For core GeoB18105-1, the obtained ten CWC ages range from 121.8 to 106.3 kyr BP, with two ages (121.8 kyr BP and 118.4 kyr BP) corresponding to Marine Isotope Stage (MIS) 5e, seven ages (114.5-110.6 kyr BP) corresponding to MIS 5d, and one age (106.3 kyr BP) corresponding to MIS 5c (Table 5-2; Fig. 5-2). The three ages in the range of 121.8-114.5 kyr BP are older than those deeper in the core and form a distinct package between 249.5-176.5 cm core depths. Thus, only the ages above and below this package were used to calculate AR. Although the four coral ages ranging from 111.2 kyr BP to 112.3 kyr BP (core depth: 565-302.5 cm) overlap within their error ranges, considering the oldest age at the base and the youngest at the top of this core interval, a AR of 240 cm kyr^{-1} can be calculated. For the uppermost section of the core, no ARs have been calculated due to the occurrence of possibly reworked corals.

Table 5-2. U/Th dates, uranium and thorium isotope concentrations and ratios obtained from CWC fragments collected from the on-mound cores GeoB18120-1 and GeoB18105-1. Coral mound aggradation rates (ARs) are calculated based on a linear interpolation of the coral ages.

Core ID [GeoB]	Core Depth [cm]	Lab-code [IUP-]	Coral Species	Age [kyr BP]	± [kyr]	^{238}U [ppm]	± [ppm]	^{232}Th [ppb]	± [ppb]	δ^{234}U$_0$ [‰]	error	AR [cm kyr^{-1}]
18120-1	18.5	9660	M. oculata	4.71	0.015	3.97379	0.00010	0.22609	0.00060	148.56	0.46	6.5
18120-1	64	9661	M. oculata	11.68	0.034	3.82411	0.00007	0.10256	0.00018	148.79	0.47	
18120-1	114	9662	L. pertusa	12.47	0.029	3.75425	0.00010	0.26755	0.00043	148.29	0.50	
18120-1	134	9663	L. pertusa	12.39	0.032	3.52376	0.00010	0.41536	0.00078	149.02	0.44	
18120-1	176.5	9664	L. pertusa	12.39	0.039	3.55363	0.00009	0.56418	0.00094	148.82	0.50	216.0
18120-1	366.5	9665	L. pertusa	13.35	0.033	3.20746	0.00010	0.16559	0.00032	149.68	0.46	
18120-1	456.5	9666	L. pertusa	13.37	0.033	3.67551	0.00010	0.30440	0.00048	149.46	0.52	
18120-1	466	9667	L. pertusa	13.27	0.035	3.74078	0.00010	0.05291	0.00014	148.92	0.49	
18120-1	534	9668	L. pertusa	13.85	0.042	3.04562	0.00009	0.13565	0.00032	150.38	0.65	
18120-1	555	9669	L. pertusa	52.82	0.11	3.03420	0.00008	0.16097	0.00028	144.62	0.57	0.5
18120-1	623	9670	L. pertusa	72.23	0.19	2.72166	0.00007	0.21414	0.00043	140.88	0.65	3.5
18120-1	635	9671	L. pertusa	71.49	0.21	3.15141	0.00008	0.14236	0.00029	139.76	0.55	47.3
18120-1	754	9672	M. oculata	75.00	0.21	3.62813	0.00010	0.14294	0.00037	140.14	0.64	-
18120-1	859.5	9673	M. oculata	78.01	0.22	3.39076	0.00011	0.08538	0.00029	141.15	0.69	86.0
18120-1	1013	9674	M. oculata	78.01	0.25	2.95216	0.00009	0.07352	0.00023	142.15	0.68	
18105-1	44	9675	M. oculata	106.27	0.41	3.24843	0.00013	0.29877	0.00098	146.38	0.88	-
18105-1	50	9676	M. oculata	110.60	0.36	3.34451	0.00011	0.06923	0.00036	146.61	0.88	-
18105-1	119	9677	M. oculata	111.84	0.38	3.75647	0.00012	0.16142	0.00048	146.45	0.62	-
18105-1	176.5	9678	M. oculata	*114.51	0.44	3.22468	0.00010	0.21010	0.00046	146.93	0.82	-
18105-1	204	9679	M. oculata	*121.79	0.40	3.21831	0.00009	0.4346	0.0010	151.31	0.77	-
18105-1	249.5	9680	M. oculata	*118.43	0.46	3.49797	0.00010	0.32635	0.00062	149.69	0.90	-
18105-1	302.5	9681	M. oculata	111.24	0.36	3.14450	0.00009	0.17851	0.00058	146.26	0.79	
18105-1	328	9682	M. oculata	112.23	0.38	3.31544	0.00011	0.17030	0.00043	146.86	0.72	240
18105-1	414.5	9683	M. oculata	111.60	0.28	3.25027	0.00013	0.16802	0.00040	147.29	0.57	
18105-1	565	9684	M. oculata	112.34	0.33	3.69792	0.00014	0.25514	0.00051	146.39	0.73	

*: Age reversals. Ages in italic are not used for the calculation of coral mound AR. See text for explanation. The measured initial δ^{234}U values are in the range of 146±10‰ in comparison to the modern seawater (Anderson et al., 2010). These data obtained from the two cores, therefore, are redliable.
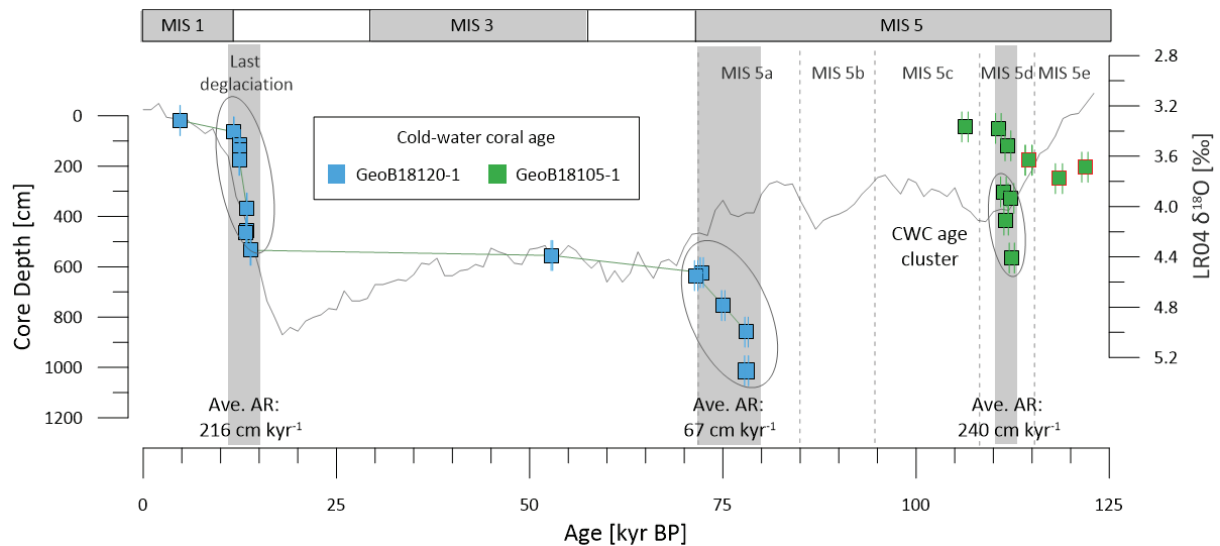
Figure. 5-2. Coral ages and corresponding mound aggradation rates (AR) from on-mound cores GeoB18120-1 (blue squares) and GeoB18105-1 (green squares) from the East Melilla cold-water coral mound province (EMCP). For core GeoB18120-1, two main age clusters were obtained, suggesting pronounced coral growth and mound formation (highlighted by ovals) during the marine isotope stage (MIS) 5a and the last deglaciation. The corresponding average coral mound aggradation rate (AR) amounts to 67 and 216 cm kyr^{-1}, respectively. For core GeoB18105-1, coral ages cluster in MIS 5d, indicating remarkable coral growth and associated mound formation (highlighted by oval) with high mound AR of 240 cm kyr^{-1} for the lower section of the core (112.3-111.2 kyr BP). Age reversals are indicated as green squares bounded by red lines. The thin grey line represents to LR04 Global benthic $\delta^{18}O$ stack of Lisiecki and Raymo (2005). The scheme of the MIS 5 substages is according to Railsback et al. (2015)

5.4.2 Off-mound core record

5.4.2.1 Chronology

The age model of core MD13-3457 is based on eight AMS ^{14}C ages, ranging from 0.4 kyr BP to 35.3 kyr BP, supported by seven tie points resulting from the comparison of the $\delta^{18}O_{Cib}$ record with the LR04 $\delta^{18}O$ stack (Lisiecki and Raymo, 2005; Table 5-3; Fig. 5-3). The $\delta^{18}O_{Cib}$ record ranges between of 4.4‰ and 1.1‰ revealing a glacial-interglacial offset of >3‰. According to the correlation to the LR04 stack, the core represents the last ~129 kyr (Fig. 5-3) with sedimentation rates in the range of ~5-44 cm kyr^{-1}. The sedimentation rate during the MIS 5e and 5d is high, showing values of ~25 cm kyr^{-1}. During MIS 5c, 5b and 5a, relatively low sedimentation rates in the range of ~8-12 cm kyr^{-1} are obtained. During the last glacial period, sedimentation rates fluctuate in the range of ~5-28 cm kyr^{-1}. Since the last deglaciation, the sedimentation rate increases from ~8 cm kyr^{-1} (the last deglaciation) to 44 cm kyr^{-1} (since the Mid Holocene) (Fig. 5-3).

Table 5-3. AMS ^{14}C dates of mixed planktonic foraminifers obtained from the off-mound core MD13-3457. The ages were corrected for ^{13}C using a reservoir age of 400 years. The calendar age (kiloyears before present, kyr BP, P=1950 CE) were obtained by converting the ages with the web-based CALIB 7.10 (Stuiver and Reimer, 1993; http://calib.org/calib/calib.html), using the MARINE-13 curve (Reimer et al., 2013). At the core depths of 448-803 cm, the age model is based on visual tie-point correlation between the δ^{18}O record of core GeoB18121-1 and the LR04 δ^{18}O stack record (Lisiecki and Raymo, 2005). Sedimentation rates are calculated based on a linear interpolation of the AMS ^{14}C dates and tie points

Core ID	Core Depth [cm]	Lab-code	Conventional Age [kyr]		2σ range cal. age [cal kyr BP P=AD 1950]		Median Probability Age [cal kyr BP]	Sedimentation Rate [cm kyr^{-1}]
			^{14}C age	± error				
MD13-3457	3	Poz-72322	0.75	0.03	0.305	0.463	0.4	-
MD13-3457	303	Poz-72323	6.67	0.05	7.104	7.340	7.2	43.9
MD13-3457	338	Poz-72324	8.59	0.05	9.085	9.394	9.2	17.5
MD13-3457	373	Poz-77253	10.54	0.06	11.407	12.024	11.8	13.7
MD13-3457	403	Poz-72325	13.47	0.08	15.329	15.931	15.7	7.7
MD13-3457	453	Poz-72326	22.51	0.15	25.973	26.731	26.3	4.7
MD13-3457	538	Poz-77254	22.37	0.40	25.528	27.182	*26.3*	-
MD13-3457	708	Poz-77255	31.80	0.50	34.371	36.287	35.3	28.4

Core ID	Core Depth [cm]		Tie-Point Age [kyr BP]	Sedimentation Rate [cm kyr^{-1}]
MD13-3457	1038		58	14.5
MD13-3457	1228	Tie points to the LR04 δ^{18}O stack record (Lisiecki & Raymo, 2005)	70	15.8
MD13-3457	1308		85	5.3
MD13-3457	1378		91	11.7
MD13-3457	1518		108	18.2
MD13-3457	1688		115	24.3
MD13-3457	2028		127	28.3

Ages in italic are not used for the calculation of sedimentation rate.

5.4.2.2 Paleo-environmental proxies
Stable carbon isotopes

The δ^{13}C$_{Cib}$ record ranges from -0.72‰ to 1.20‰ (Fig. 5-4). During the last interglacial, the δ^{13}C$_{Cib}$ shows several step-wise increasing trends, with values rising from ~0.19‰ to ~0.50‰ between 120 and 110 kyr BP (MIS 5e-5c), from -0.13‰ to ~0.96‰ between 100 and 86 kyr BP (MIS 5c-5b), and from~0.55‰ to ~1.11‰ between 84 and 60 kyr BP (MIS 5a-early MIS 4). During the last glacial, the δ^{13}C$_{Cib}$ is relatively heavy, oscillating between 0.31‰ and 1.20‰. It decreases from ~0.93‰ to ~0.49‰ during the last deglaciation. Since the Holocene, the δ^{13}C$_{Cib}$ values is low and relatively stable, fluctuating between -0.05‰ and 0.68‰ (Fig. 5-4).

Mean grain size

The mean grain size ranges between 3.9 and 30.4 μm. During extensive periods of the last 127 kyr, the sediments are rather fine with mean grain sizes of <8 μm (Fig. 5-4). It is slightly enhanced during MIS

5d reaching almost 10 µm. Significantly coarser sediments with mean grain sizes of >20 µm have been deposited only during the transition from MIS 5c to MIS 5b, mid 5a and early-to-mid MIS 3 (Fig. 5-4). During the last deglaciation, the mean grain size increased again to >18 µm (Fig. 5-4).
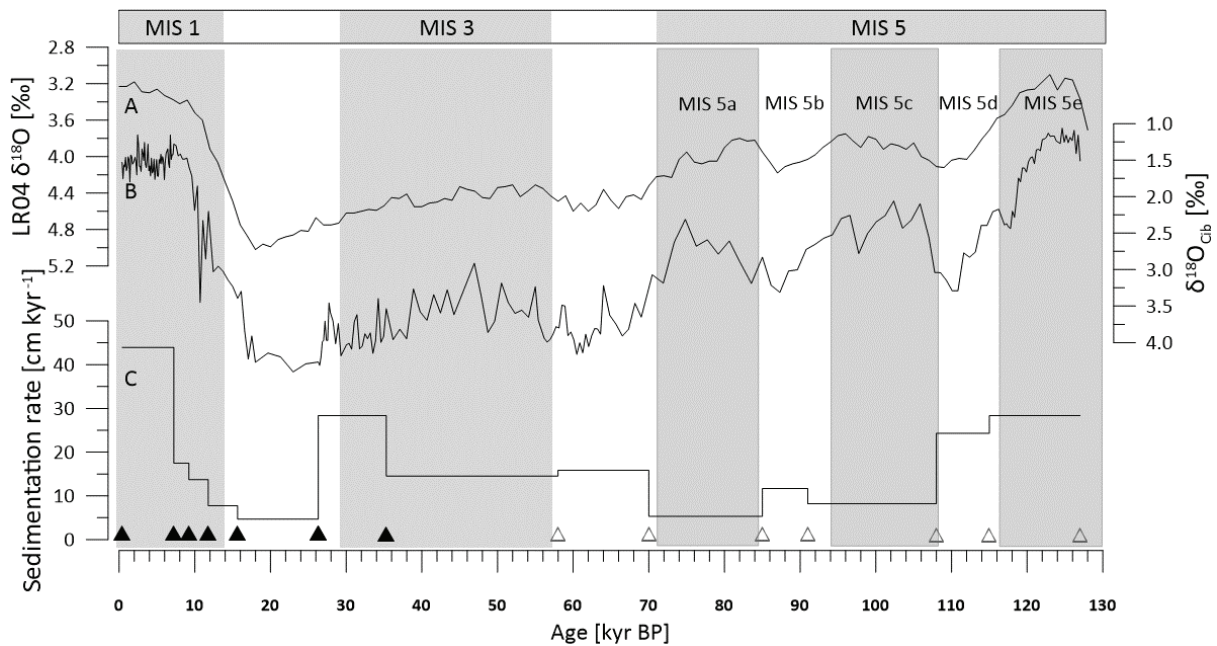

Figure. 5-3. Age model of the off-mound core MD13-3457 from the East Melilla cold-water coral mound province (EMCP). A: LR04 global benthic $\delta^{18}O$ stack (grey line; Lisiecki and Raymo, 2005). B:Stable oxygen isotopes ($\delta^{18}O$) obtained from the benthic foraminifera *Cibicidoides mundulus*. C: Calculated sedimentation rate. Black filled triangles represent the seven AMS ^{14}C ages. Open triangles mark tie points obtained by comparing the $\delta^{18}O_{Cib}$ record with the LR04 stack (Lisieck and Raymo, 2005). MIS: Marine Isotope Stages. Scheme of the MIS 5 substages is according to Railsback et al. (2015).

XRF scanning

The Ca/(Ca+Fe) ratio ranges between 0.65 and 0.86 while the relative Mn content (given as Mn counts as percentage off the total counts) ranges between 0.13 % and 0.27 % (based on the 15-point-running average) (Fig. 5-4). Both records show a cyclic behaviour with high Ca/(Ca+Fe) ratios roughly corresponding to low Mn contents (Fig. 5-4).

5.5 Discussion

In the Mediterranean Sea, most of the known CWC mounds have been found in the southern Alboran Sea, primarily in the EMCP (Fink et al., 2013) and the WMCP (Lo Iacono et al., 2014). In particular, coral mounds in the EMCP are impressive as they display diverse morphologies and dimensions along a N-S trending depth transect (Hebbeln, 2019). It is most likely that subtle circulation changes at the different water depths in the study area impacted on food and sediment supply and, thus, on mound formation. Up to present, the development of coral mounds in the northern and western sub-clusters of the EMCP since the last deglaciation (at ~14 kyr BP) has been described (Fink et al., 2013; Stalder et

al., 2015; 2018). Here, we extent the knowledge about past mound formation in the EMCP spatially by including records from the central and the southern sub-cluster and temporary by extending it from approximately the last 15 kyr BP to >120 kyr BP (Fig. 5-2).

5.5.1 Timing and duration of coral mound formation in the EMCP, southern Alboran Sea

The obtained U/Th age clusters indicate two phases of enhanced mound formation in the central (78.0-71.5 kyr BP and 13.9-11.7 kyr BP, core GeoB18120-1) and one phase in the southern (112.3-110.6 kyr BP, core GeoB18105-1) sub-clusters of the EMCP (Fig. 5-2). Both cores reveal high CWC abundance prior to the last deglacial, which up to now has never been documented in the Mediterranean Sea. So far, only individual specimen of *L. pertusa* and *M. oculata* yielded ages >16 kyr with only two single dated samples (Adriatic: 17.5 kyr; Strait of Sicily: 47.9 kyr) having been recorded from the last ~130 kyrs (McCulloch et al., 2010). The obtained Mound average ARs of 67 and 240 cm kyr^{-1}, now established for the EMCP, however, clearly document for the first time not only high CWC abundance but also intense mound formation prior to the last deglaciation. Mound ARs as reported here for the last deglaciation, 216 cm kyr^{-1}, are within the range of > 200 cm kyr^{-1} reported earlier for the EMCP for this period (Fink et al., 2013; Stalder et al., 2015).

The duration of intense mound formation (CWC occurrences partly cover a longer time span) for all three documented phases is 6.5 kyrs (MIS 5a), 2.2 kyrs (last deglaciation) and 1.7 kyrs (MIS 5d), revealing that intense mound formation at a given site is a rather short-living event. This is in agreement with other studies focusing on deglacial mound formation in the Alboran Sea (Fink et al., 2013; Stalder et al., 2015; 2018; Wang et al., 2019). As found in most coral mounds also in the North Atlantic (e.g., Dorschel et al., 2005; Matos et al., 2017), periods between phases of coral growth are only poorly – if at all – preserved in the mound records. Individual coral ages apart from pronounced age clusters, as e.g., the ages of 52.8 and 4.7 kyr in core GeoB18120-1, most likely reflect short periods of coral presence, however, without offering conditions triggering enhanced mound formation.

Interestingly, in contrast to all other EMCP sub-clusters experiencing mound formation during the Early Holocene (Fink et al., 2013; Stalder et al., 2015; 2018; and core GeoB18120-1, this study), coral mound formation ceased much earlier (~106 kyr BP; core GeoB18105-1, water depth: 224 m) in the southern sub-cluster, the shallowest part of the EMCP. The coral mounds in this area only reach ~10 m above the surrounding seabed and get gradually buried towards the coast in the south (Hebbeln, 2019). As our off-mound core located much further off the coast reveals an average sedimentation rate of 15 cm kyr^{-1} (Table 5-3), probably much higher sedimentation rates can be expected for the southernmost sub-cluster being close to the main regional sediment source, the Moulouya River. Thus, assuming an average sedimentation rate for this region in the order of ~30 cm kyr^{-1}, would yield a sedimentation in the order of ~10 m between the mound formation phases in MIS 5d and MIS 5a. This amount of sediment might have reduced the relative height of the mounds in this sub-cluster to an extent

disrupting the local hydrodynamic effect of the mounds in enhancing bottom currents to support the lateral food supply to the corals.

To what extent the mound formation phases during MIS 5d and MIS 5a are documented in the other sub-clusters of the EMCP (in addition to site GeoB18120-1 documenting the MIS 5a phase) is unknown as all published cores did not penetrate in sediments older than the last deglaciation. During the deglacial, the very high AR of >200 cm kyr^{-1} recorded in core GeoB18020-1 is well in line with the deglacial coral boom in the region described before (Fink et al., 2013; Stalder et al., 2015; Wang et al., 2019). However, comparisons between all these deglacial records show slightly different ages for the highest mound ARs for individual sites within the deglacial time window of ~15-10 kyr BP pointing to some yet unexplained local variability.

5.5.2 paleo-environmental conditions controlled coral mound formation in the southern Alboran Sea since the last deglaciation

Coral mound formation results from the complex interplay between coral growth and sediment deposition (Hebbeln et al., 2016; Wienberg and Titschack, 2017). In the oligotrophic Mediterranean Sea, high food supply to the corals is a key factor driving coral proliferation, preconditioning mound formation (e.g., Fink et al., 2013; Stalder et al., 2015; 2018). For the WMCP, internal waves significantly enhancing the lateral food supply to the corals have been identified as a key factor triggering the fast coral growth and, thus, coral mound formation during the last deglaciation (Wang et al., 2019). Apart from the food supply to the corals, sediment supply to the mounds also is of crucial importance for mound formation, as a high sediment supply on one hand stabilizes the coral framework preventing it from physical fragmentation and biogenic degradation and on the other hand provides most of the material making up the coral mounds (e.g., Titschack et al., 2015; 2016). In this context, we reconstruct surface water productivity, water column structure, and bottom water hydrodynamics as well as the oxygenation state using the off-mound core to unravel the environmental conditions driving coral mound formation in the different sub-clusters of the EMCP.

5.5.2.1 Water column structure and bottom water hydrodynamics controlled the formation of coral mounds in the EMCP, southern Alboran Sea

Given the offset between the δ^{13}C values of the isotopically heavier MAW (~1.4‰) and the lighter LIW (~0.9‰) in the Alboran Sea (Pierre, 1999), here the δ^{13}C$_{Cib}$ data are used to reconstruct varying influences of both water masses in the EMCP. Considering sea level variations in the order of ~120 m (Waelbroeck et al., 2002) and internal tides at the LIW-MAW interface with amplitudes of ~90 m (Van Haren, 2014), the relative influence of both water masses on the coral mounds in the EMCP most likely varied considerably over the last ~130 kyr. By using δ^{13}C values of benthic foraminifera, Wang et al. (2019) showed that coral mound formation during the deglaciation in the WMCP and in the

northernmost EMCP was most intense when the $\delta^{13}C$ data revealed a lasting decreasing trend most likely reflecting a gradual shift of dominant water mass from the MAW to LIW probably triggered by the rising sea level. Along this trend mound formation coincided with relatively coarse mean grain sizes pointing to enhanced bottom water hydrodynamics most likely stimulated by internal waves propagating along the by-passing LIW-MAW interface (Wang et al., 2019). In addition, for the WMCP (Wang et al., 2019) and the EMCP (Fink et al., 2013), the deglacial mound formation phase was marked by enhanced surface water productivity. Thus, previous data indicate enhanced vertical and lateral food supply, the latter increased by internal waves along the LIW-MAW water mass boundary, as key factors for the deglacial mound formation phase in both provinces.
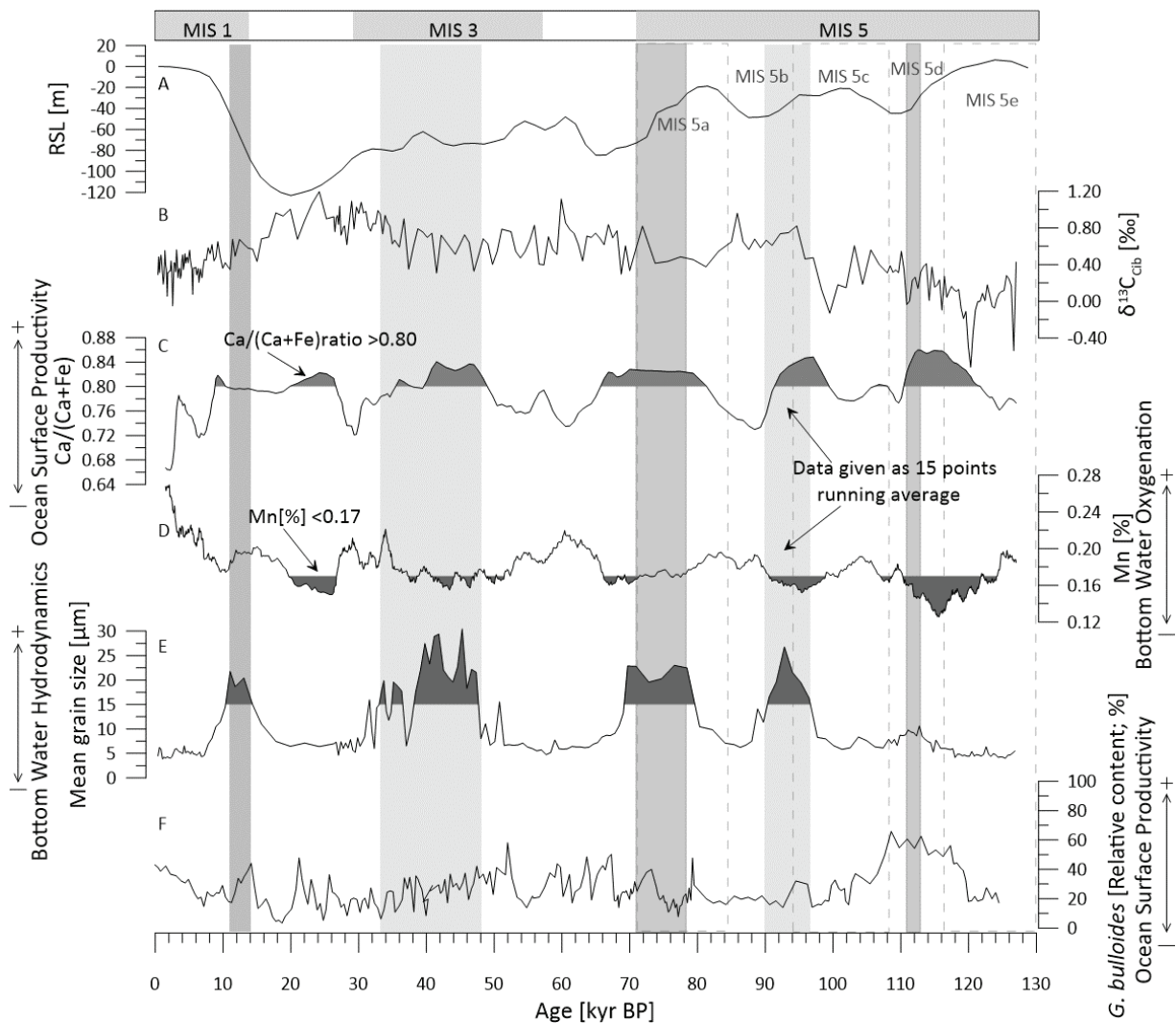
Figure. 5-4. Multi-proxy data obtained from off-mound core MD13-3457 from the East Melilla cold-water coral mound province (EMCP) covering the past 130 kyr BP. A: relative sea level (RSL) record from Waelbroeck et al. (2002) B: Stable carbon isotopes ($\delta^{13}C$) from the epi-benthic foraminifera *Cibicidoides mundulus*, used to reconstruct the water column structure in the EMCP. C: Ca/(Ca+Fe) ratio (given as 15 points running average) as a proxy for surface water productivity. D: Mn content (%, relative to total counts, given here as 15 points running average) as an indicator for bottom water oxygenation. E: Mean grain size data as a proxy for bottom water hydrodynamics. F: Relative content of the planktonic foraminifera *Globigerina bulloides* from Ocean Drilling Program (ODP) Site 977 in the eastern Alboran Sea (Pérez-Folgado et al., 2004). Dark grey vertical bars correspond to coral mound formation phases reported here, while light grey bars indicate periods seemingly suitable for mound formation (see text).

57

The new data presented here reveal an almost identical pattern for the deglacial record in the central EMCP, where mound formation between 13.9 and 11.7 kyr BP coincides with an overall decreasing $\delta^{13}C$ trend, relative coarse mean grain sizes and high productivity (Fig. 5-4). A similar pattern can be observed for the previous mound formation phase during MIS 5a. The only difference is the opposite $\delta^{13}C$ trend from ~0.40‰ during the MIS 5a to ~1.1‰ during the early MIS 4 (Fig. 5-4). The corresponding gain in influence of the MAW would be in line with the sea level lowering during this period. Consequently, for MIS 5a the same mechanisms controlling mound formation as for the last deglaciation can be assumed.

Interestingly, the mound formation phase during MIS 5d appears to be characterized by a different paleoenvironmental setting. The most prominent feature is the lack of a clear grain size signal in the off-mound record (Fig. 5-4). Rather low mean grain sizes during this period point to relatively weak bottom water hydrodynamics possibly limiting the lateral food supply to the corals. This is in line with the $\delta^{13}C_{Cib}$ record showing lower values for this period in comparison to the two younger mound formation phases. These lower values point to the dominant influence of the LIW at the off-mound site, most likely in pace with a reduced effect of internal tides as indicated by the mean grain size data (Fig. 5-4). This difference in the oceanographic setting of the MIS 5d mound formation phase compared to the later phases might be controlled by the higher sea level during MIS 5d, probably also placing the MAW-LIW water mass boundary higher up in the water column. This, of course, also might have affected the setting at the individual mounds, with site GeoB18105-1, documenting the MIS 5d mound formation phase, corresponding to the shallowest site (Table 5-1). Although the two younger mound formation phases documented at site GeoB18120-1, which is situated only 25 m deeper in the water column as site GeoB18105-1, correlate with the grain size data from the off-mound core taken even 100 m deeper, an upward movement of the MAW-LIW interface might have put the off-mound site out of the range of the internal tides. As the mound formation phase during MIS 5d corresponds to a comparatively high sea level, which accounts even more for the even older coral ages corresponding to MIS 5e, we suppose that also during MIS 5d internal tides supported coral growth at site GeoB18105-1, however, without leaving a clear trace in the off-mound site 120 m deeper.

Further support for coral mound formation during this period, most likely was provided by enhanced primary productivity in the surface waters. The highest Ca/(Ca+Fe) ratios in our record (Fig. 5-4) coinciding with the highest relative abundances (>50%) of the high productivity-related planktic foraminifera *Globigerina bulloides* in near-by ODP site 977 (Pérez-Folgado et al., 2004) provides clear indications for a very high surface water productivity during this period. This is further corroborated by low Mn values suggesting relatively low oxygen conditions at the seabed, another major difference in the paleoenvironmental setting compared to the two younger mound formation phases described above (Fig. 5-4). Nevertheless, the overall good negative correlation between the productivity indicator (Ca/(Ca+Fe) ratio) and the oxygenation proxy (Mn values) points to a local,

productivity-driven control of the bottom water oxygenation probably resulting from the remineralization of locally produced organic matter (Fig. 5-4).

Low bottom water oxygenation, on one hand, has been shown to potentially disrupt coral growth (Fink et al., 2012; Tamborrino et al., 2019). On the other hand, the additional energy demand of the corals to cope with low oxygen conditions (Diaz and Rosenberg, 1995) might be balanced by extremely enhanced food supply through enhanced surface water productivity as, e.g., suggested for the Angolan cold-water corals presently thriving under hypoxic conditions (Hanz et al., 2019; Hebbeln et al., subm.). Thus, for MIS 5d we propose that very high surface water productivities, as best exemplified by the highest percentages of the productivity planktonic foraminifera indicator species *G. bulloides* of the last 150 kyr in ODP Site 977 in the eastern Alboran Sea (Pérez-Folgado et al., 2004; Fig. 5-4), were sufficient for compensating for the impact of low bottom water oxygenation on the metabolic activity of the corals. Of course, 120 m higher up in the water column within the range of the internal tides, oxygenation at site GeoB18105-1 also might have been better as at the off-mound site.

5.5.2.2 Poor bottom water oxygenation might have hampered coral mound formation during the last glacial and the MIS 5c in the EMCP

Interestingly, also between 48 and 33 kyr BP the environmental conditions seem to be optimal for coral mound formation, however, no corals have been found although this period should be covered in core GeoB18120-1. The $\delta^{13}C_{Cib}$ record (mostly in the range of 0.40‰-0.80‰) during this period likely suggested the presence of the LIW-MAW interface in the study area, which is in line with strong bottom water hydrodynamics as indicated by high mean grain sizes. In terms of surface water productivity, the high Ca/(Ca+Fe) ratios seem to indicate high production, although lower ratios and lower contents of *G. bulloides* at ODP Site 977 point to lower productivities as e.g., during MIS 5d. The main difference of this 48-33 kyr BP period compared to the two mound formation phases (MIS 5a and deglaciation) documented in core GeoB18120-1 is the low Mn level pointing to rather low bottom water oxygenation (Fig. 5-4). In contrast to MIS 5d, these low oxygen levels probably could not have been compensated by high enough food supply, thus, hampering coral growth, a scenario described earlier for, e.g., the eastern Mediterranean Sea and areas off Mauritania and Namibia (e.g., Fink et al., 2012; Wienberg et al., 2018; Tamborrino et al., 2019).

Also for the period between 97 and 90 kyr BP, the paleoceanographic proxies at first glance point to optimal conditions for coral growth, namely triggered by strong bottom water hydrodynamics, high productivity and the influence of the LIW-MAW boundary as indicated by the $\delta^{13}C_{Cib}$ data (Fig. 5-4). However, the Mn data indicate that during this period oxygenation most likely was even worse compared to the 48-33 kyr interval, when no corals lived in the EMCP. Here, it only can be speculated what happened between 97 and 88 kyr BP in the EMCP. At the shallowest site, GeoB18105-1, corals did not thrive during this period, however, for site GeoB18120-1 any information is lacking as the corresponding core was not long enough to obtain samples from this interval. Even though, in analogy

to the 48-33 kyr interval, it might be expected that also between 97 and 88 kyr BP low bottom water oxygenation precluded extended coral growth in the EMCP.

5.5.2.3 Dominant role of sea level for coral mound formation in the southern Alboran Sea
Comparing the individual paleoceanographic proxies with each other and with respect to the occurrence of cold-water corals in the EMCP, some interesting patterns can be observed. The obvious correlation between productivity (Ca/(Ca+Fe)) and bottom water oxygenation (Mn content) (Fig. 5-5A) points to a clear productivity control on the oxygen conditions at the seabed. Coral occurrence is linked to higher productivities and, thus, to poorer bottom water oxygenation. However, there seems to be a threshold for coral proliferation, when bottom water oxygen contents get too low (except for the shallowest site, where bottom water conditions were probably different from those recorded at the off-mound site, see above).

Furthermore, strong bottom water hydrodynamics (mean grain size) appear to be linked to specific water mass conditions as, e.g., demonstrated by their link to a narrow range of $\delta^{13}C_{Cib}$ data (0.3-1‰) (Fig. 5-5B). The $\delta^{13}C_{Cib}$ data obtained at the off-mound site increase continuously with lowering relative sea level (Fig. 5-5C), i.e. the lower the sea level the stronger is the influence of the MAW, which is marked by heavier $\delta^{13}C$ values (Pierre, 1999). Consequently, strong hydrodynamics at the off-mound site are linked to a specific range of past sea levels, namely the range of ~20-90m below present-day conditions (Fig. 5-5D). Overall, these observations point to a dominant control of sea level on mound formation in the EMCP, predominantly by regulating the water column structure and by controlling the depth range of the internal tides extending along the MAW-LIW interface. However, some additional control can be exerted by the state of bottom water oxygenation, which upon becoming too low might preclude further coral growth.

These data also show the limitation of the on-mound vs. off-mound approach (Hebbeln et al., 2019), when the corresponding data sets are taken from different water depths. Here, especially the MIS 5d mound formation phase documented in the shallowest core, GeoB18105-1, does only partly fit into the pattern outlined above. For this period, lowest $\delta^{13}C_{Cib}$ values in the off-mound core point to a strong LIW dominance indicative for an LIW-MAW interface somewhere higher up in the water column. Most likely, this interface was still affecting core GeoB18105-1 taken approximately 120 m shallower and providing suitable conditions for the corals at this site. Thus, utmost care should be taken, to obtain off-mound records especially in terms of water depth from as close as possible to coral mounds, which formation history should be investigated.
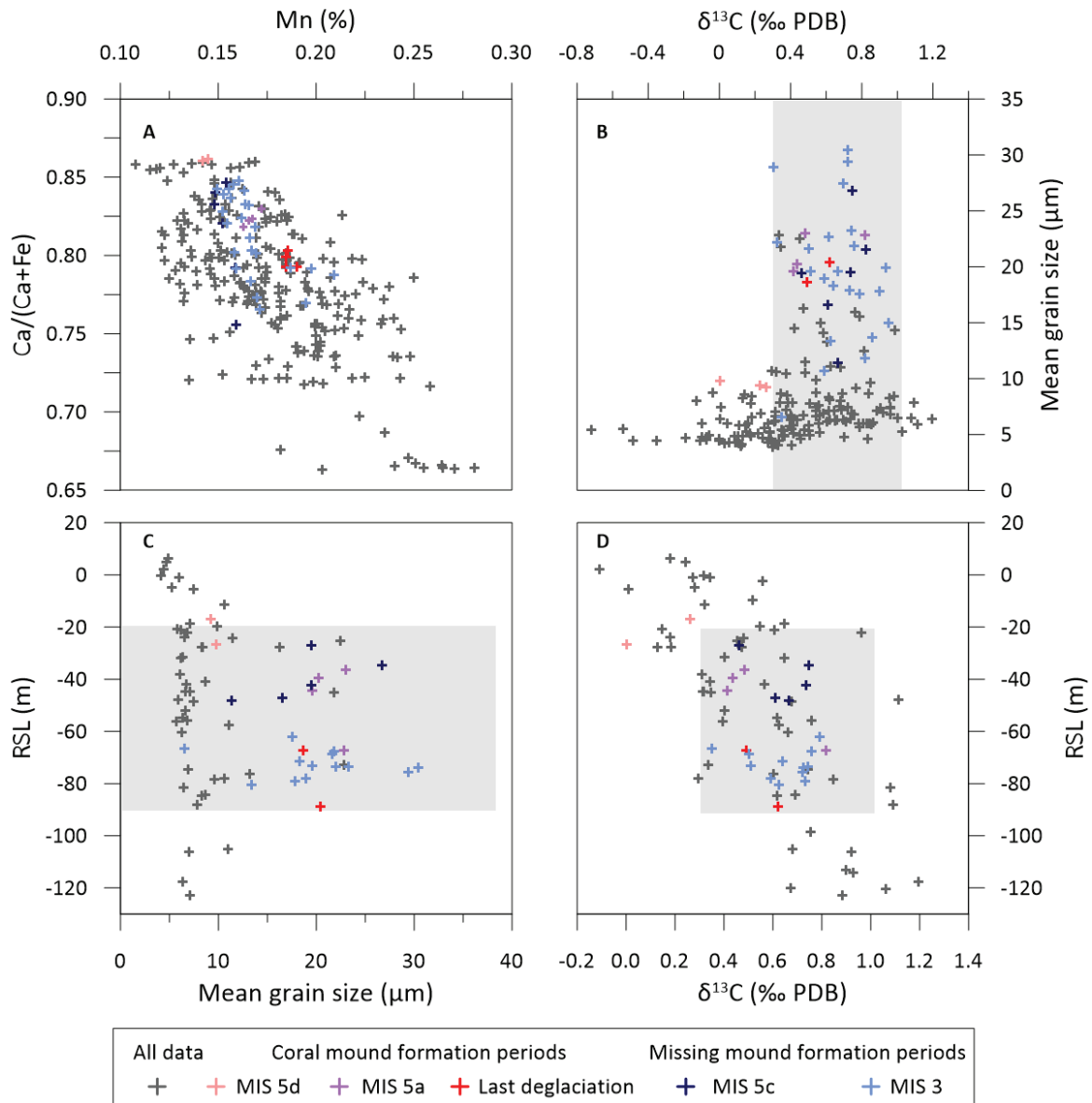
Figure. 5-5. Paleoenvironmental data obtained from off-mound core MD13-3457 in the Alboran Sea. A: Scatter plot of the productivity (Ca/(Ca+Fe)) vs. the bottom water oxygenation proxy (Mn% relative to total counts). B: Scatter plot of the hydrodynamics (mean grain size) vs. the water mass (δ¹³C) proxy, obtained on the benthic foraminifer *Cibicidoides mundulus*. The grey bar marks the δ¹³C range corresponding to elevated mean grain size data. C: Scatter plot of relative sea level (RSL) vs mean grain size. The grey bar marks the relative sea level range corresponding to elevated mean grain sizes. D: Scatter plot of relative sea level vs δ¹³C. The grey square represents the overlap of the grey bars shown in (B) and (C). The RSL data are from Waelbroeck et al. (2002). The color coding refers to the individual time periods of observed coral mound formation (deglaciation, MIS 5a and 5d) and missing mound formation (MIS 5c and MIS 3) as explained in the text.

5.6 Conclusion

On-mound cores from the central and southernmost coral mound sub-clusters of the EMCP revealed the development of CWC mound since the last interglacial. While the youngest, deglacial mound

formation phase detected in these cores coincided with previous results from the northern and westernmost sub-clusters, the older mound formation phases in MIS 5d and 5a reported here are the first ones to be reported in the Mediterranean Sea from prior to the last deglaciation. For the deglacial as well as for the MIS 5a mound formation phase, rather comparable environmental settings marked by strong bottom water hydrodynamics most likely linked to internal waves propagating along the MAW-LIW interface have been observed. For the MIS 5d period, similar evidence for enhanced bottom water hydrodynamics could not be detected in the off-mound core. However, this is probably due to the relatively great water depth offset of 120 m between the off-mound record and site GeoB18105-1, the only recorder for the MIS 5d mound formation phase so far. For other periods marked by similar environmental conditions, evidence for coral growth are lacking. Most likely, reduced bottom water ventilation hampered coral growth during these times. Overall, there seems to be a strong influence of the relative sea level on coral growth and mound formation, as suitable environmental conditions, especially in relation to the position of the MAW-LIW interface and the internal waves developing along this water mass boundary, are closely coupled to the water column structure and, thus, to sea level.

Chapter 6

Cold-water coral mounds in the southern Alboran Sea (western Mediterranean Sea): Internal waves as an important driver for mound formation since the last deglaciation

Haozhuang Wang[a], Claudio Lo Iacono[b, c], Claudia Wienberg [a], Jürgen Titschack [a, d], Dierk Hebbeln [a]

a Center for Marine Environmental Sciences (MARUM), Bremen University, Leobener Strasse 2, 28359 Bremen, Germany

b National Oceanography Centre, University of Southampton, Waterfront Campus, European Way, SO143ZH, Southampton, United Kingdom

c Marine Sciences Institute (ICM), Spanish National Research Council (CSIC), Paseo Maritimo de la Barceloneta 37-49, 08003, Barcelona, Spain

d Senckenberg am Meer (SAM), Marine Research Department, Südstrand 40, 26382 Wilhelmshaven, Germany

Abstract

Cold-water corals (CWCs) are widely distributed in the entire Alboran Sea (western Mediterranean Sea), but only along the Moroccan margin they have formed numerous coral mounds, which are constrained to the West and the East Melilla CWC mound provinces (WMCP and EMCP). While information already exists about the most recent development of the coral mounds in the EMCP, the temporal evolution of the mounds in the WMCP was unknown up to the present. In this study, we present for the first time CWC ages obtained from four sediment cores collected from different mounds of the WMCP, which allowed to decipher their development since the last deglaciation. Our results revealed two pronounced periods of coral mound formation. The average mound aggradation rates were of 75-176 cm kyr^{-1} during the Bølling-Allerød interstadial and the Early Holocene, only temporarily interrupted during the Younger Dryas, when aggradation rates decreased to <45 cm kyr^{-1}. Since the Mid Holocene, mound formation significantly slowed-down and finally stagnated until today. No living CWCs thrive at present on the mounds and some mounds became even buried. The observed temporal pattern in mound formation coincides with distinct palaeoceanographic changes that significantly influenced the local environment. Within the Alboran Sea, enhanced surface ocean productivity and seabed hydrodynamics prevailed during the Bølling-Allerød and the Early Holocene. Only with the onset of the Mid Holocene, the area turned into an oligotrophic setting. The strong hydrodynamics during the mound formation periods are most likely caused by internal waves that

developed along the water mass interface between the Modified Atlantic Water and the Levantine Intermediate Water. In analogue to observations from modern CWC settings, we assume that internal waves created turbulent hydrodynamic conditions that increased the lateral delivery of particulate material, promoting the availability of food for the sessile CWCs. Overall, our data point to the dominant role of the water column structure in controlling the proliferation of CWCs and hence the development of coral mounds in the southern Alboran Sea.

6.1. Introduction

Scleractinian framework-forming cold-water corals (CWCs) show a world-wide distribution and form important deep-sea ecosystems providing habitats for numerous marine organisms (e.g., Henry and Roberts, 2007; Roberts et al., 2009). The most prominent species *Lophelia pertusa* and *Madrepora oculata* tolerate a wide range of physico-chemical conditions in the ocean, with temperature, salinity, dissolved oxygen concentrations, pH, aragonite saturation, and water mass density being the most important properties of the surrounding water masses that influence their occurrence (e.g., Freiwald, 2002; Davies et al., 2008; Dullo et al., 2008; Davies and Guinotte, 2011; Flögel et al., 2014; Büscher et al., 2017). However, the proliferation of CWCs is even more controlled by the availability of sufficient food (phytoplankton, zooplankton, particulate organic material), which is steered by enhanced surface productivity and/or the local hydrodynamic regime (including geostrophic currents, internal tides and waves, cascading and down-welling processes), providing periodic to constant delivery of sufficient food particles (White et al., 2005; Duineveld et al., 2007; Mienis et al., 2007; Davies et al., 2009; Duineveld et al., 2012; Taviani et al., 2016).

Over geological timescales, the sustainable growth of CWCs can shape the seabed topography along the continental margins by forming three-dimensional structures, named coral mounds (Roberts et al., 2009; Wienberg and Titschack, 2017; Lo Iacono et al., 2018). In the Atlantic, coral mounds are usually found at water depths between 200 and 1000 m and are often arranged as clusters or coral mound provinces consisting of hundreds to thousands of mounds (e.g., De Mol et al., 2002; Fosså et al., 2005; de Haas et al., 2009; Correa et al., 2012a; Glogowski et al., 2015; Vandorpe et al., 2017; Hebbeln et al., 2019). Individual mounds have oval to elongated shapes, and appear as ridge-like structures, which extend over hundreds to thousands of metres (Wheeler et al., 2007). The height of individual mounds varies from a few to hundreds of metres (e.g., van Weering et al., 2003; Mienis et al., 2007; Wheeler et al., 2007; Collart et al., 2018).

Although food delivery plays a crucial role in the proliferation of CWCs, the formation of coral mounds is even more sensitive to the complex interplay between the sustained growth of CWC, their baffling capacity and sediment supply that eventually result in the formation of coral mounds (Wheeler et al., 2005; Huvenne et al., 2009a; Mienis et al., 2009a; Titschack et al., 2015; 2016; Victorero et al., 2016). Consequently, coral mounds consist of coral frameworks and fragments, remains of coral associated fauna, and hemipelagic sediments. Their development can last from thousands to even millions of years (e.g., Kano et al., 2007; Frank et al., 2011; Raddatz et al., 2011). Therefore, the coral mounds provide unique archives to reconstruct the palaeoceanographic constraints during their formation as well as the development of CWC populations in relation to changing environments.

Studies from various coral mound provinces in the NE Atlantic revealed distinct temporal patterns of mound formation which appear to be closely related to climate changes, such as those induced by

glacial-interglacial variability (e.g., Kano et al., 2007; Frank et al., 2011). On a regional scale, mound formation is controlled by strong near-bottom hydrodynamics and enhanced paleo-productivity (Dorschel et al., 2005; Rüggeberg et al., 2007; Wienberg et al., 2010; Eisele et al., 2011; Matos et al., 2015), while low dissolved oxygen concentrations might hinder the development of coral mounds (Wienberg et al., 2018). Moreover, the water column structure and water mass circulation at intermediate water depths seem to play an important role in stimulating or suppressing the formation of coral mounds (White and Dorschel, 2010; Raddatz et al., 2014; Matos et al., 2017; Wienberg et al., 2018). Nevertheless, our knowledge about environmental parameters and their complex interplay controlling coral mound formation is still limited.

In the Mediterranean Sea, coral mounds are mainly found along the Moroccan margin, in the southern Alboran Sea, where they are constrained to two coral mound provinces 35 km northwest and 15 km northeast of the Spanish enclave Melilla (Cape Tres Forcas; Fig. 6-1). Within the West Melilla CWC mound province (WMCP), more than 100 oval to elongated coral mounds occur in two clusters at water depths of 300-430 m (Fig. 6-1; Lo Iacono et al., 2014). They have diameters of 50-476 m, and arise 8-21 m above the seafloor. In addition, few isolated circular coral mounds with heights of 10-35 m were found in water depths of 450-590 m (Fig. 6-1). Today, no living CWCs are observed on the mounds of the WMCP, and some of the mounds are partly buried (Lo Iacono et al., 2014). The East Melilla CWC mound province (EMCP) displays different morphologies and dimensions of mounds. In the north, three very steep ridges occur at water depths of 250-450 m, which have heights of 50-150 m and stretch from 3 km to almost 20 km in length (Brittlestar ridges I, II and III; Hebbeln, 2019). To the south, more than 40 oval to arcuate coral mounds (height: 20-40 m) and partly buried elongated ridges (height: 10 m) occur at water depths of 200-300 m (Comas et al., 2009; Hebbeln, 2019). Spotted colonies of living CWCs have been observed on the Brittlestar ridges and on some of the smaller mounds, displaying a rather sparse distribution (Hebbeln et al., 2009; Fink et al., 2013).

Recent studies provided some first information on the temporal development of the CWCs and coral mounds in the EMCP during the past 14 kyr. CWCs experienced marked proliferation during the late Bølling-Allerød (B/A) interstadial and the Early Holocene, associated with high mound aggradation rates (ARs) of 140-420 cm kyr^{-1} (Fink et al., 2013; Stalder et al., 2015). These two periods of pronounced mound formation contrast with a period of nearly stagnation, coinciding with the Younger Dryas (YD), when ARs decreased to 30-50 cm kyr^{-1}. Since the late Early Holocene, CWC growth was reduced and coral mound formation significantly slowed down until present (Fink et al., 2013; Stalder et al., 2015). Overall, it is assumed that coral mound formation in the EMCP is controlled by a variable set of environmental parameters such as sea surface and export productivity, strong hydrodynamics, and bottom water oxygenation, which in turn seem to be steered by changes in the water column structure (Fink et al., 2013; Stalder et al., 2015). So far, nothing is known about the timing of CWC growth and coral mound formation in the WMCP. Based on seismic data, it is assumed that a simultaneous initial CWC colonisation took place in the WMCP and that some of the

mounds became buried concurrent to the effects of sea-level rise that likely induced changes in near-bottom hydrodynamics and sedimentation rates on the slope (Lo Iacono et al., 2014). However, no temporal framework for the evolution of the coral mounds in the WMCP has been established so far, mainly due to the lack of sediment cores collected in this region.

The main aims of this study are therefore (i) to reconstruct the temporal development of coral mounds in the WMCP, and (ii) to relate the derived temporal patterns in mound formation to changes in the regional environmental setting. For this purpose, coral-bearing (on-mound) cores were collected from different coral mounds in the WMCP, and complemented by one off-mound sediment core (barren of any coral fragments) retrieved close to the studied mounds. The on-mound cores were described and dated to elucidate the local coral mound formation pattern, while the off-mound core was used for multi-proxy analyses to assess the (palaeo-) environmental controls on mound development. Furthermore, we evaluated any differences in mound evolution between the WMCP and the EMCP, and addressed the decisive role of water mass circulation, in particular distinct processes at water mass boundaries, as a crucial local factor driving the development of coral mounds in the southern Alboran Sea.

6.2. Regional Setting

The Alboran Sea is located at the westernmost part of the Mediterranean Sea, and is connected to the Atlantic Ocean through the Gibraltar Strait (Fig. 6-1). The oceanography of the Alboran Sea is characterized by three different water masses, the Modified Atlantic Water (MAW), the Levantine Intermediate Water (LIW) and the Western Mediterranean Deep Water (WMDW). The MAW, formed by the mixing of Atlantic Water and the surface waters of Alboran Sea (Millot and Taupier-Letage, 2005), flows at the surface down to 150-200 m water depth (Millot, 1999). Within the Alboran Sea, the MAW forms two anti-cyclonic gyres, the quasi-permanent West and the variable East Alboran Gyres (WAG and EAG; Fig. 6-1), which have diameters of 100 km and reach down to 200-300 m water depth (Heburn and La Violette, 1990). Their intensity is closely related to the strength of the Atlantic Water inflow (Heburn and La Violette, 1990; Vargas-Yáñez et al., 2002). The LIW, which originates in the Eastern Mediterranean Sea, flows westward beneath the MAW at depths between 200 m and 600 m. The core of the LIW is found at around 400 m water depth in the Alboran Sea indicated by the salinity maximum (Millot, 2009). Its thickness decreases gradually from the European to the African continental margin (Brankart and Pinardi, 2001; Fabres et al., 2002). The WMDW is formed in the Gulf of Lions, and spreads into the Balearic Sea and further into the Alboran Sea, where it flows westward underneath the LIW, at water depths of >600 m (Millot, 1999).

The Alboran Sea is the area with the highest productivity within the overall oligotrophic Mediterranean Sea (Morán and Estrada, 2001; D'Ortenzio and Ribera d'Alcalà 2009). The increased productivity is driven by locally restricted upwelling that occurs along the edge of the WAG and at the

eastern limb of the EAG (Sarhan et al., 2000; Baldacci et al., 2001). The siliciclastic sediment fraction in the Alboran Sea is a mixture of aeolian dust, which is transported northward from the Sahara (Stuut et al., 2009), and fluvial input, which mainly derives from the Iberian Peninsula (Fabres et al., 2002). The only larger river along the Moroccan coast is the Moulouya River, which enters the Alboran Sea 50 km east of the EMCP.
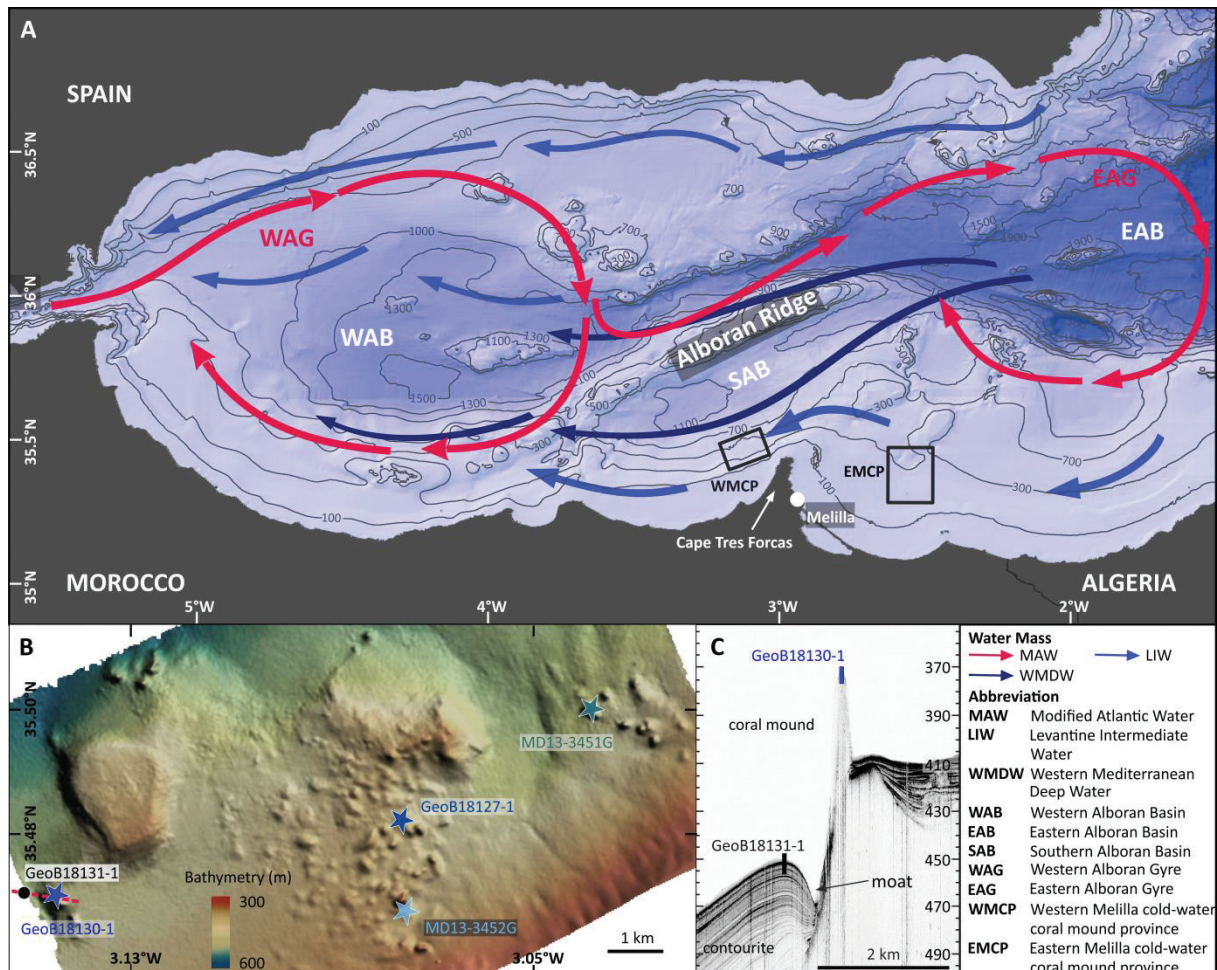
Figure. 6-1. A: Bathymetry map of the Alboran Sea (Western Mediterranean Sea) (Map: Marine Information Service (2016); EMODnet Digital Bathymetry, http://doi.org/10.12770/c7b53704-999d-4721-b1a3-04ec60c87238). Displayed is the schematic present-day oceanic circulation pattern in the Alboran Sea. Two black rectangles represent the West Melilla cold-water coral mound province (WMCP; this study) and the East Melilla cold-water coral mound province (EMCP). B: Shaded relief map of the WMCP showing the location of the four on-mound cores (stars; MD13-3451G, MD13-3452G, GeoB18127-1, and GeoB18130-1) and one off-mound core (dot; GeoB18131-1) presented in this study. C: Sub-bottom profile (parasound) from the WMCP (modified after Hebbeln et al., 2009) indicating the sampling sites of the on-mound core GeoB18130-1 and the off-mound core GeoB18131-1. The location of the cross profile is indicated as a red dashed line in (B).

6.3. Material and Methods

Within this study, four "on-mound" gravity cores retrieved from coral mounds of the WMCP and one "off-mound" gravity core collected from the adjacent seafloor were analysed (Fig. 6-1; Table 6-1). The two on-mound cores MD13-3451G and MD13-3452G were collected in 2013 during the MD194

"Gateway" Eurofleets Cruise onboard the RV Marion Dufresne (Van Rooij et al., 2013). The other two on-mound cores GeoB18127-1 and GeoB18130-1, and the off-mound core GeoB18131-1 were collected in 2014 during the MSM-36 "MoccoMebo" cruise on board the RV Maria S. Merian (Hebbeln et al., 2015). The on-mound cores have recovery lengths between 148 cm and 563 cm, and the off-mound core has a recovery length of 851 cm (Table. 6-1).

The four on-mound cores were frozen for 24 hours to -20 °C before cutting them lengthwise with a diamond saw to secure that the sediment, consisting of coral fragments embedded in hemi-pelagic sediment, is kept intact during the opening process. The cores were described, and coral fragments were sampled at various core depths for absolute dating.

The off-mound core GeoB18131-1 was split in a conventional way into working and archive halves and was used for palaeoceanographic multi-proxy analyses.

Table 6-1. Metadata of gravity cores collected in the WMCP (southern Alboran Sea) during the cruise MD 194 "GATEWAY" with the French RV Marion Dufresne and cruise MSM 36 "MoccoMeBo" with the German RV Maria S. Merian.

Cruise	Core Type	Core ID	Latitude [N]	Longitude [W]	Water depth [m]	Recovery [cm]
MD194	On-mound	MD13-3451G	35°29.996′	3°02.398′	370	522
MD194	On-mound	MD13-3452G	35°28.128′	3°04.661′	305	558
MSM-36	On-mound	GeoB18127-1	35°28.969′	3°04.641′	365	563
MSM-36	On-mound	GeoB18130-1	35°28.099′	3°08.747′	379	148
MSM-36	Off-mound	GeoB18131-1	35°28.093′	3°09.301′	457	851

6.3.1 On-mound core analyses

6.3.1.1 Sedimentological core description
Cores MD13-3451G and MD13-3452G were visually described to provide (qualitative, 2D) information on variations in coral content and clast size throughout the cores. The coral content was estimated based on its coverage on the cutting surface (unit: surface (surf.) %) of the core halves, and changes in CWC clast size were described (see Fig. 6-S1 in Supplementary Material).

In contrast, the core description provided for cores GeoB18127-1 and GeoB18130-1, is based on the analyses of computer tomography (CT) scan data. These analyses were further used to define CWC preservation pattern (CPP) by quantifying coral clast size and orientation (see Table 6-S1 in Supplementary Material) in close accordance to a CPP classification introduced by Titschack et al. (2015).

The CT scans were performed by using Toshiba Aquilion 64 computer tomography at the hospital Klinikum Bremen-Mitte (Bremen, Germany). The X-ray source voltage was 120 kV and the current was 600 mA. Images were reconstructed based on the Toshiba patented helical cone beam

reconstruction technique. The CT scan resolution was 0.35 mm in x-y and 0.5 mm in z direction (0.3 mm reconstruction interval). The CT data were processed with the Zuse Institute Berlin edition of Amira software (version 2015.37; Stalling et al., 2005; http://amira.zib.de), following the method described in Titschack et al. (2015) with only minor modification(for further processing details, see Supplementary Material).

6.3.1.2 Radiocarbon and Uranium-series dating

A total of 38 fragments of *L. pertusa* and *M. oculata* were sampled from the four on-mound cores at various depths and used for dating. Prior to the analyses, all coral fragments were cleaned mechanically to remove cortical corrosion, bioerosion holes, and adhering detritus from the coral skeletons.

Twelve coral samples collected from cores MD13-3451G and MD13-3452G, were dated by accelerator mass spectrometry (AMS) radiocarbon (^{14}C) age determination. Prior to the measurement, the coral fragments were chemically cleaned with hydrogen peroxide. The measurements were conducted at the Poznan Radiocarbon Laboratory, Poznan, Poland. All the obtained ages were corrected for ^{13}C and a mean ocean reservoir age of 400 years. The AMS ^{14}C ages were converted to calendar years using the MARINE13 curve (Reimer et al., 2013) of the web-based CALIB 7.10 software (Stuiver and Reimer, 1993; http://calib.org/calib/calib.html) and reported as kiloyears before present (kyr BP, Present=AD 1950; Table 6-2).

Twenty-six coral samples from cores GeoB18127-1 and GeoB18130-1 were collected for Uranium-series dating. Before the analyses, coral fragments were cleaned mechanically according to a procedure described by Frank et al. (2004). The U-series isotope measurements were performed on a ThermoFisher iCAP-Qs inductively coupled plasma mass spectrometer (ICP-MS) at the Institute of Environmental Physics, at the Heidelberg University (IUP), Germany. The reproducibility was assessed using the international uranium standard material HU1 (Cheng et al., 2000a; Frank et al., 2004; Wefing et al., 2017). U-series coral ages are reported as kyr BP (Table 6-3). Finally, all coral mound ARs were calculated based on the linear interpolation between the dated depths of each core (Tables. 6-2, 6-3).

6.3.2 Off-mound core analyses

6.3.2.1 Radiocarbon dating

The chronostratigraphy of the off-mound core GeoB18131-1 is based on six AMS ^{14}C dates. Therefore, around 8 mg of calcium carbonate of mixed planktonic foraminifers of the size fraction >150 μm were analysed at the Poznan Radiocarbon Laboratory, Poznan, Poland. The obtained ages were corrected as described above (Table 6-4).

6.3.2.2 Stable oxygen and carbon isotope analyses

For stable oxygen (δ^{18}O) and carbon (δ^{13}C) isotope measurements, the core was sampled at a 5 cm resolution. Each sample was wet-sieved and the >150 μm fraction was used to collect around 10 specimens of the two epibenthic foraminifera species: *Cibicidoides mundulus* (also described as *Cibicidoides kullenbergi*) and *Cibicidoides pachyderma*. To exclude a potential species-specific fractionation effect (vital effect) on the measured isotopic compositions of the paired samples, δ^{18}O and δ^{13}C of both species were measured separately on 16 samples.

The analyses were performed at MARUM, University of Bremen, Germany, using a Finnigan MAT 251 mass spectrometer coupled either to a Kiel I or Kiel IV automated carbonate preparation device. With a constant temperature of 75 °C, the measurements were conducted on CO_2 that evolved by phosphoric acid treatment. Ground Solnhofen limestone was used as internal standard, which has been calibrated against Vienna Pee Dee Belemnite (V-PDB) using the NBS 19 standard. The measured data were reported relative to the V-PDB standard. The analytical standard deviation for δ^{18}O and δ^{13}C was ± 0.04‰ and ± 0.03‰ for the paired samples and ± 0.06‰ and ± 0.03‰ for the mono-species samples, respectively. The δ^{18}O and δ^{13}C anomaly between the two species has a mean value of 0.04‰ and -0.04‰, respectively, with a standard deviation of less than 0.25 for both. Given the standard deviation during the measurement, our record from mixed samples is valid.

The benthic foraminifera δ^{18}O record (δ^{18}O$_{Cib}$) was used to establish a chronostratigraphy for the off-mound core (supplemented by the AMS ^{14}C dates). The δ^{13}C$_{Cib}$ record was applied to trace past changes in the water column structure. Epibenthic foraminifera are commonly used in palaeoceanographic studies as their tests incorporate δ^{13}C in equilibrium with the ambient water (e.g., Curry et al., 1988; Curry and Oppo, 2005; Zahn et al., 1986). However, it has been shown that *C. mundulus* and *C. pachyderma* may record lighter δ^{13}C values than those of the ambient water suggesting an occasional infaunal habitat (Schmiedl et al., 2004; Martínez-Méndez et al., 2013; Schmittner et al., 2017 and references therein).

6.3.2.3 Grain-size analysis

Grain-sizes were measured on the terrigenous fraction of the sediment (sampling interval: 5cm). Prior-to the analyses, the samples were chemically treated following the method of McGregor et al. (2009). Deionized, degassed and filtered water (filtered with mesh size: 0.2 μm) was used during the entire process to reduce the potential influence of air bubbles or particles within the used water. The analyses were performed in the Particle-Size Laboratory at MARUM, University of Bremen, Germany, with a Beckman Coulter Laser Diffraction Particle Size Analyzer LS 13320. The obtained results provide the grain-size distribution of individual sample from 0.04 μm to 2000 μm in 116 size classes. All provided statistic values are based on a geometric statistic. In this study, the mean grain size is used to trace changes in bottom current strength (see alsoFink et al., 2013).

6.3.2.4 Benthic foraminifer accumulation rate

Benthic foraminifer accumulation rates (BFARs) were analysed for the upper 368 cm of the off-mound core. From the core top to 158 cm, the sampling resolution was 10 cm whereas the resolution was increased to 5 cm between 158 cm and 368 cm core depth. The bulk samples were wet sieved and the >150 μm fraction was used for benthic foraminifer counts. Each sample was split until it contained approximately 300 individuals of benthic foraminifers, and counted (Patterson and Fishbein, 1989). All counts were corrected for splits and the BFAR (unit: x10^3 individuals cm^{-2} kyr^{-1}) was calculated according to the equation from Ehrmann and Thiede (1985):

$$BFAR = SR \times DBD \times foram/1000$$

BFAR: benthic foraminifer accumulation rate;

SR: Sedimentation Rate (unit: cm kyr^{-1});

DBD: Dry bulk sediment density (unit: g cm^{-3});

foram: number of foraminifers per gram in the dry bulk sample (unit: individuals g^{-1}).

Due to the linear relation between the BFAR and the organic matter flux to the seafloor, the BFAR represents an established proxy for the export productivity (e.g., Berger and Herguera, 1992).

6.4 Results

6.4.1 On-mound core description

6.4.1.1 Visual core description of on-mound cores MD13-3451G and MD13-3452G

For the two on-mound cores MD13-3451G and MD13-3452G, a visual core description is provided (see Fig. 6-S1 in Supplementary Material), as CT scan data, allowing for a detailed quantitative description or determining of CPPs, are not available for these cores. Core MD13-3451G reveals CWC fragments embedded in predominantly grey muddy matrix sediments. Based on distinct variations in coral content and coral clast size, the core is subdivided into three units. The lowermost part of the core (522-460 cm core depth) exhibits relatively high coral contents of around 30-50 surf.% with generally large coral clasts of 3-5 cm. Between 460 and 190 cm core depth, the coral contents decrease to around 10-30 surf.%. The size of the coral clasts varies mainly between 1-3 cm in length, while large coral clasts of about >3 cm in length occur occasionally at core depths of 495-460 cm, 415-335 cm and 250-200 cm. In the uppermost section of the core (190 cm to core top), very low coral content of <5 surf.% comprising coral clasts of 1-2 cm in size concentrated at core depths of 180-168 cm, 85-79 cm, and 20-0 cm, while in between these intervals, no coral clasts are visible.

Core MD13-3452G contains CWC fragments throughout the core, which are embedded in olive grey muddy matrix sediments. Changes in coral content and coral clast size allowed to divide the core into

three units. The lowermost three meters of the core (558-270 cm core depth) reveal the highest coral content that varies between 30 and 70 surf.%, with overall rather large coral clasts of 1-5 cm in size. Between 270 and 92 cm core depth, the coral content decreases to 30-50 surf.% and also the coral clast sizes decrease to 1-2 cm. For the uppermost part of the core (92 cm to core top), coral content again decreases to 10-30 surf.%. Coral clasts are rather small, with sizes of ~1 cm, only in the uppermost 20 cm, large coral clasts are found.

6.4.1.2 CT-based classification of cold-water coral preservation patterns of on-mound cores GeoB18127-1 and GeoB18130-1

For the two on-mound cores GeoB18127-1 and GeoB18130-1, the CT analyses allowed for the differentiation of three CPPs following the approach of Titschack et al. (2015). Considering the CWC clast size and orientation, the three CPPs are defined as (i) CPP A: coral framework in living position characterised by large average coral clast size of $>$-4.7 Φ ($>$2.6 cm) and variable orientations of up to 90°; (ii) CPP B: slightly collapsed coral framework marked by moderate average coral clast sizes of -4.7 to -4.4 Φ (~2.6-2.1 cm) and orientation $< $ 60°; and (iii) CPP C: coral rubble defined by small average coral clast sizes of $<$-4.5 Φ (~1.3 cm) and orientations of $<$45° or no clear orientation (Figs. 6-2, 6-3). The average coral content varying between 9 and 23 vol.% could not be applied to clearly distinguish between the CPPs, and the values for clast sizes and orientation of the different CPPs slightly vary between the two cores (see Table 6-S1 in Supplementary Material).

In core GeoB18127-1, CPP A occurs at core depths of 473-395 cm (CPP A_1) and 190-70 cm (CPP A_2; Fig. 6-2), and CPP B was recognized between CPP A_1 and CPP A_2 at core depths of 360-190 cm. CPP C was identified at various core depths of 563-500 cm (CPP C_1), 500-473 cm (CPP C_2), 395-360 cm (CPP C_3) and 70-0 cm (CPP C_4). It is notable that the CPP C_1, identified at the bottom of the core GeoB18127-1 directly below CPP C_2 exhibits remarkably smaller coral clasts (~2.8 Φ/0.7cm) and lower coral contents (~9 vol.%) compared to all other core sections containing coral rubble (clast size: $>$-4.2 Φ / $>$2.1 cm; average coral contents: $>$16 vol.%; Fig. 6-2; see also Table 6-S1 in Supplementary Material). In core GeoB18130-1, CPP A was identified at core depths of 106-71 cm, while CPP B occurs below and above CPP A (CPP B_1: 148-106 cm; CPP B_2: 71-34 cm). Coral rubble (CPP C) was only recognised between 34 cm and the core top (Fig. 6-3).

6.4.2 Coral ages and coral mound aggradation rates

Four AMS ^{14}C ages were obtained from core MD13-3451G, which range from 13.8 kyr BP to 4.5 kyr BP. One age (13.8 kyr BP) plots into the B/A interstadial, two ages (11.5 kyr BP and 9.5 kyr BP) into the Early Holocene, and one age (4.5 kyr BP) into the Late Holocene (Table 6-2, Fig. 6-4). Between 13.8 kyr BP and 11.5 kyr BP, the coral mound AR amounts to 46 cm kyr^{-1}. During the Early Holocene, the coral mound AR was enhanced with 96 cm kyr^{-1} before it dropped to 38 cm kyr^{-1} between 9.5 kyr BP and 4.5 kyr BP (Table 6-2, Fig. 6-4).

For core MD13-3452G, eight AMS ^{14}C dates were obtained ranging from 14.0 kyr BP to 3.5 kyr BP (Table 6-2). Four ages (14.0-12.9 kyr BP) fall into the B/A, three ages (10.9-9.3 kyr BP) into the Early Holocene, and one age (3.5 kyr BP) into the early Late Holocene (Table 6-2, Fig. 6-4). During the B/A interstadial, the average coral mound AR amounts to 176 cm kyr^{-1} (min: 132 cm kyr^{-1}, max: 205 cm kyr^{-1}). Between 12.9 kyr BP and 10.9 kyr BP, a low average coral mound AR of 43 cm kyr^{-1} was obtained. In the Early Holocene, the average coral mound AR increased to 107 cm kyr^{-1} (min: 64 cm kyr^{-1}, max: 182 cm kyr^{-1}). The mound AR dropped to 15 cm kyr^{-1} in the following period between 9.3 kyr BP and 3.5 kyr BP (Table 6-2, Fig. 6-4).

For the core GeoB18127-1, sixteen U-series ages were obtained, ranging from 14.1 kyr BP to 5.4 kyr BP. Four ages (14.1-13.3 kyr BP) coincide with the B/A interstadial, nine ages (11.1-8.2 kyr BP) with the Early Holocene and four ages (7.8-5.4 kyr BP) with the Mid Holocene (Table 6-3, Fig. 6-4). One age at 159 cm core depth (8.55±0.12 kyr BP), is in the error range of the slightly younger age obtained at 189 cm core depth (8.51±0.17 kyr BP; Table 6-3), and was ignored for the calculation of the coral mound AR. In addition, two ages obtained from *M. oculata* and *L. pertusa* at the same core depth of 79 cm, revealed slightly differing ages of 7.81±0.16 kyr BP and 8.23±0.14 kyr BP, respectively. However, this difference is most likely due to the 3-dimensional complexity of the depositional environment, potentially linked to a reduction of the mound AR (enhanced time averaging effect). The younger age may probably result from the recolonization of *M. oculata*, hence was not used for the calculation of coral mound ARs. During the B/A interstadial, the calculated average mound AR amounts to 113 cm kyr^{-1} (min: 20 cm kyr^{-1}, max: 547 cm kyr^{-1}; Table 6-3). Between 13.3 kyr BP and 11.1 kyr BP, no CWC ages were obtained, and the coral mound AR during this short interval exhibits low values of 14 cm kyr^{-1}. Between 11.1 kyr BP and 7.6 kyr BP (largely corresponding to the Early Holocene), a mean mound AR of 90 cm kyr^{-1} (min: 40 cm kyr^{-1}, max: 479 cm kyr^{-1}) was obtained. During the Mid Holocene (5.8-5.4 kyr BP; Fig. 6-4), low coral mound ARs of 21 and 37 cm kyr^{-1} are reported (Table 6-3; Fig. 6-4).
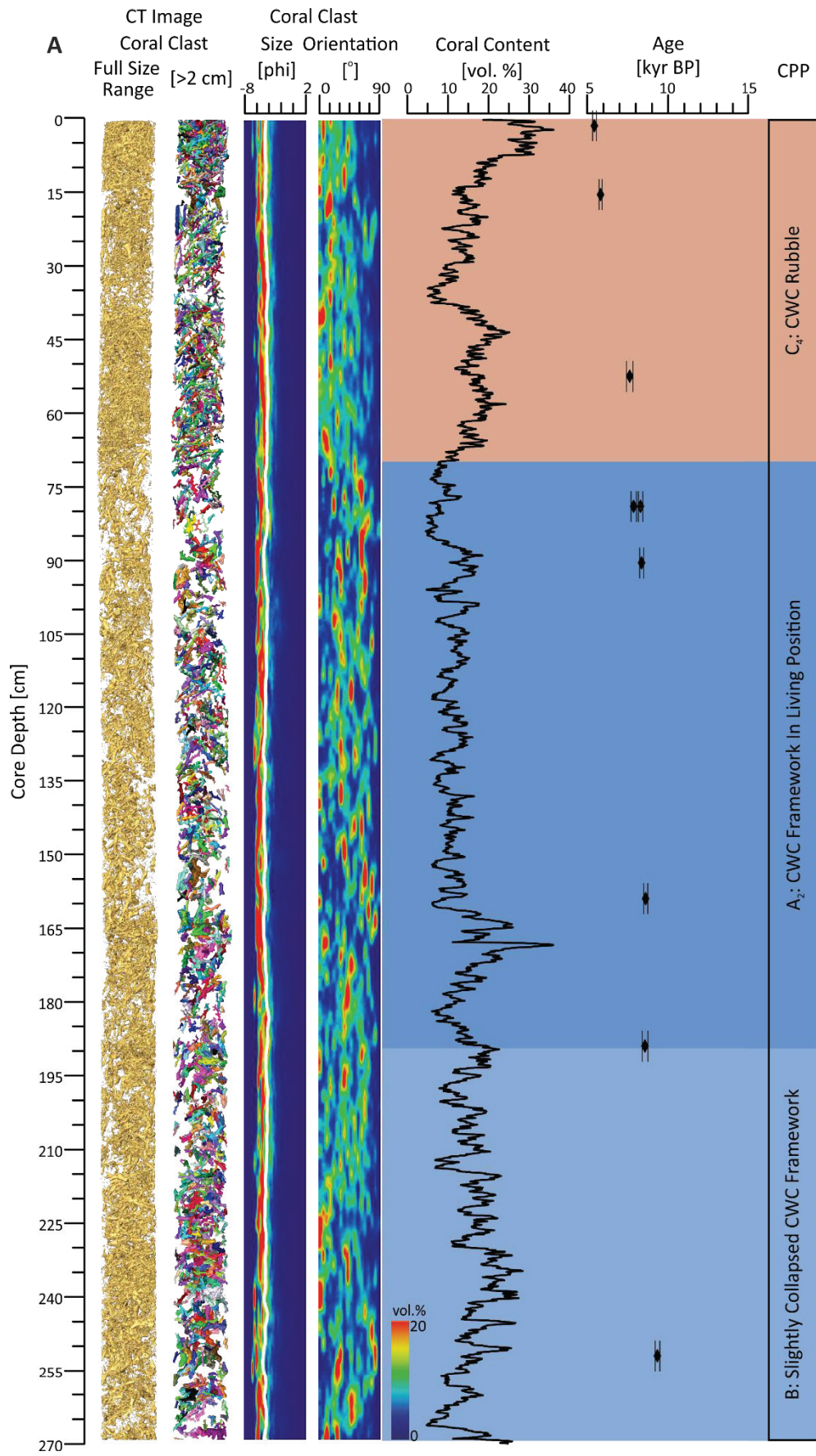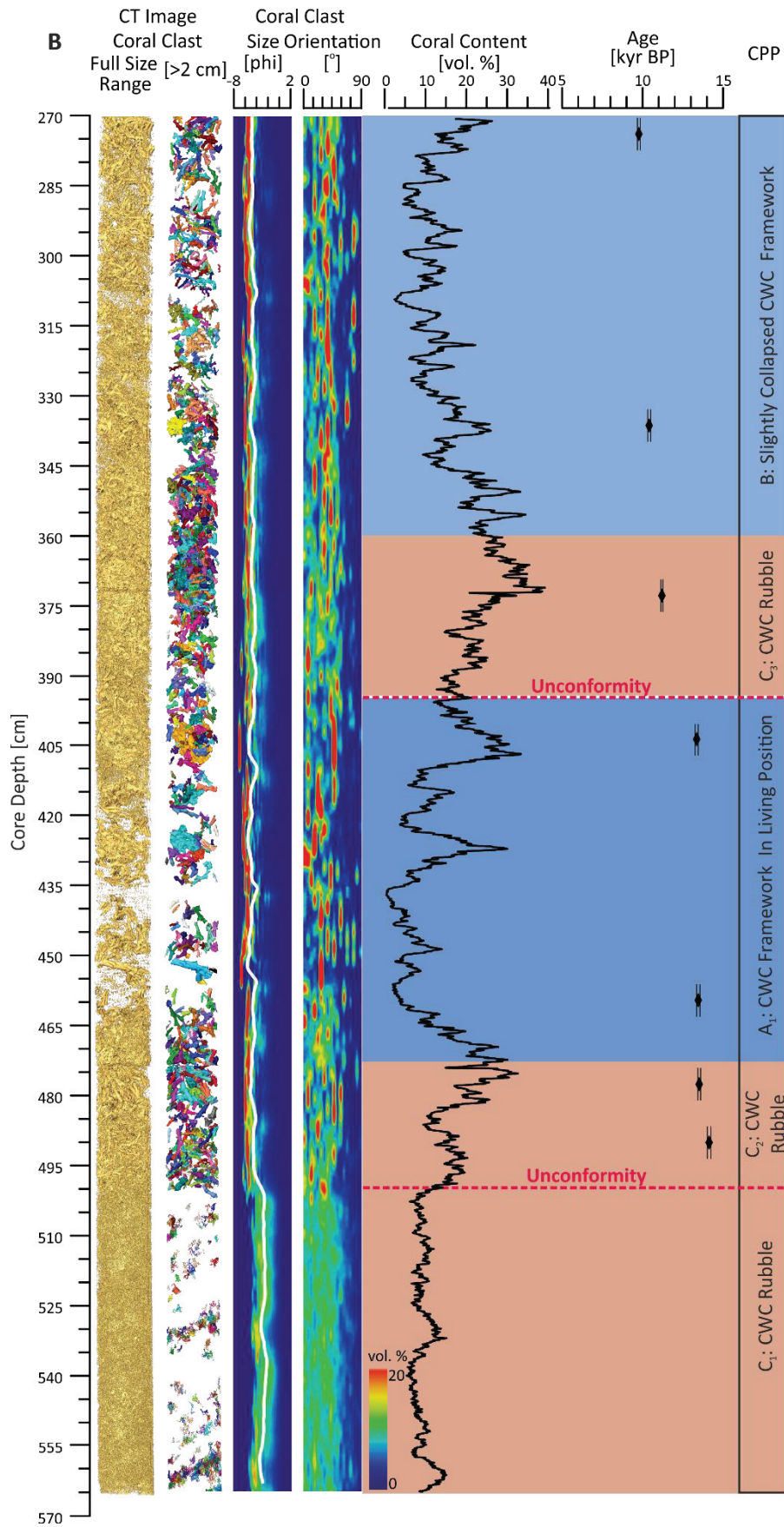
Figure. 6-2. Log of the on-mound core GeoB18127-1 (**A**: 0-269 cm, **B**: 270-563 cm core depth) retrieved from a coral mound of the West Melilla cold-water coral mound province. From left to right: Core CT 3D image of

coral clast in full size range, coral clast larger than >2 cm, coral clast size distribution (white line indicates the mean clast size), coral clast orientation, quantified coral content based on the CT data, and U-series coral ages. Three different cold-water coral (CWC) preservation patterns (CPPs) were recognized. CPP A: CWC framework in living position (highlighted by blue shading), CPP B: slightly collapsed CWC framework (highlighted by light blue shading), and CPP C, CWC rubble (highlighted by light red shading). Red dashed lines represent two unconformities identified at core depths of 500 cm and 395 cm.
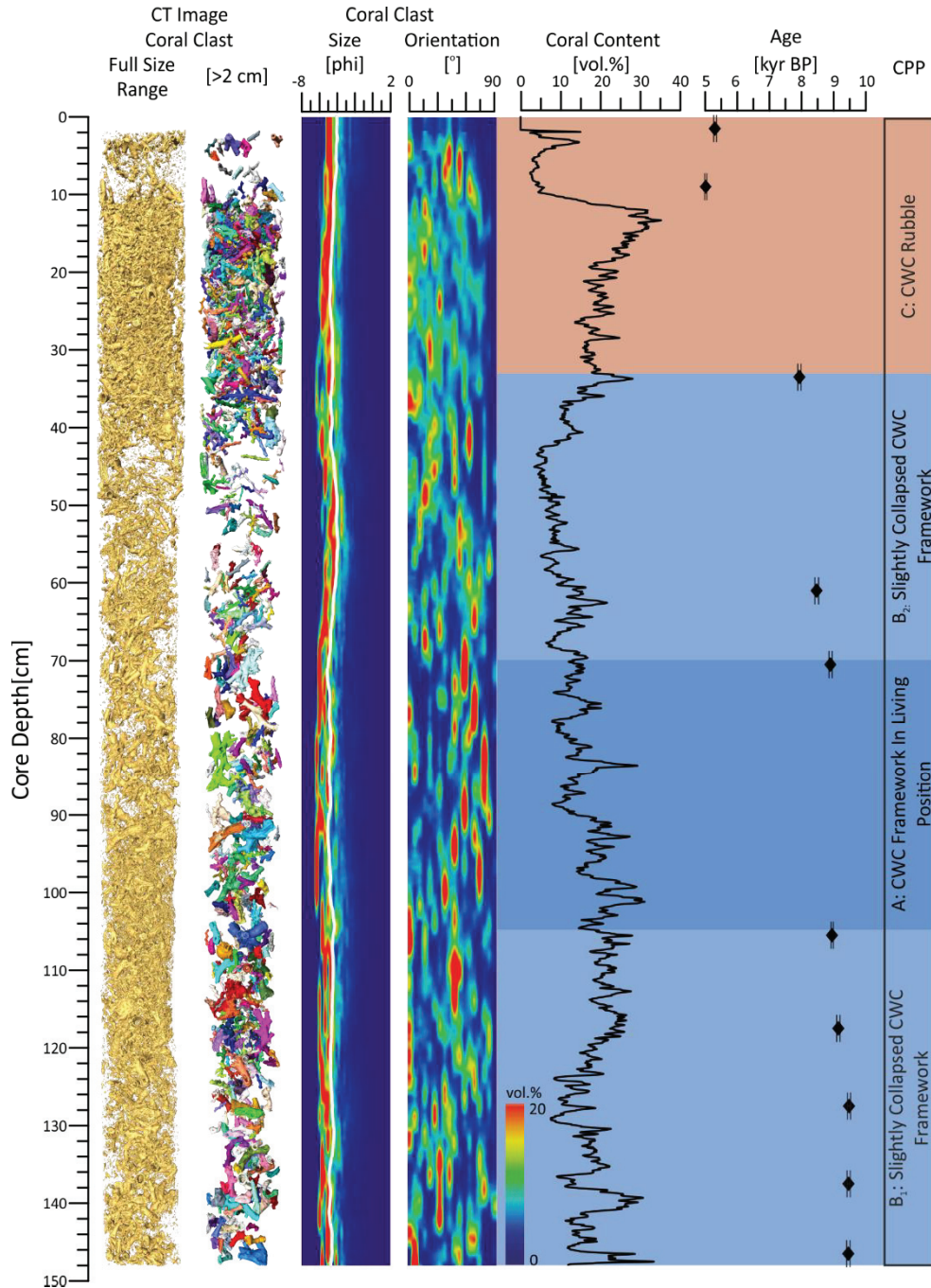
Figure. 6-3. Log of the on-mound core GeoB18130-1 (0-148 cm core depth) collected from a coral mound in the West Melilla cold-water coral mound province. From left to right: Core CT 3D image of coral clast in full size range, coral clast large than >2 cm, coral clast size distribution (white line indicates the mean clast size), coral clast orientation, quantified coral content based on the CT data, and U-series coral ages. Three different cold-water coral (CWC) preservation patterns (CPPs) were recognized. CPP A: CWC framework in living position (highlighted by blue shading), CPP B: slightly collapsed CWC framework (highlighted by light blue shading), and CPP C: CWC rubble (highlighted by light red shading).

Table 6-2. AMS ^{14}C dates obtained from CWC fragments collected from the on-mound cores MD13-3451G and MD13-3452G. The ages were corrected for ^{13}C and a reservoir age of 400 years. The AMS ^{14}C ages were converted into calendar age with the CALIB 7.10 (Stuiver and Reimer, 1993; http://calib.org/calib/calib.html), using the MARINE-13 curve (Reimer et al., 2013). Coral mound aggradation rates (ARs) are calculated based on a linear interpolation of the coral ages.

Core ID (MD13-)	Core Depth [cm]	Lab-code	Coral Species	Conventional Age [kyr] BP		2σ range cal. age [kyr BP P=AD 1950]		Median Probability Age [kyr BP]	AR [cm kyr^{-1}]
				^{14}C age	± error				
3451G	5	Poz-62332	*M. oculata*	4.37	0.03	4.41	4.61	4.51	-
3451G	197	Poz-62333	*L. pertusa*	8.90	0.04	9.47	9.66	9.54	38.1
3451G	382	Poz-62334	*L. pertusa*	10.39	0.05	11.24	11.74	11.47	96.3
3451G	488	Poz-62335	*L. pertusa*	12.32	0.05	13.63	13.95	13.79	45.5
3452G	13	Poz-62336	*M. oculata*	3.58	0.03	3.38	3.56	3.47	-
3452G	99	Poz-62337	*M. oculata*	8.61	0.04	9.13	9.40	9.28	14.8
3452G	203	Poz-62338	*M. oculata*	9.11	0.05	9.66	10.09	9.85	181.8
3452G	267	Poz-62339	*L. pertusa*	9.90	0.04	10.70	11.02	10.85	63.6
3452G	355	Poz-62340	*M. oculata*	11.45	0.05	12.75	13.08	12.91	42.7
3452G	406	Poz-62341	*L. pertusa*	11.83	0.07	13.16	13.44	13.30	131.8
3452G	467	Poz-62342	*L. pertusa*	12.17	0.05	13.46	13.78	13.62	191.8
3452G	550	Poz-62343	*L. pertusa*	12.54	0.05	13.87	14.16	14.02	204.9

Table 6-3. U/Th dates, uranium and thorium isotope concentrations and ratios obtained from CWC fragments collected from the on-mound cores GeoB18127-1 and GeoB18130-1 (n.d. not determinable). Coral mound aggradation rates (ARs) are calculated based on a linear interpolation of the coral ages.

Core ID [GeoB]	Core Depth [cm]	Lab-code	Coral Species	Age [kyr BP]	± [kyr]	^{238}U [ppm]	± [ppm]	^{232}Th [ppb]	± [ppb]	δ^{234}U$_0$ [‰]	error	AR [cm kyr^{-1}]
18127-1	1	IUP-7734	*M. oculata*	5.39	0.12	4.218	0.0006	0.282	0.009	150.5	2.7	-
18127-1	15	IUP-7735	*M. oculata*	5.76	0.09	4.233	0.0005	n.d.		146.9	3.1	37.2
18127-1	52	IUP-7736	*L. pertusa*	7.56	0.20	3.362	0.0007	n.d.		150.3	3.0	20.5
18127-1	79	IUP-7737	*M. oculata*	#7.81	0.16	4.122	0.0005	0.101	0.006	149.5	2.6	-
18127-1	79	IUP-7738	*L. pertusa*	#8.23	0.14	3.445	0.0004	0.199	0.007	149.4	3.1	40.4
18127-1	90	IUP-7739	*L. pertusa*	8.30	0.12	3.182	0.0004	0.057	0.002	149.3	3.0	158.3
18127-1	159	IUP-7740	*L. pertusa*	8.55	0.12	4.168	0.0005	0.622	0.010	150.7	2.8	-
18127-1	189	IUP-7741	*L. pertusa*	8.51	0.17	3.921	0.0005	0.229	0.007	151.9	3.4	479.0
18127-1	252	IUP-7742	*L. pertusa*	9.28	0.14	3.234	0.0004	n.d.		148.2	2.7	82.0
18127-1	274	IUP-7743	*L. pertusa*	9.70	0.08	3.659	0.0004	0.091	0.002	149.3	2.6	51.7
18127-1	337	IUP-7744	*L. pertusa*	10.35	0.09	3.420	0.0003	0.179	0.002	143.3	2.5	97.7
18127-1	373	IUP-7745	*L. pertusa*	11.14	0.07	4.177	0.0003	0.293	0.002	145.8	1.9	45.2
18127-1	404	IUP-7746	*L. pertusa*	13.30	0.10	3.398	0.0002	0.354	0.002	149.8	2.1	14.4
18127-1	460	IUP-7747	*L. pertusa*	13.40	0.10	3.712	0.0002	0.224	0.002	148.7	1.4	546.9
18127-1	478	IUP-7748	*L. pertusa*	13.45	0.09	3.758	0.0002	0.323	0.002	149.6	2.2	335.2
18127-1	491	IUP-7749	*L. pertusa*	14.07	0.11	3.288	0.0002	0.362	0.002	148.9	1.5	20.2
18130-1	2	IUP-7750	*M. oculata*	5.28	0.04	4.514	0.0003	0.166	0.001	146.8	2.0	-
18130-1	9	IUP-7751	*M. oculata*	*5.00	0.03	3.989	0.0002	0.050	0.000	149.9	1.8	-
18130-1	34	IUP-7752	*M. oculata*	7.88	0.05	3.957	0.0002	0.256	0.002	148.6	1.4	12.4
18130-1	61	IUP-7753	*M. oculata*	8.41	0.06	3.773	0.0003	0.136	0.001	148.1	1.9	51.0
18130-1	71	IUP-7754	*L. pertusa*	8.83	0.05	4.062	0.0002	0.387	0.001	149.5	0.9	23.6
18130-1	106	IUP-7755	*L. pertusa*	8.88	0.04	3.506	0.0002	0.232	0.001	149.1	0.9	704.2
18130-1	118	IUP-7756	*M. oculata*	9.07	0.05	3.735	0.0002	0.334	0.002	147.7	0.9	63.1
18130-1	128	IUP-7757	*L. pertusa*	9.40	0.05	3.483	0.0002	0.713	0.003	149.3	1.1	
18130-1	138	IUP-7758	*L. pertusa*	9.38	0.05	3.851	0.0002	0.627	0.002	149.1	0.9	> 270
18130-1	147	IUP-7759	*L. pertusa*	9.37	0.05	4.131	0.0002	0.306	0.001	148.9	1.4	

*: age reversal. #: two different ages obtained from *L. pertusa* and *M. oculata* at the same core depth, see text for explanation.

79

Within the core GeoB18130-1, ten U-series ages ranging from 9.4 kyr BP to 5.0 kyr BP were obtained, with seven ages (9.4-7.9 kyr BP) corresponding to the Early Holocene and three ages (7.9-5.0 kyr BP) to the Mid Holocene. One age reversal occurs at the top of the core, most likely due to sediment disturbance during the coring process. The age of 5.28±0.04 kyr BP at 2 cm core depth, was used for the calculation of the coral mound AR. Three ages obtained at the bottom of the core (128-147 cm core depth), show slightly increasing ages from bottom to top (9.37±0.05 kyr BP to 9.40±0.05 kyr BP), though the differences of these ages are within each other's error ranges. This points to a short phase of fast mound formation (9.37-9.40 kyr BP), during which the AR reached values of >270 cm kyr^{-1}. Between 9.1 kyr BP and 7.9 kyr BP (largely corresponding to the Early Holocene), the average coral mound AR was 76 cm kyr^{-1} (min: 24 cm kyr^{-1}, max: 704 cm kyr^{-1}; Table 6-3, Fig. 6-4), while between 7.9 kyr BP and 5.0 kyr BP, the coral mound AR declined to ~12 cm kyr^{-1} (Table 6-3).
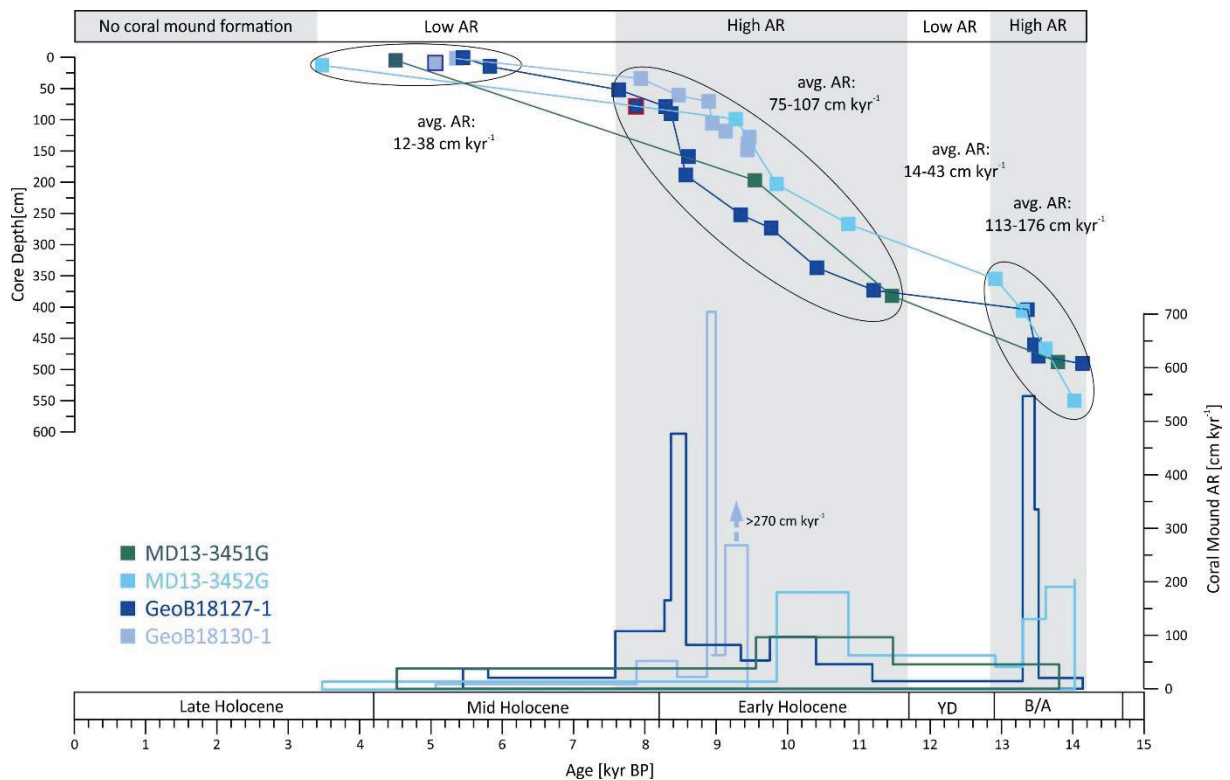

Figure. 6-4. Cold-water coral (CWC) ages (filled squares) versus core depth and corresponding calculated coral mound aggradation rates (ARs) of four on-mound cores collected in the West Melilla cold-water coral mound province (WMCP, see legend for core-ID and color code). Filled square with blue frame indicates an age reversal and filled square with red frame indicates an age obtained from *Madrepora oculata*, both of which were not used for the calculation of ARs (see text for explanation). The CWC ages cluster in three periods, which mainly correspond to the Bølling-Allerød (B/A) interstadial, the Early Holocene and the Mid Holocene (highlighted by ovals). During the B/A and the Early Holocene, highest ARs are obtained with average (avg.) values ranging between 75 and 176 cm kyr^{-1}. During the Younger Dryas (YD), the avg. ARs decreased to 14-43 cm kyr^{-1}. In the Mid Holocene, the avg. ARs range between 12 and 38 cm kyr^{-1}. Since the onset of the Late Holocene, mound formation in the WMCP seems to stagnate. The B/A, the YD and the sub-periods of the Holocene are temporally defined according to Walker et al. (2012) and Lowe et al. (2008).

6.4.3 Background palaeo-environmental record from off-mound core GeoB18131-1

6.4.3.1 Chronology

The chronology of the off-mound core GeoB18131-1 is constrained by six AMS ^{14}C ages, which range between 20.3 kyr BP (at 360 cm core depth) and 0.3 kyr BP (core top; Table 6-4). The age model is supported by the visual correlation between the $\delta^{18}O_{Cib}$ record and the LR04 $\delta^{18}O$ stack record (Lisiecki and Raymo, 2005). For the tie-point correlation of the lower part of the core (855-360 cm core depth), six visual correlation-points were selected. The obtained age model suggests an age of approximately 110 kyr BP for the bottom of the core (~850 cm core depth), hence the entire record covers the last interglacial (Marine Isotope Stage 5, MIS 5), the last glacial (MIS 2-4) and the recent interglacial (MIS 1; Fig. 6-S2 in Supplementary Material). The $\delta^{18}O_{Cib}$ record shows values of 4.0-1.9‰ for the last interglacial, heavy values of 4.3-3.1‰ for the last glacial, and light values of 3.3-1.5‰ for the Holocene. The calculated sedimentation rate displays an increasing trend towards the Holocene. During the MIS 5, the sedimentation rate was less than 5 cm kyr^{-1}, while during most of the last glacial period, it amounts to 6-9 cm kyr^{-1}. Only during the Last Glacial Maximum (LGM), the sedimentation rate significantly increased to 27 cm kyr^{-1}. During the Holocene, the sedimentation rate varied between 8 cm kyr^{-1} and 21 cm kyr^{-1} (Fig. 6-S2 in Supplementary Material).

6.4.3.2 Palaeo-environmental proxies

The main aim of this research is to relate the temporal occurrence of CWCs and coral mound development to distinct changes in the palaeo-environment. As the herein presented coral ages reach only 14.1 kyr BP back in time, all presented proxy records are restricted to the last 26 kyr to elucidate any changes across the last glacial-interglacial transition (the entire off-mound core proxy records are presented in Fig. 6-S2 in the Supplementary Material).

During the last 26 kyr, the $\delta^{13}C$ values of the mixed benthic foraminifera ($\delta^{13}C_{Cib}$) range from 1.1‰ to 0.3‰ (Fig. 6-5A). Before ~13.3 kyr BP, the $\delta^{13}C$ values fluctuate between 0.6‰ and 1.1‰. Between 13.3 kyr BP and 7.6 kyr BP, the $\delta^{13}C_{Cib}$ record displays a conspicuous decreasing trend, declining from 1.0‰ to 0.5‰. Since 7.6 kyr BP, the $\delta^{13}C_{Cib}$ values fluctuate between 0.3‰ and 0.6‰ (Fig. 6-5B).

The mean grain size ranges from ~17 μm to 5 μm during the last 26 kyr (Fig. 6-5B). Between 26 kyr BP and ~16 kyr BP, the mean grain size is low with values mainly below 8 μm. Since 16 kyr BP, the mean grain size gradually increases, reaching a maximum value of 17 μm at ~12 kyr BP. Since then it shows a decreasing trend, and the mean grain size value remains again below 8 μm for the last 8 kyr (Fig. 6-5C).

The BFARs vary between 1 and 27 $\times 10^3$ individuals cm^{-2} kyr^{-1} during the last 26 kyr (Fig. 6-5D). Before ~17 kyr BP, the BFARs are low, only showing peak values of up to 13 $\times 10^3$ individuals cm^{-2} kyr^{-1} during the LGM. Since ~17 kyr BP, the BFARs show a gradually increasing trend until the

highest BFARs of up to ~27 ×10^3 individuals cm^{-2} kyr^{-1} at ~10.8 kyr BP. Between 10.8 kyr BP and 7.6 kyr BP, the BFARs rapidly decline to ~8 ×10^3 individuals cm^{-2} kyr^{-1}. Afterwards, the BFARs remain low, with values of below 5 ×10^3 individuals cm^{-2} kyr^{-1} (Fig. 6-5D).

Table 6-4. AMS ^{14}C dates of mixed planktonic foraminifers obtained from the off-mound core GeoB18131-1. The ages were corrected for ^{13}C and a reservoir age of 400 years. The AMS ^{14}C ages were converted into calendar age with the CALIB 7.10 (Stuiver and Reimer, 1993; http://calib.org/calib/calib.html), using the MARINE-13 curve (Reimer et al., 2013). Below 400 cm core depth, the age model is based on visual tie-point correlation between the δ^{18}O record of core GeoB18131-1 and the LR04 δ^{18}O stack record (Lisiecki and Raymo, 2005). Sedimentation rates are calculated based on a linear interpolation of the AMS ^{14}C dates and tie points.

Core ID [GeoB]	Core Depth [cm]	Lab-code	Conventional Age		2σ range cal. age [kyr BP P=AD 1950]		Median Probability Age [kyr BP]	Sedimentation Rate [cm kyr^{-1}]
			^{14}C age [kyr]	± error [kyr]				
18131-1	3	Poz-84167	0.63	0.03	0.189	0.376	0.3	-
18131-1	168	Poz-84348	7.84	0.05	8.183	8.394	8.3	20.5
18131-1	193	Poz-84349	9.49	0.05	10.217	10.484	10.3	12.3
18131-1	198	Poz-84350	9.74	0.05	10.506	10.793	10.6	16. 5
18131-1	273	Poz-84351	17.50	0.1	20.335	20.913	20.6	7.5
18131-1	363	Poz-84300	20.27	0.32	23.040	24.697	23.9	27.5

Core ID [GeoB]	Core Depth [cm]					Tie-Point Age [kyr BP]	Sedimentation Rate [cm kyr^{-1}]
18131-1	423	Tie points to the LR04 δ^{18}O stack record (Lisiecki & Raymo, 2005)				32	7.4
18131-1	608					52.5	9.0
18131-1	708					68	6.5
18131-1	758					80	4.2
18131-1	768					82	3.0
18131-1	848					110	2.9

6.5 Discussion

Within the Alboran Sea, the two most common framework CWC species, *L. pertusa* and *M. oculata*, have been found on various seamounts and volcanic banks along the continental slope off Spain, on ridges (e.g., Alboran ridge), and on some mud volcanoes in the western Alboran Sea (Lo Iacono et al., 2008; Margreth et al., 2011; Palomino et al., 2011; De Mol et al., 2012; Lo Iacono et al., 2012; Palomino et al., 2015; Wienberg, 2019). Coral mounds are far more seldom and mainly concentrate in the southern Alboran Sea, comprising the mound clusters of the EMCP and the WMCP (Lo Iacono et al., 2014; Hebbeln, 2019; Wienberg, 2019). The discrepancy between the restricted occurrence of coral mounds in contrast to the widespread distribution of CWCs, though today mainly occurring as fossil accumulations rather than as living occurrences, hints to far more constrained (palaeo-)environmental conditions controlling coral mound formation compared to those promoting CWC growth (Wienberg and Titschack, 2017). The proliferation of CWCs, which is steered by various biotic and abiotic factors such as food supply, water masses properties, local hydrodynamic regime (e.g. Roberts et al., 2006; Davies and Guinotte, 2011) is a prerequisite for coral mound formation. Nevertheless, the construction of coral mounds as complex geological structures is the result of a well-

balanced interplay between a sustained growth of CWC, which form coral frameworks with high sediment baffling capacity, and a contemporaneous supply of sediments stabilizing the biogenic construction (e.g., Thierens et al., 2013; Titschack et al., 2015).

Any variations in the temporal development of coral mounds are reflected by varying ARs as well as by changes in the preservation state of the deposited CWC clasts (see Titschack et al., 2015; Titschack et al., 2016). In this context, high vertical mound aggradation is the result of pronounced CWC growth and enhanced sediment supply, thereby current-transported sediments become entrapped within the coral framework. The fast burying of CWC frameworks prevents them from biodegradation and physical fragmentation, and may even allow the deposition of CWC framework in living position (Titschack et al., 2015). In contrast, during times of reduced CWC growth, coral mounds aggradation is slowed down and can eventually stagnate, the latter being documented as unconformities in the sedimentary record. Furthermore, when the dead coral framework (not covered by an organic tissue) remains exposed for a prolonged time on the mound's surface due to lack of substantial sediment cover, degradation and fragmentation of the coral skeletons may occur, eventually resulting in the formation of coral rubble. Thus, mound ARs calculated from coral dates in combination with the CPPs can be used to reconstruct the temporal development of coral mounds in much detail.

6.5.1 Cold-water coral mound formation in the southern Alboran Sea since the last deglaciation

6.5.1.1 Re-activation of coral mound formation during the B/A interstadial
While quite some information exists already on the formation of the coral mounds of the EMCP since the last deglaciation (Fink et al., 2013; Stalder et al., 2015), up to this study no information was available about the temporal development of the mounds in the neighbouring WMCP. Considering their present-day average height of 8-35 m above the seafloor and their additional subsurface extension on one hand (Lo Iacono et al., 2014), and the maximum on-mound core recovery of less than 6 m on the other hand (Table 6-1), this study, can however only decipher the most recent period(s) of mound development.
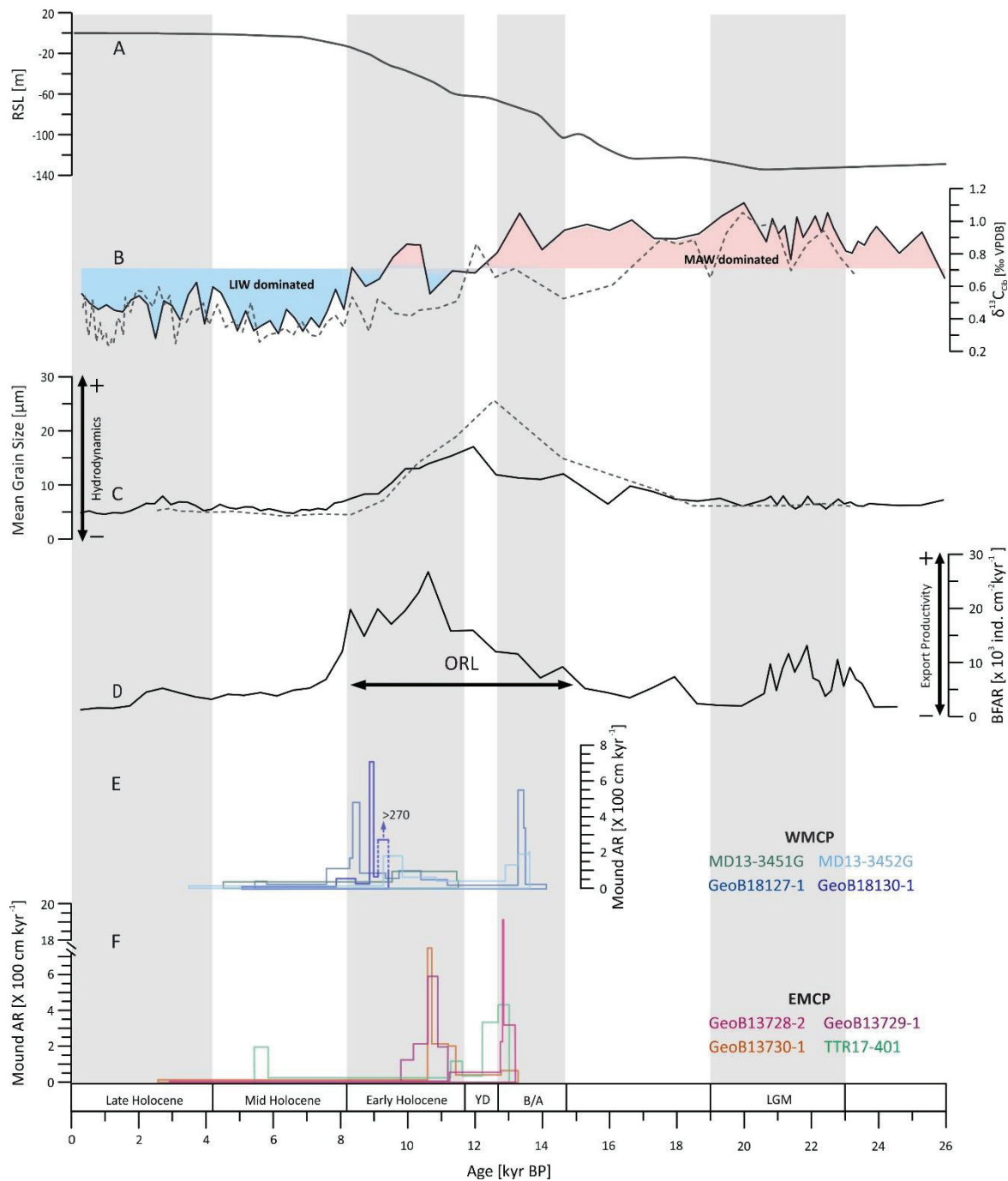
Figure. 6-5. Compilation of paleoceanographic multi-proxy data obtained from the off-mound core GeoB18131-1 collected in the West Melilla cold-water coral mound province (WMCP) focusing on the past 26 kyr supplemented by other paleoceanographic records. A: Relative Sea Level (RSL) record (Lambeck et al., 2014). B: $\delta^{13}C_{Cib}$ records of mixed benthic foraminifers (*Cibicidoides mundulus* and *Cibicidoides pachyderma*) obtained for the WMCP (black line; this study) and of *Cibicidoides kullenbergi* obtained for the East Melilla cold-water coral mound province (EMCP; grey dashed line; Fink et al., 2013) used as a proxy for water column structure. Pink shading indicates a dominance of the Modified Atlantic Water (MAW) during the last glacial, while light blue shading marks a dominance of the Levantine Intermediate Water (LIW) since the Mid Holocene. C: Mean grain size used as proxy for bottom current strength (WMCP: black line, this study; EMCP: grey dashed line, Fink et al., 2013). D: Benthic foraminifera accumulation rate (BFAR) record obtained from the WMCP and used as a proxy for export productivity. (E-F) Cold-water coral mound aggradation rates (ARs) obtained from various on-mound cores collected from (E) the WMCP (this study) and (F) the EMCP (Fink et al., 2013; Stalder et al., 2015). The Last Glacial Maximum (LGM) and rapid events during the deglaciation (B/A: Bølling-Allerød, YD: Younger Dryas) and sub-periods of the Holocene are temporally defined according to Walker et al. (2012) and Lowe et al. (2008). MIS: Marine Isotope Stage.

The oldest ages obtained from the coral mounds of the WMCP range between 14.1 kyr BP and 12.9 kyr BP, and represent a pronounced coral mound formation stage during the B/A interstadial with high ARs of 113-176 cm kyr^{-1} on average (and even maximum ARs of up to 500 cm kyr^{-1}; Tables 6-2, 6-3, Fig. 6-4). The CPP obtained from the core GeoB18127-1 indicate that coral rubble of B/A age (defined as CPP C_2 in Fig. 6-2) rest on small-sized CWC rubble (defined as CPP C_1 in Fig. 6-2). Both CWC rubble-dominated sections are separated by a distinct unconformity. The high fragmentation grade of the pre-B/A CWC rubble deposits indicate that these coral clasts rested for a long time exposed on the mound's surface without any coverage (by sediments or living CWCs). Unfortunately, these CWC clasts were too small and showed strong corrosion avoiding their usage for absolute dating. Therefore, without the support of longer dated core records, the timing of coral mound development before the last deglaciation cannot be further constrained.

Nevertheless, the re-initiation of coral mound formation during the last deglaciation started at ~14.1 kyr BP, interestingly fitting with similar observations obtained from various coral mound records of the EMCP (~13.3-13 kyr BP; Fink et al., 2013; Stalder et al., 2015). The slight temporal off-set (~800 years) in the timing of the deglacial coral re-colonization, and hence, re-initiation in mound formation between both provinces might simply be explained by the limited length of the mound core records available for the EMCP, avoiding to collect coral fragments of early B/A-age. The CPP displayed in core GeoB18127-1, with CWC rubble (CPP C_2) being present at the base of the B/A period along with the associated initial low AR of 21 cm kyr^{-1} (Figs. 6-2, 6-4), point to a rather slow post-glacial start-up phase in coral mound formation for the WMCP. This observation contrasts with results from the EMCP, which suggest a sudden and fast start-up phase of CWC colonization (Fink et al., 2013; Titschack et al., 2016). Since ~13.5 kyr BP, the CPP in core GeoB18127-1 changed from CWC rubble to CWC framework being preserved in living position (CPP A_1; Fig. 6-2), which indicates enhanced CWC growth as well as increased sediment deposition. Also both MD cores show rather large coral clasts (3-5 cm in size) in their lower core intervals that correspond to the B/A (see Fig. 6-S1 in the Supplementary Material), indicating that coral frameworks were rapidly buried by sediments, preventing them from being strongly fragmented. This is further supported by a significant increase of the coral mound ARs to average values of 176-493 cm kyr^{-1} (calculated for cores MD13-3452G and GeoB18127-1; Tables 6-2, 6-3, Fig. 6-4), which are in the range of coeval average ARs of 385-416 cm kyr^{-1} obtained from mounds in the EMCP (Fink et al., 2013; Stalder et al., 2015).

6.5.1.2 Temporal stagnation in mound formation during the YD cold event
During the YD, coral mound formation significantly slowed down. No coral ages were obtained between 12.9 kyr BP and 11.5 kyr BP, and coral mound ARs significantly decreased to 14-43 cm kyr^{-1} (calculated for cores MD13-3452G and GeoB18127-1; Tables 6-2, 6-3, Fig. 6-4). Moreover, a distinct unconformity was identified in core GeoB18127-1 marked by an abrupt change in the CPPs from

CWC framework preserved in living position (CPP A$_1$) to CWC rubble (CPP C$_3$; Fig. 6-2). Also for the coral mounds of the EMCP, a distinct reduction in mound aggradation was indicated during the YD (AR: 31-38 cm kyr^{-1}; see also Fig. 6-5; Fink et al., 2013; Stalder et al., 2015), although based on the available datings it appears that this reduction seems to encompass a shorter time period only corresponding to the late YD (12.2-11.6 kyr BP; Stalder et al., 2015).

6.5.1.3 Coral mound formation during the Early Holocene
The most recent period of coral mound formation in the WMCP started at ~11.5 kyr BP during the onset of the Early Holocene, and simultaneously to the start of the Early Holocene mound formation period indicated for the EMCP (11.6-11.4 kyr BP; see Fig. 6-5; Fink et al., 2013; Stalder et al., 2015). As already identified for the B/A mound formation period, there seems to be again a slow start-up phase in mound formation in the WMCP. The CPP in core GeoB18127-1 reveals at the beginning of this period the deposition of CWC rubble (CPP C$_3$; Fig. 6-2), and also for the cores MD13-3451G and MD13-3452G, the lower Early Holocene deposits are marked by small sized coral clasts (see Fig. 6-S1 in Supplementary Material). This overall points to hampered CWC growth and low sediment deposition, which is further evidenced by rather low to moderate ARs of 46-97 cm kyr^{-1}. However, already within a few hundreds of years, ARs increased to values of >100 cm kyr^{-1} (even temporarily reaching values of up to 700 cm kyr^{-1}; Tables 6-2, 6-3, Fig. 6-4), although the available CWC ages do not allow to temporally constrain this transition. The increased ARs are accompanied by CPPs that vary between slightly collapsed CWC framework and CWC framework preserved in living position (indicated for cores GeoB18127-1 and GeoB18130-1; Figs. 6-2, 6-3). Overall, the average coral mound ARs during the Early Holocene range between 75 and 107 cm kyr^{-1} (Tables 6-2, 6-3, Fig. 6-4). Hence, in comparison to average ARs obtained for the EMCP, which varied between 140 and 291 cm kyr^{-1} (Fink et al., 2013; Stalder et al., 2015), coral mound formation in the WMCP seems to be less pronounced. In addition, while the highest mound aggradation in the EMCP (ARs mainly above 190 cm kyr^{-1}) already occurred directly at the beginning of the Early Holocene mound formation period at 11.6 kyr BP and lasted until ~10.2 kyr BP, the coral mounds of the WMCP experienced their most pronounced Holocene aggradation (ARs mainly above 150 cm kyr^{-1}) between ~9.9 and 8.3 kyr BP, thus about 1700 years later than the boost of the EMCP mound formation (Fig. 6-5).

6.5.1.4 Slow-down in coral mound formation since the Mid Holocene
Coral mound formation in the WMCP significantly slowed down since the early Mid Holocene (at ~7.6 kyr BP), which is mainly reflected by a strong decrease of the coral mounds ARs to values of 12-38 cm kyr^{-1} (indicated for all cores; Tables 6-2, 6-3, Fig. 6-4). Moreover, in both GeoB cores, the CPPs abruptly changed from coral framework to CWC rubble (Geob18127-1: CPP A$_2$ to C$_4$, Fig. 6-2; GeoB18130-1: CPP B$_2$ to C, Fig. 6-3) during this period, as also shown in both MD cores, where only

a sparse occurrence of small-sized coral clasts was indicated, pointing to a reduced CWC growth and a low sediment input, both favouring the fragmentation of coral clasts. For the EMCP, a slow-down in mound formation with a significant decrease of the ARs to 4-22 cm kyr^{-1} already started at ~9.8 kyr BP (Fink et al., 2013; Stalder et al., 2015), thus over 2,000 years earlier compared to the WMCP.

The youngest CWC ages (n=5) obtained for the coral mounds of the WMCP range between 5.8 and 3.5 kyr BP (Tables 6-2, 6-3, Fig. 6-4), hence coral mound formation likely stagnated since the Late Holocene. Present day conditions suggest that CWCs seem to be completely absent from the coral mounds of the WMCP, with some of the ground-truthed mounds being buried by coral-barren sediments (Lo Iacono et al., 2014; Hebbeln et al., 2015). Also for the EMCP, the youngest obtained CWC ages (~2.9-2.6 kyr BP) are of Late Holocene ages, but in contrast to the WMCP, these mounds actually are covered by dead coral framework/rubble with sparse living CWC colonies (Hebbeln et al., 2009; Fink et al., 2013).

6.5.2 Palaeo-environmental controls on coral mound formation in the southern Alboran Sea

The temporal pattern in mound formation obtained for the coral mounds of the WMCP since the last deglaciation correlates well with distinct changes in the local palaeo-environmental conditions. In particular variations in the surface productivity and food supply, the water column structure, and the near-bottom hydrodynamics were identified to be the most important local or regional driver on the development of the CWC mounds (Fig. 6-5). Nevertheless, the reactivation of mound formation during the B/A interstadial, both in the WMCP and the EMCP, coincide with a major re-organisation of the thermohaline circulation in the entire Mediterranean basin. The rapid last deglacial sea-level rise (Fig. 6-5; Lambeck et al., 2014) resulted in an increased injection of low saline Atlantic waters due to a deepening of the Gibraltar sill (Sierro et al., 2005). Moreover, the enhanced glacial melting in the Alps and Apennines increased the inflow of freshwater into the Mediterranean Basin (e.g., Cacho et al., 2002; Ivy-Ochs et al., 2007; Rogerson et al., 2008), both leading to a freshening and reduced density of the surface waters. Concurrently, the sea surface temperatures increased up to 14 °C (e.g., Balearic Sea; Dubois-Dauphin et al., 2017). All these processes resulted in a slowdown of the Mediterranean Sea thermohaline circulation and caused a collapse of deep-water (WMDW) production in the Western Mediterranean Sea (Gulf of Lion), which led to an increased stratification of the water column and weakened ventilation of intermediate and deep-water masses (Cacho et al., 2001; Sierro et al., 2005; Rogerson et al., 2008; Toucanne et al., 2012). At the same time, the production of LIW in the eastern Mediterranean Sea (Levantine Basin) was enhanced, which caused intensification and increased inflow of the LIW into the western basin (Jiménez-Espejo et al., 2015). The strong influence of the LIW at the intermediate depths in the Alboran Sea since the last deglaciation is also documented in the neodymium isotopic composition of CWCs collected from the EMCP, though the Alboran Sea seems

to be rather insensitive to hydrological variations of the LIW, at least since 13.5 kyr BP until present (Dubois-Dauphin et al., 2017).

Studies from various sites in the western Mediterranean Sea revealed that the surface productivity gradually increased during the B/A (Fig. 6-5) due to a shoaling of the nutricline, and consequently also the export of organic matter was enhanced (Cacho et al., 2002; Jimenez-Espejo et al., 2008; Rogerson et al., 2008; Ausín et al., 2015) resulting in the deposition of the organic rich layer 1 (ORL1; 14.5-8.2 kyr BP) in the deep western Mediterranean Sea (Cacho et al., 2002). The BFAR record from the WMCP reveals a low export production during the last glacial before it significantly increased since 14 kyr BP, reached its maximum during the Early Holocene and dropped rapidly at the onset of the Mid Holocene (Fig. 6-6). This suggests a more or less synchronous increase of the BFAR export production with the formation of the ORL1, supporting the enhanced surface productivity, and even more important, highlighting an improved food delivery to the WMCP during this time interval since the deglaciation until the Mid Holocene has likely favoured the proliferation of CWCs and mound formation within the region, by contributing to their food supply (Fig. 6-5).

However, considerable differences in the BFAR between the two main mound formation phases marked by similar mound aggradation rates call for additional parameters in addition to palaeo-productivity that control mound formation. Interestingly, the grain-size distribution shows a similar pattern as the BFAR with coarser sediments occurring between 15 and 8 kyr BP (Fig. 6-5). The enhanced hydrodynamic energy reflected by this coarsening of the sediments further contributed to the food supply of the CWCs. The change in the grain size distribution coincides with our $\delta^{13}C_{Cib}$ record, which here is adopted to trace past changes in the water column structure (Fig. 6-5). During the last glacial, the intermediate depths of the WMCP were influenced by waters with relatively high $\delta^{13}C_{Cib}$ values (0.8-1.1‰; Fig. 6-5), which we interpret to represent the effect of a dominant influence of the MAW coinciding with the sea level considerably lower than today. On the contrary after the cessation of deglacial sea-level rise and the final establishment of the modern circulation, the intermediate depths of the WMCP were mainly bathed by waters with relatively low $\delta^{13}C_{Cib}$ values (0.3-0.6‰; Fig. 6-5), which are likely due to the predominance of the LIW. However, from the B/A interstadial to the Mid Holocene (~13.3-7.6 kyr BP), the $\delta^{13}C_{Cib}$ record shows a gradual change from MAW to LIW dominance, though also revealing strong fluctuations (Fig. 6-5). Thus, we assume that in pace with the deglacial sea level rise, the coral mounds of the WMCP, which today occur at water depths of 300-490 m (Lo Iacono et al., 2014), were bathed by the MAW before the B/A interstadial. Between the B/A interstadial and Early Holocene the mounds became affected by the interface between the MAW and the LIW, and were mainly influenced by the LIW since the Mid Holocene, when the water mass interface was shifted towards shallower depths above the coral mounds (Fig. 6-6). Interestingly, the time interval when the coral mounds of the WMCP were placed within the interface between the MAW and the LIW – marked by the strong gradient in the $\delta^{13}C_{cib}$ record - almost exactly encompasses

the timing of mound formation in the WMCP during the B/A interstadial (14.1-12.9 kyr BP) and the Early Holocene (11.6-7.6 kyr BP; Figs. 6-4, 6-5).
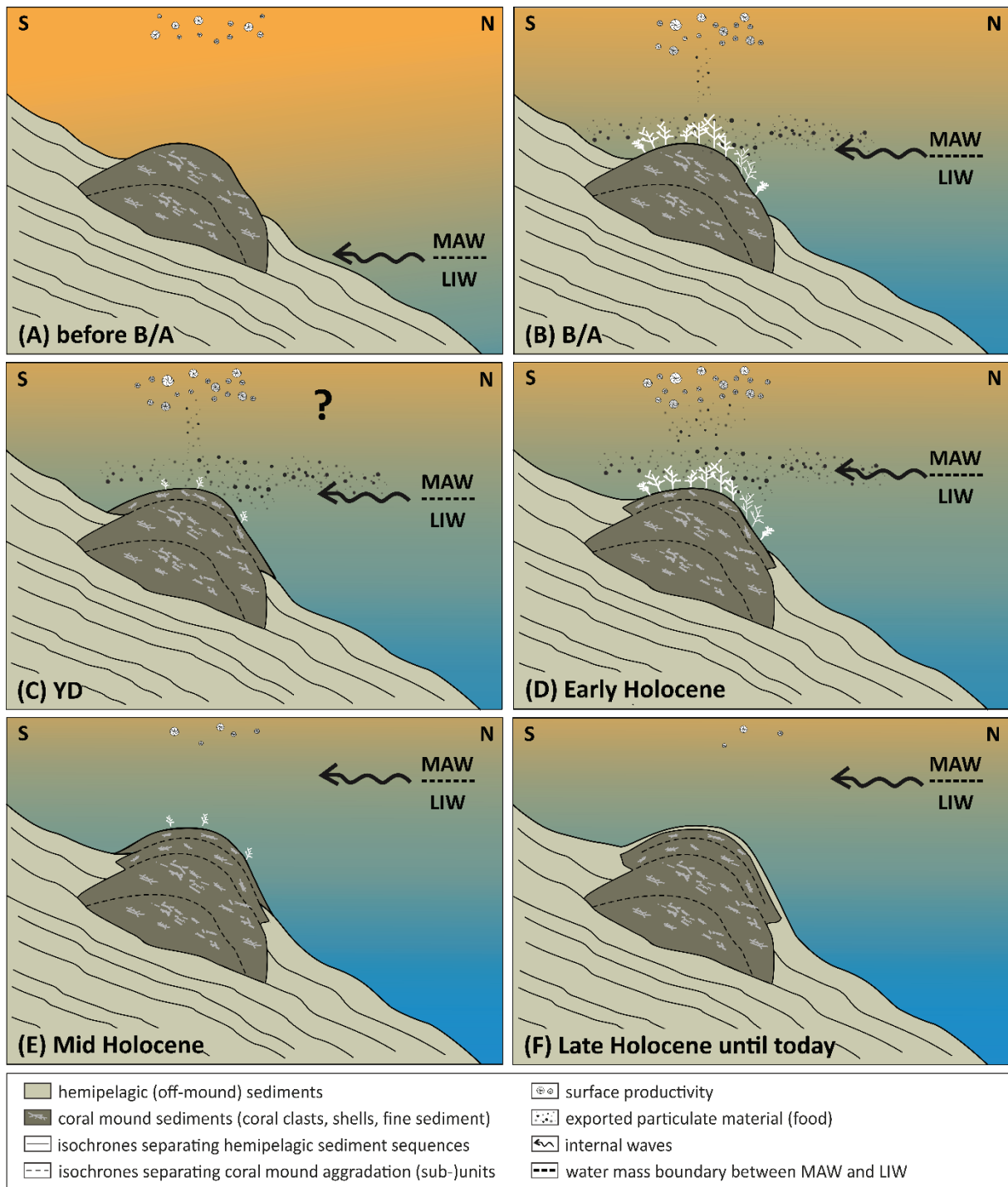

Figure. 6-6. Schematic model showing the chronology of coral mound formation for the West Melilla cold-water coral mound province (WMCP) since the last deglaciation. The blue/green-colored water column represents a predominance of the westward-flowing Levantine Intermediate Water (LIW) in the depth level of coral mound occurrence, while the yellow/orange shading indicates a predominance of the eastward-flowing Modified Atlantic Water (MAW). Curved arrow indicates internal waves that develop due to enhanced interactions at the interface between the MAW and the LIW. A: Before the Bølling-Allerød (B/A) interstadial: Coral mounds of the WMCP were in a dormant state. B: B/A interstadial: Enhanced coral mound formation. The interface between the MAW and the LIW were placed towards the coral mounds. Internal waves that likely

89

developed along this interface (indicated by enhanced bottom current strength) promoted increased delivery of food particles to the CWCs. At the same time, increased sea surface productivity also contributed to the enhanced export of particulate material. C: Younger Dryas (YD): Temporary slow-down of coral mound formation despite overall optimal environmental conditions for CWC growth. D: Early Holocene to early Mid-Holocene: Enhanced coral mound formation. Similar environmental conditions prevailed as indicated for the B/A interstadial. E: Mid Holocene: Slow-down of coral mound formation. Coral mounds became submerged by the LIW and a relatively stable hydrodynamic setting was established. Surface and export productivity significantly decreased. F: Late Holocene until present. CWCs completely declined, mound formation stagnated and some coral mounds in the WMCP became buried by sediments.

Common features that occur at the interface between two water masses of different densities are internal waves (Small and Martin, 2002; Pomar et al., 2012). Such waves propagate along the pycnocline, due to friction between the two water bodies caused by different flow velocities, and eventually break against facing slopes (Pomar et al., 2012). Therefore, internal waves are a potentially relevant source of turbulent energy as they enable mixing and particle re-suspension, and hence the lateral transportation of particulate organic materials. Moreover, these features can force the accumulation of particulate material, and hence, the formation of nepheloid layers (Mienis et al., 2007). The positive feedback of internal waves on mound formation is described for various modern coral mound settings in the NE Atlantic (Frederiksen et al., 1992; White et al., 2005; Mienis et al., 2007; Davies et al., 2009; White and Dorschel, 2010; Hebbeln et al., 2014). Internal waves transport fresh or re-suspend recently deposited food particles with increased velocity to the CWCs thriving on mounds (Mienis et al., 2007). Thereby, they act as a nutritional pump that makes food particles repeatedly available for CWCs, flushing particles laterally through the CWC framework, thus enhancing the chance for the coral polyps to catch them (Davies et al., 2009; Mienis et al., 2009a; Hebbeln et al., 2016). Also for the fossil record, a strong relationship between the existence of a water mass interface and coral mound formation has already been postulated. For example, mound aggradation along the Irish margin (Porcupine Seabight) was active when the interface between the Mediterranean Outflow Water and the Eastern North Atlantic Water was placed towards the depth level of the mounds, thereby the stable water mass stratification between both water masses caused enhanced food supply (Raddatz et al., 2014). Recently, the positive effect of internal waves has been hypothesised for a coral mound province in the Gulf of Mexico (Campeche Bank; Matos et al., 2017). There, mound formation is restricted to interglacial periods, when internal waves propagated along the pycnocline between the Atlantic Intermediate Water and the Tropical Atlantic Central Water, while during glacial times this water mass interface was shifted away from the coral mounds (Matos et al., 2017). It is very likely that such a scenario is also valid for the WMCP, where internal waves propagating along the MAW-LIW-interface enhanced the supply of food particles to the CWCs and hence promoted the pronounced aggradation of the mounds during the B/A and Early Holocene (Fig. 6-6). The enhanced hydrodynamic energy resulting from the internal waves along the water mass interface is reflected by the grain size data from the off-mound record in the WMCP and the EMCP (Figs. 6-5, 6-6).

By comparing the palaeo-environmental conditions between the WMCP and the neighbouring EMCP, very similar trends with respect to export production and near-bottom hydrodynamics are indicated for

the past 23 kyr (Fig. 6-5; see also Fink et al., 2013). However, the mounds of the EMCP experienced a slightly earlier (at ~9.8 kyr BP) slow-down in mound formation during the Early Holocene (Fink et al., 2013; Stalder et al., 2015) compared to the mounds of the WMCP (at ~7.6 kyr BP; Fig. 6-5). This might simply reflect the natural mound formation variability along continental margins as was recently shown by Wienberg et al. (2018). These authors identified distinct temporal differences in mound formation stages within a giant coral mound province off Mauritania, even for directly neighbouring coral mounds. Alternatively, the temporal offset in mound formation between the EMCP and the WMCP might be related to the influence of the Cape Tres Forcas, which today separates both provinces and whose morphology probably significantly modified the circulation pattern in pace with the rising sea level since the last deglaciation. During the LGM, the sea level was ~130 m lower than at present (Fig. 6-5), and the Moroccan coastline was located much further off-shore, thus much closer to the coral mounds of the WMCP and the EMCP (see also Lo Iacono et al., 2014). At ~14.5 kyr BP the sea-level rapidly rose about 20 m in about 500 years (Deschamps et al., 2012), and reached the present-day level between 8 and 6 kyr BP (Lambeck and Chappell, 2001; Lambeck et al., 2014; Fig. 6-5). As suggested by Lo Iacono et al. (2014), the morphological alteration of the Cape Tres Forcas due to the sea-level rise probably modified the current regime and subsequent sedimentation rates in the WMCP, leading to the demise of coral mounds.

One period that remains enigmatic is the YD cold event, when mound formation temporarily stagnated, though our off-mound record reveals significant enhancement of productivity and hydrodynamics (Figs. 6-5, 6-6). Enhanced productivity conditions in combination with a well-ventilated, high energetic intermediate water mass regime during the YD was also assumed for other sites in the western Mediterranean Sea (Bárcena et al., 2001; Rogerson et al., 2008; McCulloch et al., 2010; Margreth et al., 2011; Toucanne et al., 2012). However, while these overall optimal environmental conditions explain the frequent reports of corals of YD-age from various sites in the Mediterranean Sea (Balearic, Tyrrhenian, Ionian and Aegean Seas; McCulloch et al., 2010; Taviani et al., 2011; Fink et al., 2015), the reduced occurrence (or even absence) of CWCs in the southern Alboran Sea point to rather local environmental controls that suppressed their proliferation. Fink et al. (2015) assumed that this local control on CWC growth in the southern Alboran Sea might be related to changes in the two-gyres-system that induced upwelling and density fronts in the upper 200-300 m (Heburn and La Violette, 1990).

6.6. Conclusions

Within the Alboran Sea, coral mounds formed by the scleractinian framework-forming CWCs *L. pertusa* and *M. oculata* were so far only discovered along its southern margin just 15-30 km off the Moroccan coastline. These mounds are grouped in two provinces, the WMCP and EMCP, which are located east and west of the Spanish enclave Melilla (Cape Tres Forcas) in intermediate water depths

of 200-450 m (Lo Iacono et al., 2014; Hebbeln, 2019). This study provided for the first time insight into the temporal evolution of the coral mounds in the WMCP and clearly revealed that mound formation re-initiated (almost) simultaneously in both provinces with the onset of the last deglaciation. Subsequently, the mounds experienced periods of pronounced aggradation corresponding to the B/A interstadial and the Early Holocene. Highest ARs were reached during the B/A, with average ARs of 1-2 m kyr^{-1} obtained for the WMCP. These ARs are in the range of or even above the values found for mound provinces in the NE Atlantic (e.g., Frank et al., 2009; Wienberg and Titschack, 2017). The CPPs identified for the mounds of the WMCP indicate for both periods a slow start-up phase rapidly followed by a "booster" stage in mound formation which partly supports an early mound evolution model introduced by Henriet and Guidard (2002).

The re-initiation of mound formation and subsequent mound development in the southern Alboran Sea was likely the result of (i) the strong hydrodynamics triggered by internal waves related to the sea level-driven re-organisation of the water column structure, and (ii) the concurrently enhanced ocean productivity. For modern Atlantic coral mound settings, internal waves are frequently observed to develop along pycnoclines related to water mass boundaries. They create enhanced turbulent energy and lateral transport (and/or enrichment) of particulate material (food, sediments; e.g., Mienis et al., 2007; White et al., 2005), thus supporting CWC growth as well as mound formation. We assume that such a scenario also promoted mound formation in the southern Alboran Sea from the last deglaciation until the end of the Early Holocene (see also Fink et al., 2013). During the Mid Holocene, the MAW-LIW-interface shifted to shallower water depths above the mounds and altered the environmental conditions at the sea floor to a less turbulent condition. At the same time, the area turned into an oligotrophic setting. These caused a significant slow-down (EMCP) and even stagnation (WMCP) in mound formation that persists until today.

The water column structure most likely played a dominant role in controlling mound formation in the southern Alboran Sea. However, the locally and temporarily restricted processes might also have influenced the development of the coral mounds. During the YD, mound formation was suppressed in both provinces which might be related to the changes of the two gyre circulation that triggering upwelling and density fronts at intermediate water depths (Fink et al., 2015; Heburn and La Violette, 1990). Moreover, slight temporal offsets in mound formation identified between the two provinces might be related to the Cape Tres Forcas that acts as a morphological barrier possibly affecting the hydrodynamic processes in both provinces in a different manner. However, these offsets also simply might reflect the natural variability in mound formation, which according to recent studies seems to be a common pattern (even between directly neighboring coral mounds) rather than an exceptional feature (e.g., Wienberg et al., 2018).

While this study provides detailed insight into the most recent coral mound development in the southern Alboran Sea, the timing and environmental controls of mound formation before the last

deglaciation remains unknown. Only with the recovery of longer sedimentary records, we may possibly elucidate any large-scale pattern related to older climate fluctuations, as identified for NE Atlantic mound provinces (e.g., Frank et al., 2011).

Supplementary Material

Material and Methods

CT data processing
The obtained CT data were processed with the Zuse Insitute Berlin edition of Amira software (version 2015.37; Stalling et al., 2005; http://amira.zib.de).

First, the liner and approximately 2 mm of the core rims (to avoid artefacts that were caused by the coring process) were deleted from the data with the *Segmentation* editor and the *Arithmetic* module. The processed core sections were then merged into two datasets for core GeoB18127-1 (0-269 cm and 270-472 cm core depth) and one dataset for core GeoB18130-1 (0-148 cm core depth) with the *Merge* module. Afterwards, the CWC-dominated-sediment constituents larger than approximately 1 mm and the matrix sediment were segmented with the *MultiThresholding* module. Thereby, the threshold value had to be adjusted. While for the upper part of the core GeoB18127-1 (0-472 cm) and the entire core GeoB18130-1, a threshold value of 1400 HU (HU: Hounsfield Units, a quantitative scale for radiodensity) could be used (coral clasts: >1400 HU; matrix sediment: <1400 HU), the threshold values for the basal 83 cm of core GeoB18127-1 (472-563 cm) had to be adjusted to 1700 HU to obtain a good coral clast – matrix sediment separation. The sediment composition was subsequently quantified in each slice using the *MaterialStatistics* module (volume per slice).

To investigate the CWC preservation, the previous segmented coral clasts were separated from each other with the *ContourTreeSegmentation* module (persistence values: 1150) and parameterized with the *ShapeAnalysis* module that calculates various shape parameters for every clast, including a minimum-bounding box and the eigenvalues of the clasts. The *GrainSizeDistribution* module uses the longest axis of the minimum-bounding boxes for the coral clast size analysis (measured in $\Phi=-\log_2[\text{length(mm)}/1\text{ mm}]$). The *GrainAngelDistribution* module relies on the angle between the longest clast axis and the horizontal plane (XY-plane within the CT scans), calculated from the clast eigenvalues. For both analyses, each clast within 5 cm core interval (167 CT slices) was considered and the result was written to the central slice. The grain size range was defined between -8 Φ and 2 Φ being divided into 32 bins. The coral clast orientation was determined between 0° (horizontal) and 90° (vertical) in 18 bins (equal to 5° dip angle). Finally, coral clasts >2 cm were visualized with the *SurfaceGen* and *SurfaceView* module (for each identified clast, a different colour was used; see also Fig. 6-2, 6-3 in the manuscript).

Results

Logs of sediment cores MD13-3451G, MD13-3452G, GeoB18127-1 and GeoB18130-1 collected from the West Melilla cold-water coral mound province (WMCP)
Core logs of MD13-3451G and MD13-3452G were obtained with a line scan camera. Based on a visual core description, both cores were divided into three units describing significant variations in

coral content and coral clast size (Fig. 6-S1; see also detailed description in the manuscript in sub-chapter '4.4.1.1 Visual core description of on-mound cores MD13-3451G and MD13-3452G'). The core logs of GeoB18127-1 and GeoB18130-1 were obtained from CT imaging. The CT data were also used to define CWC preservation patterns (CPPs), which mainly derive from variations in coral clast size and orientation (Fig. 6-S1; see also detailed description in the manuscript in sub-chapter '6.4.1.2 CT-based classification of cold-water coral preservation patterns of on-mound cores GeoB18127-1 and GeoB18130-1).

All on-mound cores show varying contents of scleractinian cold-water coral clasts embedded in muddy matrix sediment (Fig. 6-S1). *Lophelia pertusa* is the dominant coral species and occurs throughout the four cores. While *Madrepora oculata* occurs mainly at the top of the four cores (MD13-3451G: 50 cm; MD13-3452G: 121-91 cm, 385-355 cm; GeoB18127-1: 150-0 cm; GeoB18130-1: 70-0 cm). Sparse occurrence of *Dendrophyllia* spp. and *Desmophyllum dianthus* are also observed especially from the top of cores GeoB18127-1 (28-13cm; 244-238 cm; 255-246 cm) and GeoB18130-1 (37-0 cm; 130-101 cm).

CT-based classification of cold-water coral preservation patterns of on-mound cores GeoB18127-1 and GeoB18130-1

For the two on-mound cores GeoB18127-1 and GeoB18130-1, the CT analyses allowed for the differentiation of three CWC preservation patterns (CPPs) following the approach of Titschack et al. (2015). These are CPP A: coral framework in living position, CPP B: slightly collapsed coral framework and CPP C: coral rubble (see also Fig. 6-S1). The definition of CPPs is mainly based on average CWC clast size and orientation, while the mean coral content (varying between 9 and 23 vol.%) could not be applied to clearly differentiate between the different CPPs (see also detailed description of the defined CPPs in the manuscript in sub-chapter '6.4.1.2 CT-based classification of cold-water coral preservation patterns of on-mound cores GeoB18127-1 and GeoB18130-1).
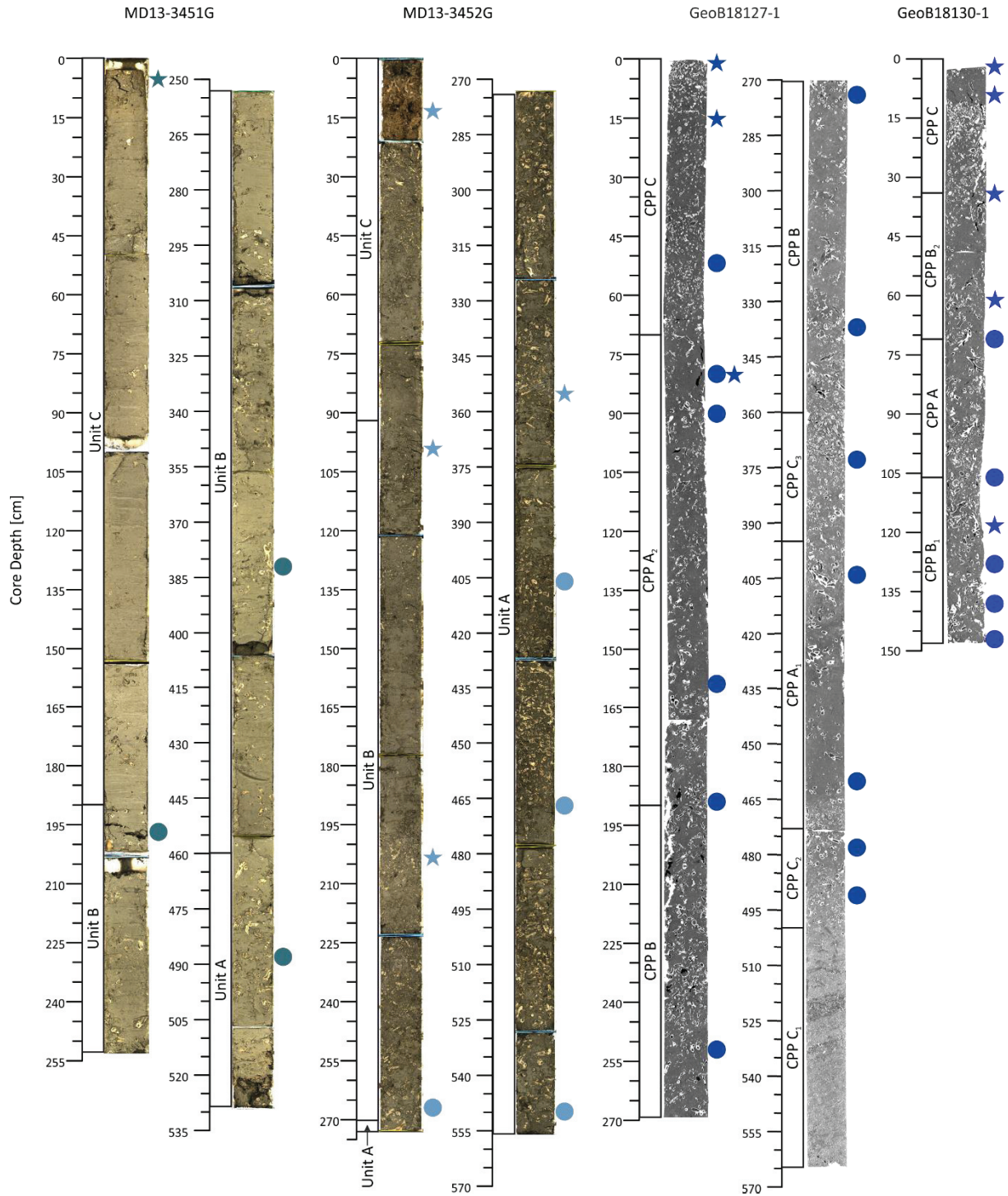
Figure 6-S1. Logs of on-mound sediment cores MD13-3451G, MD13-3452G, GeoB18127-1 and GeoB18130-1 collected from the West Melilla cold-water coral mound province (WMCP; for core locations please refer to Fig. 6-1 in the manuscript). Logs of the MD cores derive from line scan camera images, while the GeoB cores were obtained from CT scan imaging. Dots and stars are sampling depths for U/Th dating, representing *Lophelia pertusa* and *Madrepora oculata*, respectively. The core units for MD cores and cold-water coral preservation patterns (CPPs) for GeoB cores are indicated.

The values obtained for clast sizes and orientation slightly vary between the two cores (see Table 6-S1). In core GeoB18127-1, CPP A is characterised by an average coral clast sizes between -4.8 Φ (~2.8 cm) and -4.7Φ (~2.6 cm) and a mean coral content of ~12 vol.%. Coral clast orientation maxima

96

were well-defined between 0° and 90°. CPP A occurs at two different core depths: 473-395 cm (CPP A_1) and 190-70 cm (CPP A_2). CPP B exhibits coral clast sizes of -4.7 Φ (~2.6 cm) on average and a mean coral content of ~15 vol.%. The coral clasts exhibited predominantly orientations below 60°. This CCP was recognised at core depths of 360-190 cm. The CPP C_1 is characterised by the mean coral clast size of -2.8 Φ (~0.7 cm), and the average coral content is ~9 vol.%. No clear coral clast orientation was recognized. The CPP C_1 is distinguished at core depths of 563-500 cm. In contrast, CPPs C_2, C_3 and C_4 were identified at core depths of 500-473 cm, 395-360 cm, and 70-0 cm, respectively. Within intervals of the above three CPPs, the average coral clast size of -4.5 Φ (~2.3 cm) and average coral content (~16 vol.% - ~23 vol.%) is enhanced.

In core GeoB18130-1, CPP A was identified at core depths of 106-71 cm and is attributed to an average coral clast size of -4.8 Φ (~2.8 cm) and a coral content of ~17 vol.%. The coral clasts have a predominant orientation between 60° and 90°. CPP B was indicated at depths of 148-106 cm (CPP B_1) and 71-34 cm (CPP B_2). The average coral clast sizes range between -4.4 Φ (~2.1 cm) and -4.6 Φ (~2.4 cm), with coral contents of 10-18 vol.%. The orientation of the coral clasts mainly varies between 0° and 60°. CPP C, recognised between 34 cm and the core top, is characterized by an average mean coral clast size of -4.4 Φ (~2.1 cm) and a coral content of around 16 vol.%. The clast orientation is predominantly below 45°.

Table 6-S1. Characteristics of cold-water coral preservation patterns (CPPs) identified for the on-mound cores GeoB18127-1 and GeoB18130-1 based on CT data analyses. Shown are the average coral content (in vol.%), average CWC clast size (unit: Φ; $\Phi = -\log_2[\text{length(mm)}/1 \text{ mm}]$ and cm), the CWC clast orientation (0-90°) and the corresponding core depths of the respective CPPs. CPP A: CWC framework in living position; CPP B: Slightly collapsed CWC framework; CPP C: CWC rubble (see main manuscript for definition).

Core ID [GeoB]	Core Depth [cm]	Average Coral Content [vol.%]	Average CWC Clast Size [Φ]	Average CWC Clast Size [cm]	CWC Clast Orientation [°]	CPP
	473-395	~ 12	-4.8	-~2.8	0-90	A_1
	190-70	~ 12	-4.7	~2.6	0-90	A_2
	360-190	~ 15	-4.7	~2.6	<60	B
18127-1	563-500	~ 9	-2.8	~0.7	not clear	C_1
	500-473					C_2
	395-360	~ 16-23	-4.5	~2.3	not clear	C_3
	70-0					C_4
	106-71	~ 17	-4.8	~2.8	60-90	A
18130-1	148-106	~ 10-18	-4.4~-4.6	~2.1-2.4	0-60	$B_{1,2}$
	71-34					
	34-0	~ 16	-4.4	~2.1	<45	C

Palaeo-environmental proxies obtained for the off-mound core GeoB18131-1
The chronology of the off-mound core GeoB18131-1 is based on six AMS ^{14}C ages, which range from 20.3 kyr BP (360 cm core depth) to 0.3 kyr BP (core top), and a linear interpolation between these dates. The age model is further supported by a visual correlation between the benthic foraminifera

(*Cibicidoides mundulus* and *Cibicidoides pachyderma*) δ^{18}O dataand the LR04 δ^{18}O stack record (Lisiecki and Raymo, 2005). For the visual correlation of the lower part of the off-mound core, six tie points were selected assuming an age of 110 kyr BP for the core bottom (855 cm core depth; Fig. 6-S2). Hence, the established age model of the off-mound core shows that the record covers the last interglacial (MIS 5), the last glacial (MIS4-2) and the recent interglacial (MIS 1). The δ^{18}O$_{Cib}$ record displays light values of 4.0-1.9‰ during the last interglacial, and heavy values of 4.3-3.1‰ during the last glacial, and before the values rapidly decrease with the onset of the deglaciation with light values of 1.5 ‰ predominating during the Holocene (Fig. 6-S2). The δ^{13}C$_{Cib}$ record displays values of 0.9-0.3 ‰ during the last interglacial, heavy values of 1.4-0.4‰ during the last glacial, and light values of 0.6-0.3‰ for the Holocene. The calculated sedimentation rate exhibits a generally increasing trend, showing low values (< 10 cm kyr^{-1}) during the last interglacial and last glacial. Only during the Last Glacial Maximum (LGM), the sedimentation rate increases to very high values of 27 cm kyr^{-1}. Since the Holocene, the sedimentation rate varies between 8 cm kyr^{-1} and 21 cm kyr^{-1}, showing an increasing trend during the early to late Holocene (Fig. 6-S2).

The mean grain sizes of the off-mound record range from ~25 μm to ~5 μm during the last 110 kyr. During the last interglacial (MIS 5), the mean grain size varied between ~19 μm and ~8 μm, with peak values occurring in the MIS 5a and MIS 5c. During the last glacial (MIS2-4), the mean grain size was low (< 10 μm), showing high values of 18-25 μm only between ~52 kyr BP and 44 kyr BP. With the onset of the last deglaciation, the mean grain size reaches values of 11-17 μm before it decreased significantly to <8 μm in the Early Holocene. Since the Early Holocene, the mean grain size was low (< 8 μm) (Fig. 6-S2).
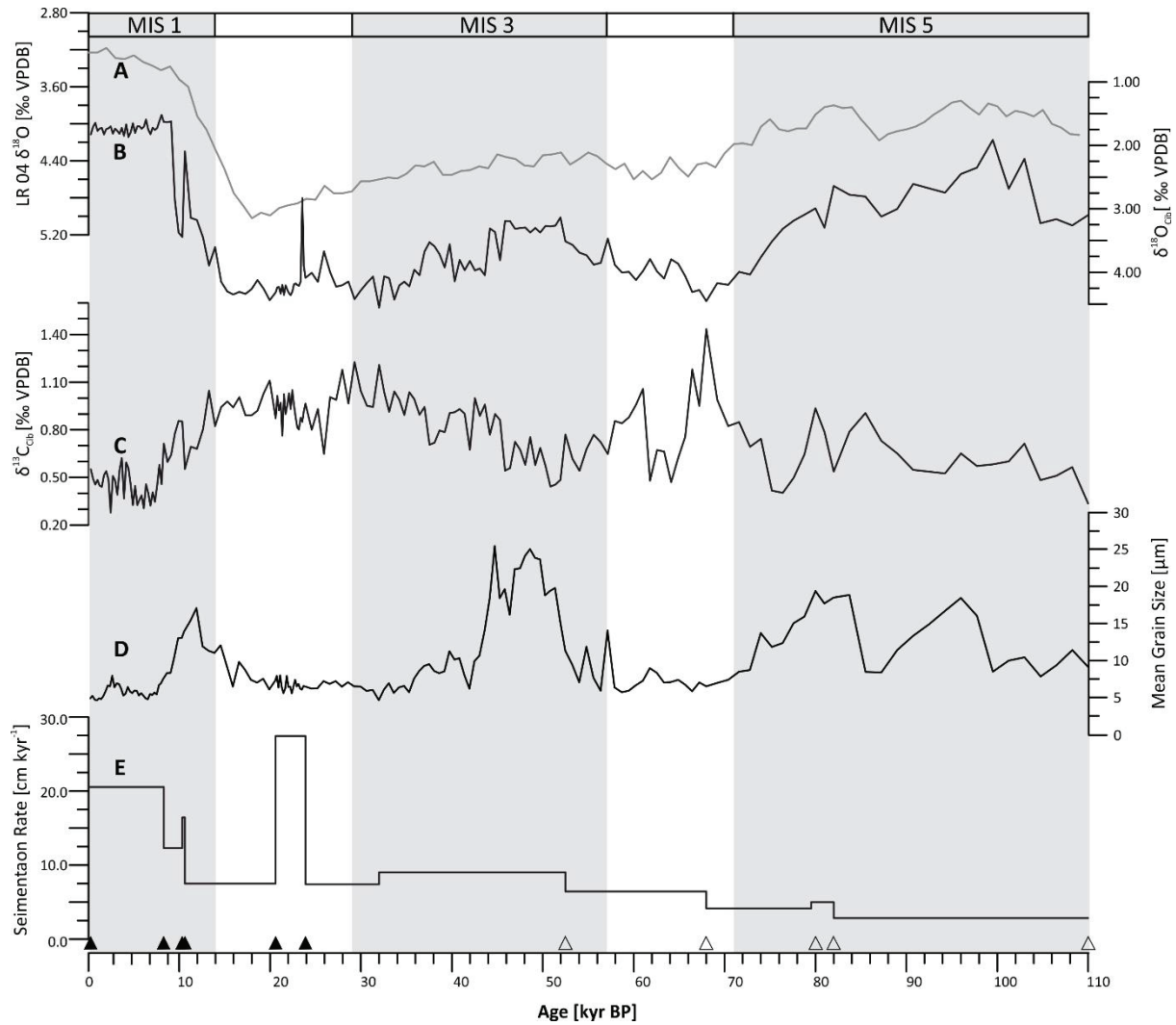
Figure 6-S2. Age model and multi-proxy data of the off-mound core GeoB18131-1 collected from the West Melilla cold-water coral mound province covering the past 110 kyr. A: LR04 $\delta^{18}O$ stack isotope (grey line, Lisiecki and Raymo, 2005). B: $\delta^{18}O_{Cib}$ record of mixed benthic foraminifera *C. mundulus* and *C. pachyderma*. **C:** $\delta^{13}C_{Cib}$ record of mixed benthic foraminifera *C. mundulus* and *C. pachyderma*. D: Mean grain size. E: Sedimentation rate. The age model of core GeoB18131-1 is based on the six AMS ^{14}C ages (black triangles) presented in kilo-years before present (kyr BP) and six correlation points (open triangles) to the LR04 $\delta^{18}O$ stack record (Lisiecki and Raymo, 2005). Shaded areas represent the Marine Isotope Stages. MIS: Marine Isotope Stage.

99

Chapter 7

Synthesis and Outlook

7.1 Synthesis

In this thesis, a comprehensive picture of the CWC mound formation in the southern Alboran Sea since the last interglacial (MIS 5) is illustrated. The presented results are largely depending on the comparison of records between CWC mounds and the adjacent seafloor derived from the two CWC mound provinces, i.e., the EMCP and the WMCP.

To begin with, we firstly reconstructed the sedimentary processes controlling mound formation. Based on two sediment cores, one collected from a coral mound and one from the near-by seafloor, we provide for the first time pivotal information about sediment transportation and deposition contributing to the mound's vertical growth:

i> The grain-size distributions of siliciclastic sediments from the coral mound show a major mode of ~7 Φ (8 µm), which is significantly finer than the simultaneously deposited sediment on the adjacent seafloor displaying a major mode of ~4 Φ (63 µm). The coarse sediment on the seafloor adjacent to the coral mound is due to strong bottom hydrodynamics under the influence of internal waves. In contrast, the occurrence of coral frameworks on the coral mound reduced the local current velocity and created a low-energy coral-derived ecological accommodation space. The prevailing calm bottom water hydrodynamics within the ecological accommodation space favored the deposition of current-transported fine sediment.

ii> The difference in the average grain-size distribution of the siliciclastic sediment between the on-mound and the off-mound records is rather stable throughout the entire core. The accumulation rate of siliciclastic sediment on the mound is extremely high, amounting to ~324 g cm^{-2} kyr^{-1}, ~30 times more than on the adjacent seafloor (average: ~10.8 g cm^{-2}kyr^{-1}). This high amount of sediment most likely was transported horizontally by internal waves. Besides, the coral content of the coral mound deposits is not positively correlated to the mound AR, suggesting that the sediment supply primarily fills the coral-derived ecological accommodation space. Overall, the obtained results clearly suggest that the baffling capacity of the coral frameworks is a prerequisite for coral mound formation, and that the aggradation of coral mounds is predominantly driven by the sediment supply and the provision of coral-generated ecological accommodation space.

The sedimentary processes controlling mound formation are of great importance also for the well-being of the corals as the enhanced hydrodynamics are crucial for the food supply to the corals. The food supply controls coral growth, which in turn defines the ecological accommodation space as well as the final mound morphology and dimension. Indeed, the CWC mounds in the four sub-clusters of the EMCP reveal different morphologies and dimensions, which most likely result from varying

hydrodynamic regimes (Hebbeln, 2019). Nonetheless, the few attempts to reconstruct coral mound development in the EMCP were made predominantly for its northern and westernmost sub-clusters (Fink et al., 2013; Stalder et al., 2015; 2018). We, therefore, utilized the sediment cores from the unexplored sub-clusters of the EMCP to unravel the history of CWC mound development:

i> Uranium series dating from CWC fragments from core GeoB18120-1 retrieved from the central sub-cluster of the EMCP (230-320 m water depth) yielded two coral age clusters: 78.1-71.6 kyr BP and 13.9-11.7 kyr BP, indicating fast mound formation during MIS 5a and during the last deglaciation, with average mound AR of 67 and 216 cm kyr^{-1}, respectively. GeoB18105-1 retrieved from the southern sub-cluster of the EMCP (200-240 m water depth), reveals one age cluster between 112.6-106.3 kyr BP with an associated mound AR of 240 cm kyr^{-1} (112.3-111.2 kyr BP), suggesting a pronounced mound formation period during MIS 5d. Since ~106.3 kyr BP, this mound became dormant.

ii> The documented three phases of CWC mound formation correspond well with periods of strong bottom water hydrodynamics triggered by the development of internal waves along the MAW-LIW interface. Along with a slightly enhanced ocean surface productivity, especially the lateral food availability to the corals was significantly enhanced, resulting in the fast aggradation of the coral mounds. During MIS 3, reduced bottom water oxygenation probably caused the absence of coral growth and the cessation of mound aggradation. The vertical positioning of the LIW-MAW interface at the depth level of coral mounds in the study area was controlled by the relative sea level, which, thus, was the (indirect) pacemaker controlling coral mound formation in the southern Alboran Sea.

Finally, we explored for the first time the development of CWC mounds in the WMCP (southern Alboran Sea). With sediment cores from coral mounds in the WMCP and a supplementary sediment core from the adjacent seafloor, we reconstructed the most recent development of coral mounds in this area since the last deglaciation.

i> U/Th datings of corals show that CWC mounds experienced remarkable aggradation during the B/A interstadial and the Early to Mid Holocene until ~7.6 kyr BP. This is reflected by high average mound AR of 75-176 cm kyr^{-1}.

ii> Coral mound aggradation coincided with high vertical and – even more prominently – lateral food supply, which is controlled by the water column structure in the southern Alboran Sea. A high food supply to the corals originates from strong bottom water hydrodynamics deriving also in the WMCP from internal wave propagation along the LIW-MAW interface. Reduced mound formation since ~7.6 kyr BP corresponds well with the establishment of an oligotrophic and low bottom water energy setting in the WMCP marked by the absence of internal waves. It is proposed that also in the WMCP variations in the water column structure since the last deglaciation controlled the formation of coral mounds.

7.2 Outlook

Given the conclusions outlined above, interests about the CWC mound formation in the entire Mediterranean Sea also beyond the Alboran Sea arise. Up to now, in the Mediterranean Sea coral mounds have also been discovered in the Strait of Sicily and off Santa Maria di Leuca (SML) (Taviani et al., 2005; Martorelli et al., 2011). However, seeing the wide distribution of framework forming CWC in the Mediterranean Sea (Chimienti et al., 2019), also a much wider distribution of coral mounds can be expected, particularly along the continental slopes based on the fact that coral mound formation results from the interplay of coral growth and sediment deposition (Hebbeln et al., 2016; Wienberg and Titschack, 2017).

A shared feature in the known distribution of coral mounds and further coral occurrences is their predominant location under the influence of the LIW (water depth: 200-700 m; Astraldi et al., 2002; Martorelli et al., 2011). The coral mounds in the Strait of Sicily, featuring a coral-barren surface, mainly occur at water depths of 300-600 m well within the influence of the LIW. Off SML, coral mounds occur at water depths between 300 and 1100 m (Freiwald et al., 2009; and references therein) with the majority being found at water depths of 556-630 m. These mounds are colonized by thriving CWCs on the surface (Freiwald et al., 2009). This depth level of coral mound occurrence is at the bottom limit of the LIW in the Ionian Sea, where it predominantly occurs between 200 and 600 m (Cushman-Roisin et al., 2001). In addition, past basin-wide occurrences of CWCs across the entire Mediterranean Sea were compiled (McCulloch et al., 2010; Fink et al., 2015) with most of the dated coral fragments having been collected at water depths of 200-1000 m, coinciding with the flowing path of the LIW in the Mediterranean Sea.

In the Mediterranean Sea, the intermediate thermohaline circulation is controlled by the orbital change of insolation-driven freshwater budgets (e.g., Bahr et al., 2015), and sea level changes on glacial-interglacial time-scales (Grant et al., 2014). Thus, it is plausible to anticipate that coral mound formation in the entire Mediterranean Sea is related to sea level as reported here for the Alboran Sea, where coral mound development appears to be linked to the position of the LIW-MAW water mass boundary. Therefore, future work on the development of coral mounds in the Mediterranean Sea should invoke the following aspects: i> mapping the distribution of coral mounds along the continental slopes of the Mediterranean Sea, with emphasis on those regions from which CWC occurrences have been reported. ii> unravelling coral mound development all over the Mediterranean Sea over geological time scales. iii> investigating the link of coral mound formation between the Mediterranean Sea and the North Atlantic since the intermediate water circulation in the Mediterranean Sea is coupled to North Atlantic climate variability through global sea level changes as well as African monsoon variability (e.g., Bahr et al., 2015) .

Apart from the possible similarity in coral mound formation across the Mediterranean Sea over glacial-interglacial cycles, local environmental factors, like the anoxic conditions in the eastern Mediterranean Sea during the Sapropel events, can also exert a significant impact on coral mound formation by hampering the coral growth (e.g., Fink et al., 2012). Thus, comparing coral mound formation in different areas in the Mediterranean Sea will in addition allow to assess the different environmental factors finally controlling coral mound formation.

References

Al-Awwad, S.F., Pomar, L., 2015. Origin of the rudstone–floatstone beds in the Upper Jurassic Arab-D reservoir, Khurais Complex, Saudi Arabia. Marine and Petroleum Geology 67, 743-768.

Andersen, M.B., Stirling, C.H., Zimmermann, B., Halliday, A.N., 2010. Precise determination of the open ocean $^{234}U/^{238}U$ composition. Geochemistry, Geophysics, Geosystems 11.

Arnone, R.A., Wiesenburg, D.A., Saunders, K.D., 1990. The origin and characteristics of the Algerian Current. Journal of Geophysical Research: Oceans 95, 1587-1598.

Astraldi, M., Gasparini, G.P., Vetrano, A., Vignudelli, S., 2002. Hydrographic characteristics and interannual variability of water masses in the central Mediterranean: a sensitivity test for long-term changes in the Mediterranean Sea. Deep Sea Research Part I: Oceanographic Research Papers 49, 661-680.

Ausín, B., Flores, J.A., Sierro, F.J., Bárcena, M.A., Hernández-Almeida, I., Francés, G., Gutiérrez-Arnillas, E., Martrat, B., Grimalt, J.O., Cacho, I., 2015. Coccolithophore productivity and surface water dynamics in the Alboran Sea during the last 25kyr. Palaeogeography, Palaeoclimatology, Palaeoecology 418, 126-140.

Bahr, A., Kaboth, S., Jiménez-Espejo, F.J., Sierro, F.J., Voelker, A.H.L., Lourens, L., Röhl, U., Reichart, G.J., Escutia, C., Hernández-Molina, F.J., Pross, J., Friedrich, O., 2015. Persistent monsoonal forcing of Mediterranean Outflow Water dynamics during the late Pleistocene. Geology 43, 951-954.

Baldacci, A., Corsini, G., Grasso, R., Manzella, G., Allen, J.T., Cipollini, P., Guymer, T.H., Snaith, H.M., 2001. A study of the Alboran sea mesoscale system by means of empirical orthogonal function decomposition of satellite data. Journal of Marine Systems 29, 293-311.

Bárcena, M.A., Cacho, I., Abrantes, F., Sierro, F.J., Grimalt, J.O., Flores, J.A., 2001. Paleoproductivity variations related to climatic conditions in the Alboran Sea (western Mediterranean) during the last glacial–interglacial transition: The diatom record. Palaeogeography, Palaeoclimatology, Palaeoecology 167, 337-357.

Bard, E., 1988. Correction of accelerator mass spectrometry ^{14}C ages measured in planktonic foraminifera: paleoceanographic implications. Paleoceanography 3, 635-645.

Bender, M.M., 1971. Variations in the $^{13}C/^{12}C$ ratios of plants in relation to the pathway of photosynthetic carbon dioxide fixation. Phytochemistry 10, 1239-1244.

Berger, W.H., Herguera, J.C., 1992. Reading the sedimentary record of the ocean's productivity, in: Falkowski, P.G., Woodhead, A.D., Vivirito, K. (Eds.), Primary Productivity and Biogeochemical Cycles in the Sea. Springer US, Boston, MA, pp. 455-486.

Beyer, A., Schenke, H.W., Klenke, M., Niederjasper, F., 2003. High resolution bathymetry of the eastern slope of the Porcupine Seabight. Marine Geology 198, 27-54.

Blum, P., 1997. Physical properties handbook: A guide to the shipboard measurement of physical properties of deep-sea cores. ODP Tech. Note, 26 [Online]

Bonneau, L., Colin, C., Pons-Branchu, E., Mienis, F., Tisnérat-Laborde, N., Blamart, D., Elliot, M., Collart, T., Frank, N., Foliot, L., Douville, E., 2018. Imprint of Holocene climate variability on cold-water coral reef growth at the SW Rockall Trough margin, NE Atlantic. Geochemistry, Geophysics, Geosystems.

Boyle, E.A., 1997. Characteristics of the deep ocean carbon system during the past 150,000 years: ΣCO_2 distributions, deep water flow patterns, and abrupt climate change. Proceedings of the National Academy of Sciences 94, 8300.

Brankart, J.-M., Pinardi, N., 2001. Abrupt cooling of the Mediterranean Levantine Intermediate Water at the beginning of the 1980s: Observational evidence and model simulation. Journal of Physical Oceanography 31, 2307-2320.

Brooke, S., Ross, S.W., 2014. First observations of the cold-water coral *Lophelia pertusa* in mid-Atlantic canyons of the USA. Deep Sea Research Part II: Topical Studies in Oceanography 104, 245-251.

Büscher, J.V., Form, A.U., Riebesell, U., 2017. Interactive effects of ocean acidification and warming on growth, fitness and survival of the cold-water coral *Lophelia pertusa* under different food availabilities. Frontiers in Marine Science 4.

Cacho, I., Grimalt, J.O., Canals, M., 2002. Response of the Western Mediterranean Sea to rapid climatic variability during the last 50,000 years: A molecular biomarker approach. Journal of Marine Systems 33-34, 253-272.

Cacho, I., Grimalt, J.O., Canals, M., Sbaffi, L., Shackleton, N.J., Schönfeld, J., Zahn, R., 2001. Variability of the western Mediterranean Sea surface temperature during the last 25,000 years and its connection with the Northern Hemisphere climatic changes. Paleoceanography 16, 40-52.

Calvert, S.E., Pedersen, T.F., 2007. Chapter Fourteen Elemental Proxies for Palaeoclimatic and Palaeoceanographic Variability in Marine Sediments: Interpretation and Application, in: Hillaire–Marcel, C., De Vernal, A. (Eds.), Developments in Marine Geology. Elsevier, pp. 567-644.

Chang, S., Elkins, C., Alley, M., Eaton, J., Monismitha, S., 2009. Flow inside a coral colony measured using magnetic resonance velocimetry. Limnology and Oceanography 54, 1819-1827.

Cheng, H., Adkins, J., Edwards, R.L., Boyle, E.A., 2000a. U-Th dating of deep-sea corals. Geochimica et Cosmochimica Acta 64, 2401-2416.

Cheng, H., Edwards, R.L., Hoff, J., Gallup, C.D., Richards, D.A., Asmerom, Y., 2000b. The half-lives of uranium-234 and thorium-230. Chemical Geology 169, 17-33.

Chimienti, G., Bo, M., Taviani, M., Mastrototaro, F., 2019. 19 Occurrence and Biogeography of Mediterranean Cold-Water Corals, in: Orejas, C., Jiménez, C. (Eds.), Mediterranean Cold-Water Corals: Past, Present and Future: Understanding the Deep-Sea Realms of Coral. Springer International Publishing, Cham, pp. 213-243.

Collart, T., Verreydt, W., Hernández-Molina, F.J., Llave, E., León, R., Gómez-Ballesteros, M., Pons-Branchu, E., Stewart, H., Van Rooij, D., 2018. Sedimentary processes and cold-water coral mini-mounds at the Ferrol canyon head, NW Iberian margin. Progress in Oceanography 169, 48-65.

Colman, J.G., Gordon, D.M., Lane, A.P., Forde, M.J., Fitzpatrick, J.J., 2005. Carbonate mounds off Mauritania, Northwest Africa: status of deep-water corals and implications for management of fishing and oil exploration activities, Cold-water corals and ecosystems. Springer, pp. 417-441.

Comas, M., Pinheiro, L., Ivanov, M., TTR-17 Leg 1 Scientific Party, 2009. Geo-Marine Research on the Mediterranean and European-Atlantic Margins. International Conference and TTR-17 Post-Cruise Meeting of the Training-through-Research Programme. Granada, Spain, 2-5 February 2009, in: Comas, M., Suzyumov, A. (Eds.), Deep-water coral mounds in the Alboran Sea: the Melilla mound field revisited. IOC Workshop Report, NO. 220 (English), UNESCO, 2009, p. 52.

Correa, T.B.S., Eberli, G.P., Grasmueck, M., Reed, J.K., Correa, A.M.S., 2012a. Genesis and morphology of cold-water coral ridges in a unidirectional current regime. Marine Geology 326-328, 14-27.

Correa, T.B.S., Grasmueck, M., Eberli, G.P., Reed, J.K., Verwer, K., Purkis, S.A.M., 2012b. Variability of cold-water coral mounds in a high sediment input and tidal current regime, Straits of Florida. Sedimentology 59, 1278-1304.

Cyr, F., Haren, H., Mienis, F., Duineveld, G., Bourgault, D., 2016. On the influence of cold-water coral mound size on flow hydrodynamics, and vice versa. Geophysical Research Letters 43, 775-783.

D'Ortenzio, F., Ribera d'Alcalà, M., 2009. On the trophic regimes of the Mediterranean Sea: A satellite analysis. Biogeosciences 6, 139-148.

Davies, A.J., Duineveld, G.C., Lavaleye, M.S., Bergman, M.J., van Haren, H., Roberts, J.M., 2009. Downwelling and deep-water bottom currents as food supply mechanisms to the cold-water coral *Lophelia pertusa* (Scleractinia) at the Mingulay Reef Complex. Limnology and Oceanography 54, 620-629.

Davies, A.J., Guinotte, J.M., 2011. Global habitat suitability for framework-forming cold water corals. PLoS ONE 6, e18483.

Davies, A.J., Wisshak, M., Orr, J.C., Murray Roberts, J., 2008. Predicting suitable habitat for the cold-water coral *Lophelia pertusa* (Scleractinia). Deep Sea Research Part I: Oceanographic Research Papers 55, 1048-1062.

De Clippele, L.H., Huvenne, V.A.I., Orejas, C., Lundälv, T., Fox, A., Hennige, S.J., Roberts, J.M., 2017. The effect of local hydrodynamics on the spatial extent and morphology of cold-water coral habitats at Tisler Reef, Norway. Coral Reefs 37, 253-266.

de Haas, H., Mienis, F., Frank, N., Richter, T.O., Steinacher, R., de Stigter, H., van der Land, C., van Weering, T.C.E., 2009. Morphology and sedimentology of (clustered) cold-water coral mounds at the south Rockall Trough margins, NE Atlantic Ocean. Facies 55, 1-26.

De Mol, B., Amblas, D., Calafat, A., Canals, M., Duran, R., Lavoie, C., Muñoz, A., Rivera, J., 2012. 60 - Cold-Water Coral Colonization of Alboran Sea Knolls, Western Mediterranean Sea A2 - Harris, Peter T, in: Baker, E.K. (Ed.), Seafloor Geomorphology as Benthic Habitat. Elsevier, London, pp. 819-829.

De Mol, B., Van Rensbergen, P., Pillen, S., Van Herreweghe, K., Van Rooij, D., McDonnell, A., Huvenne, V., Ivanov, M., Swennen, R., Henriet, J.P., 2002. Large deep-water coral banks in the Porcupine Basin, southwest of Ireland. Marine Geology 188, 193-231.

Degens, E.T., 1969. Biogeochemistry of Stable Carbon Isotopes, in: Eglinton, G., Murphy, M.T.J. (Eds.), Organic Geochemistry: Methods and Results. Springer Berlin Heidelberg, Berlin, Heidelberg, pp. 304-329.

Deschamps, P., Durand, N., Bard, E., Hamelin, B., Camoin, G., Thomas, A.L., Henderson, G.M., Okuno, J.i., Yokoyama, Y., 2012. Ice-sheet collapse and sea-level rise at the Bølling warming 14,600 years ago. Nature 483, 559.

Diaz, R., Rosenberg, R., 1995. Marine benthic hypoxia: A review of its ecological effects and the behavioural response of benthic macrofauna. Oceanography and marine biology. An annual review [Oceanogr. Mar. Biol. Annu. Rev.] 33, 245-303.

Dodds, L.A., Black, K.D., Orr, H., Roberts, M., 2009. Lipid biomarkers reveal geographical differences in food supply to the cold-water coral *Lophelia pertusa* (Scleractinia). Marine Ecology Progress Series 397, 113-124.

Dorschel, B., Hebbeln, D., Foubert, A., White, M., Wheeler, A.J., 2007a. Hydrodynamics and cold-water coral facies distribution related to recent sedimentary processes at Galway Mound west of Ireland. Marine Geology 244, 184-195.

Dorschel, B., Hebbeln, D., Rüggeberg, A., Dullo, C., 2007b. Carbonate budget of a cold-water coral carbonate mound: Propeller Mound, Porcupine Seabight. International Journal of Earth Sciences 96, 73-83.

Dorschel, B., Hebbeln, D., Ruggeberg, A., Dullo, W., Freiwald, A., 2005. Growth and erosion of a cold-water coral covered carbonate mound in the Northeast Atlantic during the Late Pleistocene and Holocene. Earth and Planetary Science Letters 233, 33-44.

Dubois-Dauphin, Q., Montagna, P., Siani, G., Douville, E., Wienberg, C., Hebbeln, D., Liu, Z., Kallel, N., Dapoigny, A., Revel, M., Pons-Branchu, E., Taviani, M., Colin, C., 2017. Hydrological variations of the intermediate water masses of the western Mediterranean Sea during the past 20 ka inferred from neodymium isotopic composition in foraminifera and cold-water corals. Climate of the Past 13, 17-37.

Duineveld, G.C., Lavaleye, M.S., Bergman, M.J., De Stigter, H., Mienis, F., 2007. Trophic structure of a cold-water coral mound community (Rockall Bank, NE Atlantic) in relation to the near-bottom particle supply and current regime. Bulletin of Marine Science 81, 449-467.

Duineveld, G.C.A., Jeffreys, R.M., Lavaleye, M.S.S., Davies, A.J., Bergman, M.J.N., Watmough, T., Witbaard, R., 2012. Spatial and tidal variation in food supply to shallow cold-water coral reefs of the Mingulay Reef complex (Outer Hebrides, Scotland). Marine Ecology Progress Series 444, 97-115.

Dullo, W.-C., Flögel, S., Rüggeberg, A., 2008. Cold-water coral growth in relation to the hydrography of the Celtic and Nordic European continental margin. Marine Ecology Progress Series 371, 165-176.

Ehrmann, W.U., Thiede, J., 1985. History of mesozoic and cenozoic sediment fluxes to the-North Atlantic Ocean, Contributions to Sedimentology E. Schweizerbart, Stuttgart, pp. 105-109.

Eisele, M., Frank, N., Wienberg, C., Hebbeln, D., López Correa, M., Douville, E., Freiwald, A., 2011. Productivity controlled cold-water coral growth periods during the last glacial off Mauritania. Marine Geology 280, 143-149.

Esat, T.M., Yokoyama, Y., 2006. Variability in the uranium isotopic composition of the oceans over glacial–interglacial timescales. Geochimica et Cosmochimica Acta 70, 4140-4150.

Fabres, J., Calafat, A., Sanchez-Vidal, A., Canals, M., Heussner, S., 2002. Composition and spatio-temporal variability of particle fluxes in the Western Alboran Gyre, Mediterranean Sea. Journal of Marine Systems 33, 431-456.

Faure, G., 1986. Principles of isotope geology. Second edition. John Wiley and Sons Inc.,New York, NY, United States.

Fink, H.G., Wienberg, C., De Pol-Holz, R., Hebbeln, D., 2015. Spatio-temporal distribution patterns of Mediterranean cold-water corals (*Lophelia pertusa* and *Madrepora oculata*) during the past 14,000 years. Deep Sea Research Part I: Oceanographic Research Papers 103, 37-48.

Fink, H.G., Wienberg, C., De Pol-Holz, R., Wintersteller, P., Hebbeln, D., 2013. Cold-water coral growth in the Alboran Sea related to high productivity during the Late Pleistocene and Holocene. Marine Geology 339, 71-82.

Fink, H.G., Wienberg, C., Hebbeln, D., McGregor, H.V., Schmiedl, G., Taviani, M., Freiwald, A., 2012. Oxygen control on Holocene cold-water coral development in the eastern Mediterranean Sea. Deep Sea Research Part I: Oceanographic Research Papers 62, 89-96.

Flögel, S., Dullo, W.C., Pfannkuche, O., Kiriakoulakis, K., Rüggeberg, A., 2014. Geochemical and physical constraints for the occurrence of living cold-water corals. Deep Sea Research Part II: Topical Studies in Oceanography 99, 19-26.

Flügel, E., 2004. Microfacies of carbonate rocks: Analysis, interpretation and application. Springer Science & Business Media.

Fontanier, C., Jorissen, F.J., Licari, L., Alexandre, A., Anschutz, P., Carbonel, P., 2002. Live benthic foraminiferal faunas from the Bay of Biscay: Faunal density, composition, and microhabitats. Deep Sea Research Part I: Oceanographic Research Papers 49, 751-785.

Fosså, J.H., Lindberg, B., Christensen, O., Lundälv, T., Svellingen, I., Mortensen, P.B., Alvsvåg, J., 2005. Mapping of Lophelia reefs in Norway: Experiences and survey methods, Cold-water corals and ecosystems. Springer, pp. 359-391.

Foubert, A., Huvenne, V.A.I., Wheeler, A., Kozachenko, M., Opderbecke, J., Henriet, J.P., 2011. The Moira Mounds, small cold-water coral mounds in the Porcupine Seabight, NE Atlantic: Part B—Evaluating the impact of sediment dynamics through high-resolution ROV-borne bathymetric mapping. Marine Geology 282, 65-78.

Frank, N., Freiwald, A., Correa, M.L., Wienberg, C., Eisele, M., Hebbeln, D., Van Rooij, D., Henriet, J.P., Colin, C., van Weering, T., de Haas, H., Buhl-Mortensen, P., Roberts, J.M., De Mol, B., Douville, E., Blamart, D., Hatte, C., 2011. Northeastern Atlantic cold-water coral reefs and climate. Geology 39, 743-746.

Frank, N., Paterne, M., Ayliffe, L., van Weering, T., Henriet, J.-P., Blamart, D., 2004. Eastern North Atlantic deep-sea corals: Tracing upper intermediate water Δ^{14}C during the Holocene. Earth and Planetary Science Letters 219, 297-309.

Frank, N., Ricard, E., Lutringer-Paquet, A., van der Land, C., Colin, C., Blamart, D., Foubert, A., Van Rooij, D., Henriet, J.-P., de Haas, H., van Weering, T., 2009. The Holocene occurrence of cold water corals in the NE Atlantic: Implications for coral carbonate mound evolution. Marine Geology 266, 129-142.

Frederiksen, R., Jensen, A., Westerberg, H., 1992. The distribution of the scleractinian coral *Lophelia pertusa* around the Faroe islands and the relation to internal tidal mixing. Sarsia 77, 157-171.

Freiwald, A., 2002. Reef-forming cold-water corals, Ocean margin systems. Springer, pp. 365-385.

Freiwald, A., Beuck, L., Rüggeberg, A., Taviani, M., Hebbeln, D., 2009. The white coral community in the central Mediterranean Sea revealed by ROV surveys. Oceanography 22, 58-74.

Freiwald, A., Roberts, J.M., 2006. Cold-water corals and ecosystems. Springer Science & Business Media.

Ginsburg, R.N., Lowenstam, H.A., 1958. The influence of marine bottom communities on the depositional environment of sediments. The Journal of Geology 66, 310-318.

Glogowski, S., Dullo, W.-C., Feldens, P., Liebetrau, V., von Reumont, J., Hühnerbach, V., Krastel, S., Wynn, R.B., Flögel, S., 2015. The Eugen Seibold coral mounds offshore western Morocco: Oceanographic and bathymetric boundary conditions of a newly discovered cold-water coral province. Geo-Marine Letters 35, 257-269.

Grant, K.M., Rohling, E.J., Ramsey, C.B., Cheng, H., Edwards, R.L., Florindo, F., Heslop, D., Marra, F., Roberts, A.P., Tamisiea, M.E., Williams, F., 2014. Sea-level variability over five glacial cycles. Nature Communications 5, 5076.

Grasmueck, M., Eberli, G.P., Viggiano, D.A., Correa, T., Rathwell, G., Luo, J., 2006. Autonomous underwater vehicle (AUV) mapping reveals coral mound distribution, morphology, and oceanography in deep water of the Straits of Florida. Geophysical Research Letters 33.

Guihen, D., White, M., Lundälv, T., 2013. Boundary layer flow dynamics at a cold-water coral reef. Journal of Sea Research 78, 36-44.

Hanz, U., Wienberg, C., Hebbeln, D., Duineveld, G., Lavaleye, M., Juva, K., Dullo, W.-C., Freiwald, A., Tamborrino, L., Reichart, G.-J., Flögel, S., Mienis, F., 2019. Environmental factors influencing cold-water coral ecosystems in the oxygen minimum zones on the Angolan and Namibian margins. Biogeosciences Discussions, 1-37.

Hebbeln, D., 2019. 8 Highly Variable Submarine Landscapes in the Alborán Sea Created by Cold-Water Corals, in: Orejas, C., Jiménez, C. (Eds.), Mediterranean Cold-Water Corals: Past, Present and Future: Understanding the Deep-Sea Realms of Coral. Springer International Publishing, Cham, pp. 61-65.

Hebbeln, D., Bender, M., Gaide, S., Titschack, J., Vandorpe, T., Van Rooij, D., Wintersteller, P., Wienberg, C., 2019. Thousands of cold-water coral mounds along the Moroccan Atlantic continental margin: Distribution and morphometry. Marine Geology 411, 51-61.

Hebbeln, D., Samankassou, E., 2015. Where did ancient carbonate mounds grow — In bathyal depths or in shallow shelf waters? Earth-Science Reviews 145, 56-65.

Hebbeln, D., Van Rooij, D., Wienberg, C., 2016. Good neighbours shaped by vigorous currents: Cold-water coral mounds and contourites in the North Atlantic. Marine Geology 378, 171-185.

Hebbeln, D., Wienberg, C., André, F., Mienis, F., Orejas, C., Titschack, J., Cold-water coral reefs thriving under hypoxia. Submitted to Coral Reefs.

Hebbeln, D., Wienberg, C., Bartels, M., Bergenthal, M., Fraink, N., Henriet, J.-P., Kaszemeik, K., Klar, S., Klein, T., Krengel, T., Kuhnert, M., Meyer-Schack, B., Noorlander, C., Reuter, M., Rosiak, U., Schmidt, W., Seeba, H., Seiter, C., Stange, N., Terhzaz, L., Van Rooij, D., cruise participants, 2015. MoccoMeBo Climate-driven development of Moroccan cold-water coral mounds revealed by MeBo-drilling: Atlantic vs. Mediterranean settings - Cruise MSM36 - February 18 - March 17, 2014 - Malaga (Spain) - Las Palmas (Spain). MARIA S. MERIAN-Berichte, MSM36, 47 pp., DFG-Senatskommission für Ozeanographie.

Hebbeln, D., Wienberg, C., Beuck, L., Freiwald, A., Wintersteller, P., cruise participants, 2009. Report and preliminary results of RV POSEIDON Cruise POS 385 "Cold-Water Corals of the Alboran Sea (western Mediterranean Sea)", Faro–Toulon, May 29–June 16, 2009. Berichte, Fachbereich Geowissenschaften, Universität Bremen, No. 273, 79 pages. Bremen, 2009, p. 79.

Hebbeln, D., Wienberg, C., Wintersteller, P., Freiwald, A., Becker, M., Beuck, L., Dullo, C., Eberli, G.P., Glogowski, S., Matos, L., Forster, N., Reyes-Bonilla, H., Taviani, M., 2014. Environmental forcing of the Campeche cold-water coral province, southern Gulf of Mexico. Biogeosciences 11, 1799-1815.

Heburn, G.W., La Violette, P.E., 1990. Variations in the structure of the anticyclonic gyres found in the Alboran Sea. Journal of Geophysical Research: Oceans 95, 1599-1613.

Henriet, J.P., Guidard, S., 2002. Carbonate mounds as a possible example for microbial activity in geological processes, in: Wefer, G., Billett, D., Hebbeln, D., Jørgensen, B.B., Schlüter, M., van Weering, T.C.E. (Eds.), Ocean Margin Systems. Springer Berlin Heidelberg, Berlin, Heidelberg, pp. 439-455.

Henry, L.-A., Roberts, J.M., 2007. Biodiversity and ecological composition of macrobenthos on cold-water coral mounds and adjacent off-mound habitat in the bathyal Porcupine Seabight, NE Atlantic. Deep Sea Research Part I: Oceanographic Research Papers 54, 654-672.

Herguera, J.C., 2000. Last glacial paleoproductivity patterns in the eastern equatorial Pacific: Benthic foraminifera records. Marine Micropaleontology 40, 259-275.

Herguera, J.C., Berger, W.H., 1991. Paleoproductivity from benthic foraminifera abundance: Glacial to postglacial change in the west-equatorial Pacific. Geology 19, 1173-1176.

Holden, N.E., 1989. Total half-lives for selected nuclides, Pure and Applied Chemistry, pp. 941-958.

Hughen, K.A., 2007. Chapter Five Radiocarbon Dating of Deep-Sea Sediments, in: Hillaire–Marcel, C., De Vernal, A. (Eds.), Developments in Marine Geology. Elsevier, pp. 185-210.

Huvenne, V.A.I., Masson, D.G., Wheeler, A.J., 2009a. Sediment dynamics of a sandy contourite: the sedimentary context of the Darwin cold-water coral mounds, Northern Rockall Trough. International Journal of Earth Sciences 98, 865-884.

Huvenne, V.A.I., Van Rooij, D., De Mol, B., Thierens, M., O'Donnell, R., Foubert, A., 2009b. Sediment dynamics and palaeo-environmental context at key stages in the Challenger cold-

water coral mound formation: Clues from sediment deposits at the mound base. Deep Sea Research Part I: Oceanographic Research Papers 56, 2263-2280.

Ivy-Ochs, S., Kerschner, H., Schlüchter, C., 2007. Cosmogenic nuclides and the dating of Lateglacial and Early Holocene glacier variations: The Alpine perspective. Quaternary International 164-165, 53-63.

Jaffey, A.H., Flynn, K.F., Glendenin, L.E., Bentley, W.C., Essling, A.M., 1971. Precision measurement of half-lives and specific activities of ^{235}U and ^{238}U. Physical Review C 4, 1889-1906.

Jimenez-Espejo, F.J., Martinez-Ruiz, F., Rogerson, M., González-Donoso, J.M., Romero, O.E., Linares, D., Sakamoto, T., Gallego-Torres, D., Rueda Ruiz, J.L., Ortega-Huertas, M., Perez Claros, J.A., 2008. Detrital input, productivity fluctuations, and water mass circulation in the westernmost Mediterranean Sea since the Last Glacial Maximum. Geochemistry, Geophysics, Geosystems 9, Q11U02.

Jiménez-Espejo, F.J., Pardos-Gené, M., Martínez-Ruiz, F., García-Alix, A., van de Flierdt, T., Toyofuku, T., Bahr, A., Kreissig, K., 2015. Geochemical evidence for intermediate water circulation in the westernmost Mediterranean over the last 20kyr BP and its impact on the Mediterranean Outflow. Global and Planetary Change 135, 38-46.

Johansen, J.L., 2014. Quantifying water flow within aquatic ecosystems using load cell sensors: A profile of currents experienced by coral reef organisms around Lizard Island, Great Barrier Reef, Australia. PLoS One 9, e83240.

Kano, A., Ferdelman, T.G., Williams, T., Henriet, J.-P., Ishikawa, T., Kawagoe, N., Takashima, C., Kakizaki, Y., Abe, K., Sakai, S., 2007. Age constraints on the origin and growth history of a deep-water coral mound in the northeast Atlantic drilled during Integrated Ocean Drilling Program Expedition 307. Geology 35, 1051-1054.

Kiriakoulakis, K., Freiwald, A., Fisher, E., Wolff, G.A., 2007. Organic matter quality and supply to deep-water coral/mound systems of the NW European continental margin. International Journal of Earth Sciences 96, 159-170.

Kroopnick, P.M., 1985. The distribution of ^{13}C of ΣCO_2 in the world oceans. Deep Sea Research Part A. Oceanographic Research Papers 32, 57-84.

Lambeck, K., Chappell, J., 2001. Sea Level Change Through the Last Glacial Cycle. Science 292, 679-686.

Lambeck, K., Rouby, H., Purcell, A., Sun, Y., Sambridge, M., 2014. Sea level and global ice volumes from the Last Glacial Maximum to the Holocene. Proceedings of the National Academy of Sciences 111, 15296-15303.

Libby, W.F., 1955. Radiocarbon dating. University of Chicago Press, Chicago.

Lisiecki, L.E., Raymo, M.E., 2005. A Pliocene-Pleistocene stack of 57 globally distributed benthic δ^{18}O records. Paleoceanography 20, PA1003.

Lo Iacono, C., Gràcia, E., Bartolomé, R., Coiras, E., Jose Dañobeitia, J., Acosta, J., 2012. 49 - Habitats of the Chella Bank, Eastern Alboran Sea (Western Mediterranean) A2 - Harris, Peter T, in: Baker, E.K. (Ed.), Seafloor Geomorphology as Benthic Habitat. Elsevier, London, pp. 681-690.

Lo Iacono, C., Gràcia, E., Diez, S., Bozzano, G., Moreno, X., Dañobeitia, J., Alonso, B., 2008. Seafloor characterization and backscatter variability of the Almería Margin (Alboran Sea, SW Mediterranean) based on high-resolution acoustic data. Marine Geology 250, 1-18.

Lo Iacono, C., Gràcia, E., Ranero, C.R., Emelianov, M., Huvenne, V.A.I., Bartolomé, R., Booth-Rea, G., Prades, J., 2014. The West Melilla cold water coral mounds, Eastern Alboran Sea: Morphological characterization and environmental context. Deep Sea Research Part II: Topical Studies in Oceanography 99, 316-326.

Lo Iacono, C., Savini, A., Basso, D., 2018. Cold-Water Carbonate Bioconstructions, pp. 425-455.

Lobo, F.J., Fernández-Salas, L.M., Moreno, I., Sanz, J.L., Maldonado, A., 2006. The sea-floor morphology of a Mediterranean shelf fed by small rivers, northern Alboran Sea margin. Continental Shelf Research 26, 2607-2628.

Lohrenz, S.E., Wiesenburg, D.A., DePalma, I.P., Johnson, K.S., Gustafson, D.E., 1988. Interrelationships among primary production, chlorophyll, and environmental conditions in frontal regions of the western Mediterranean Sea. Deep Sea Research Part A. Oceanographic Research Papers 35, 793-810.

López Correa, M., Montagna, P., Joseph, N., Rüggeberg, A., Fietzke, J., Flögel, S., Dorschel, B., Goldstein, S.L., Wheeler, A., Freiwald, A., 2012. Preboreal onset of cold-water coral growth beyond the Arctic Circle revealed by coupled radiocarbon and U-series dating and neodymium isotopes. Quaternary Science Reviews 34, 24-43.

Lowe, J.J., Rasmussen, S.O., Björck, S., Hoek, W.Z., Steffensen, J.P., Walker, M.J.C., Yu, Z.C., 2008. Synchronisation of palaeoenvironmental events in the North Atlantic region during the Last Termination: a revised protocol recommended by the INTIMATE group. Quaternary Science Reviews 27, 6-17.

Lowe, R.J., Falter, J.L., 2015. Oceanic forcing of coral reefs. Annual Review of Marine Science 7, 43-66.

Mackensen, A., Schmiedl, G., 2019. Stable carbon isotopes in paleoceanography: atmosphere, oceans, and sediments. Earth-Science Reviews 197, 102893.

Margreth, S., Gennari, G., Rüggeberg, A., Comas, M.C., Pinheiro, L.M., Spezzaferri, S., 2011. Growth and demise of cold-water coral ecosystems on mud volcanoes in the West Alboran Sea: The messages from the planktonic and benthic foraminifera. Marine Geology 282, 26-39.

Martínez-Méndez, G., Hebbeln, D., Mohtadi, M., Lamy, F., De Pol-Holz, R., Reyes-Macaya, D., Freudenthal, T., 2013. Changes in the advection of Antarctic Intermediate Water to the northern Chilean coast during the last 970 kyr. Paleoceanography 28, 607-618.

Martinez-Ruiz, F., Kastner, M., Gallego-Torres, D., Rodrigo-Gámiz, M., Nieto-Moreno, V., Ortega-Huertas, M., 2015. Paleoclimate and paleoceanography over the past 20,000 yr in the Mediterranean Sea Basins as indicated by sediment elemental proxies. Quaternary Science Reviews 107, 25-46.

Martorelli, E., Petroni, G., Chiocci, F.L., and the Pantelleria Scientific, P., 2011. Contourites offshore Pantelleria Island (Sicily Channel, Mediterranean Sea): depositional, erosional and biogenic elements. Geo-Marine Letters 31, 481-493.

Masqué, P., Fabres, J., Canals, M., Sanchez-Cabeza, J., Sanchez-Vidal, A., Cacho, I., Calafat, A., Bruach, J., 2003. Accumulation rates of major constituents of hemipelagic sediments in the deep Alboran Sea: A centennial perspective of sedimentary dynamics. Marine Geology 193, 207-233.

Matos, L., Mienis, F., Wienberg, C., Frank, N., Kwiatkowski, C., Groeneveld, J., Thil, F., Abrantes, F., Cunha, M.R., Hebbeln, D., 2015. Interglacial occurrence of cold-water corals off Cape Lookout (NW Atlantic): First evidence of the Gulf Stream influence. Deep Sea Research Part I: Oceanographic Research Papers 105, 158-170.

Matos, L., Wienberg, C., Titschack, J., Schmiedl, G., Frank, N., Abrantes, F., Cunha, M.R., Hebbeln, D., 2017. Coral mound development at the Campeche cold-water coral province, southern Gulf of Mexico: Implications of Antarctic Intermediate Water increased influence during interglacials. Marine Geology 392, 53-65.

McCave, I.N., Hall, I.R., 2006. Size sorting in marine muds: Processes, pitfalls, and prospects for paleoflow-speed proxies. Geochemistry, Geophysics, Geosystems 7, Q10N05.

McCave, I.N., Swift, S.A., 1976. A physical model for the rate of deposition of fine-grained sediments in the deep sea. GSA Bulletin 87, 541-546.

McCave, I.N., Thornalley, D.J.R., Hall, I.R., 2017. Relation of sortable silt grain-size to deep-sea current speeds: Calibration of the 'Mud Current Meter'. Deep Sea Research Part I: Oceanographic Research Papers 127, 1-12.

McCulloch, M., Taviani, M., Montagna, P., López Correa, M., Remia, A., Mortimer, G., 2010. Proliferation and demise of deep-sea corals in the Mediterranean during the Younger Dryas. Earth and Planetary Science Letters 298, 143-152.

McGregor, H.V., Dupont, L., Stuut, J.-B.W., Kuhlmann, H., 2009. Vegetation change, goats, and religion: A 2000-year history of land use in southern Morocco. Quaternary Science Reviews 28, 1434-1448.

Mienis, F., Bouma, T.J., Witbaard, R., van Oevelen, D., Duineveld, G.C.A., 2019. Experimental assessment of the effects of cold-water coral patches on water flow. Marine Ecology Progress Series 609, 101-117.

Mienis, F., de Stigter, H.C., de Haas, H., van Weering, T.C.E., 2009a. Near-bed particle deposition and resuspension in a cold-water coral mound area at the Southwest Rockall Trough margin, NE Atlantic. Deep Sea Research Part I: Oceanographic Research Papers 56, 1026-1038.

Mienis, F., de Stigter, H.C., White, M., Duineveld, G., de Haas, H., van Weering, T.C.E., 2007. Hydrodynamic controls on cold-water coral growth and carbonate-mound development at the SW and SE Rockall Trough Margin, NE Atlantic Ocean. Deep Sea Research Part I: Oceanographic Research Papers 54, 1655-1674.

Mienis, F., Duineveld, G.C.A., Davies, A.J., Ross, S.W., Seim, H., Bane, J., van Weering, T.C.E., 2012. The influence of near-bed hydrodynamic conditions on cold-water corals in the Viosca Knoll area, Gulf of Mexico. Deep Sea Research Part I: Oceanographic Research Papers 60, 32-45.

Mienis, F., van der Land, C., de Stigter, H.C., van de Vorstenbosch, M., de Haas, H., Richter, T., van Weering, T.C.E., 2009b. Sediment accumulation on a cold-water carbonate mound at the Southwest Rockall Trough margin. Marine Geology 265, 40-50.

Mienis, F., van Weering, T., de Haas, H., de Stigter, H., Huvenne, V., Wheeler, A., 2006. Carbonate mound development at the SW Rockall Trough margin based on high resolution TOBI and seismic recording. Marine Geology 233, 1-19.

Millot, C., 1999. Circulation in the western Mediterranean Sea. Journal of Marine Systems 20, 423-442.

Millot, C., 2009. Another description of the Mediterranean Sea outflow. Progress in Oceanography 82, 101-124.

Millot, C., Taupier-Letage, I., 2005. Circulation in the Mediterranean Sea, in: Saliot, A. (Ed.), The Mediterranean Sea. Springer, Berlin, Heidelberg, pp. 29-66.

Monismith, S.G., 2007. Hydrodynamics of Coral Reefs. Annual Review of Fluid Mechanics 39, 37-55.

Morán, X.A.G., Estrada, M., 2001. Short-term variability of photosynthetic parameters and particulate and dissolved primary production in the Alboran Sea (SW Mediterranean). Marine Ecology Progress Series 212, 53-67.

Moreno, A., Cacho, I., Canals, M., Grimalt, J.O., Sánchez-Goñi, M.F., Shackleton, N., Sierro, F.J., 2005. Links between marine and atmospheric processes oscillating on a millennial time-scale. A multi-proxy study of the last 50,000 yr from the Alboran Sea (western Mediterranean Sea). Quaternary Science Reviews 24, 1623-1636.

Mortensen, P.B., 2001. Aquarium observations on the deep-water coral *Lophelia pertusa* (L., 1758) (scleractinia) and selected associated invertebrates. Ophelia 54, 83-104.

Mueller, C.E., Larsson, A.I., Veuger, B., Middelburg, J.J., van Oevelen, D., 2014. Opportunistic feeding on various organic food sources by the cold-water coral*Lophelia pertusa*. Biogeosciences 11, 123-133.

Muñoz, A., Ballesteros, M., Montoya, I., Rivera, J., Acosta, J., Uchupi, E., 2008. Alborán Basin, southern Spain—Part I: Geomorphology. Marine and Petroleum Geology 25, 59-73.

Murray, J.W., 2006. Ecology and Applications of Benthic Foraminifera. Cambridge University Press, Cambridge.

Opsahl, S., Benner, R., 1997. Distribution and cycling of terrigenous dissolved organic matter in the ocean. Nature 386, 480-482.

Orejas, C., Ferrier-Pagès, C., Reynaud, S., Gori, A., Beraud, E., Tsounis, G., Allemand, D., Gili, J.M., 2011. Long-term growth rates of four Mediterranean cold-water coral species maintained in aquaria. Marine Ecology Progress Series 429, 57-65.

Orejas, C., Gori, A., Lo Iacono, C., Puig, P., Gili, J.M., Dale, M.R.T., 2009. Cold-water corals in the Cap de Creus canyon, northwestern Mediterranean: Spatial distribution, density and anthropogenic impact. Marine Ecology Progress Series 397, 37-51.

Palomino, D., Alonso, B., Lo Iacono, C., Casas, D., d'Acremont, E., Ercilla, G., Gorini, C., Vazquez, J.-T., 2015. Seamounts and seamount-like structures of the Alborán Sea.

Palomino, D., Vázquez, J.-T., Ercilla, G., Alonso, B., López-González, N., Díaz-del-Río, V., 2011. Interaction between seabed morphology and water masses around the seamounts on the Motril Marginal Plateau (Alboran Sea, Western Mediterranean). Geo-Marine Letters 31, 465-479.

Patterson, R.T., Fishbein, E., 1989. Re-examination of the statistical methods used to determine the number of point counts needed for micropaleontological quantitative research. Journal of Paleontology 63, 245-248.

Pérez-Folgado, M., Sierro, F.J., Flores, J.A., Grimalt, J.O., Zahn, R., 2004. Paleoclimatic variations in foraminifer assemblages from the Alboran Sea (Western Mediterranean) during the last 150 ka in ODP Site 977. Marine Geology 212, 113-131.

Pierre, C., 1999. The oxygen and carbon isotope distribution in the Mediterranean water masses. Marine Geology 153, 41-55.

Pomar, L., 2001a. Ecological control of sedimentary accommodation: Evolution from a carbonate ramp to rimmed shelf, Upper Miocene, Balearic Islands. Palaeogeography, Palaeoclimatology, Palaeoecology 175, 249-272.

Pomar, L., 2001b. Types of carbonate platforms: A genetic approach. Basin Research 13, 313-334.

Pomar, L., Haq, B.U., 2016. Decoding depositional sequences in carbonate systems: Concepts vs experience. Global and Planetary Change 146, 190-225.

Pomar, L., Kendall, C.G.S.C., 2008. Architecture of carbonate platforms: A response to hydrodynamics and evolving ecology. 187-216.

Pomar, L., Morsilli, M., Hallock, P., Bádenas, B., 2012. Internal waves, an under-explored source of turbulence events in the sedimentary record. Earth-Science Reviews 111, 56-81.

Prieur, L., Sournia, A., 1994. Almofront 1: An interdisciplinary study of the Almeria Oran geostrophic front, SW Mediterranean Sea. J. Mar. Syst 5, 187-204.

Raddatz, J., Rüggeberg, A., Liebetrau, V., Foubert, A., Hathorne, E.C., Fietzke, J., Eisenhauer, A., Dullo, W.-C., 2014. Environmental boundary conditions of cold-water coral mound growth over the last 3 million years in the Porcupine Seabight, Northeast Atlantic. Deep Sea Research Part II: Topical Studies in Oceanography 99, 227-236.

Raddatz, J., Rüggeberg, A., Margreth, S., Dullo, W.-C., 2011. Paleoenvironmental reconstruction of Challenger Mound initiation in the Porcupine Seabight, NE Atlantic. Marine Geology 282, 79-90.

Railsback, L.B., Gibbard, P.L., Head, M.J., Voarintsoa, N.R.G., Toucanne, S., 2015. An optimized scheme of lettered marine isotope substages for the last 1.0 million years, and the climatostratigraphic nature of isotope stages and substages. Quaternary Science Reviews 111, 94-106.

Ramos, A., Sanz, J.L., Ramil, F., Agudo, L.M., Presas-Navarro, C., 2017. The giant cold-water coral mounds barrier off Mauritania, in: Ramos, A., Ramil, F., Sanz, J.L. (Eds.), Deep-Sea Ecosystems Off Mauritania: Research of Marine Biodiversity and Habitats in the Northwest African Margin. Springer Netherlands, Dordrecht, pp. 481-525.

Ravelo, A.C., Hillaire-Marcel, C., 2007. The Use of Oxygen and Carbon Isotopes of Foraminifera in Paleoceanography, in: Hillaire–Marcel, C., De Vernal, A. (Eds.), Developments in Marine Geology. Elsevier, pp. 735-764.

Reimer, P.J., Bard, E., Bayliss, A., Beck, J.W., Blackwell, P.G., Bronk Ramsey, C., Buck, C.E., Cheng, H., Edwards, R.L., Friedrich, M., 2013. IntCal13 and Marine13 radiocarbon age calibration curves 0-50,000 years cal BP. Radiocarbon 55, 1869-1887.

Roberts, J., Wheeler, A., Freiwald, A., Cairns, S., 2009. Cold-water Corals: The Biology and Geology of Deep-Sea Coral Habitats. Cambridge University Press.

Roberts, J.M., Wheeler, A.J., Freiwald, A., 2006. Reefs of the deep: The biology and geology of cold-water coral ecosystems. Science 312, 543-547.

Rogerson, M., Cacho, I., Jimenez-Espejo, F., Reguera, M.I., Sierro, F.J., Martinez-Ruiz, F., Frigola, J., Canals, M., 2008. A dynamic explanation for the origin of the western Mediterranean organic-rich layers. Geochemistry, Geophysics, Geosystems 9, Q07U01.

Rohling, E.J., Cooke, S., 1999. Stable oxygen and carbon isotope ratios in foraminiferal carbonate shells, in: Sen Gupta, B.K. (Ed.), Modern Foraminifera. Kluwer Academic, pp. 239-258.

Rüggeberg, A., Dullo, C., Dorschel, B., Hebbeln, D., 2007. Environmental changes and growth history of a cold-water carbonate mound (Propeller Mound, Porcupine Seabight). International Journal of Earth Sciences 96, 57-72.

Ruiz, J., Echevarría, F., Font, J., Ruiz, S., García, E., Blanco, J.M., Jiménez-Gómez, F., Prieto, L., González-Alaminos, A., García, C.M., Cipollini, P., Snaith, H., Bartual, A., Reul, A., Rodríguez, V., 2001. Surface distribution of chlorophyll, particles and gelbstoff in the Atlantic jet of the Alborán Sea: From submesoscale to subinertial scales of variability. Journal of Marine Systems 29, 277-292.

Sánchez, F., González-Pola, C., Druet, M., García-Alegre, A., Acosta, J., Cristobo, J., Parra, S., Ríos, P., Altuna, Á., Gómez-Ballesteros, M., Muñoz-Recio, A., Rivera, J., del Río, G.D., 2014. Habitat characterization of deep-water coral reefs in La Gaviera Canyon (Avilés Canyon System, Cantabrian Sea). Deep Sea Research Part II: Topical Studies in Oceanography 106, 118-140.

Sarhan, T., Garcı, x, a Lafuente, J., Vargas, M., Vargas, J.M., Plaza, F., 2000. Upwelling mechanisms in the northwestern Alboran Sea. Journal of Marine Systems 23, 317-331.

Schmiedl, G., Pfeilsticker, M., Hemleben, C., Mackensen, A., 2004. Environmental and biological effects on the stable isotope composition of recent deep-sea benthic foraminifera from the western Mediterranean Sea. Marine Micropaleontology 51, 129-152.

Schmittner, A., Bostock, H.C., Cartapanis, O., Curry, W.B., Filipsson, H.L., Galbraith, E.D., Gottschalk, J., Herguera, J.C., Hoogakker, B., Jaccard, S.L., Lisiecki, L.E., Lund, D.C., Martínez-Méndez, G., Lynch-Stieglitz, J., Mackensen, A., Michel, E., Mix, A.C., Oppo, D.W., Peterson, C.D., Repschläger, J., Sikes, E.L., Spero, H.J., Waelbroeck, C., 2017.

Calibration of the carbon isotope composition (δ^{13}C) of benthic foraminifera. Paleoceanography 32, 512-530.

Schroeder, W.W., 2002. Observations of *Lophelia pertusa* and the surficial geology at a deep-water site in the northeastern Gulf of Mexico. Hydrobiologia 471, 29-33.

Sierro, F.J., Hodell, D.A., Curtis, J.H., Flores, J.A., Reguera, I., Colmenero-Hidalgo, E., Bárcena, M.A., Grimalt, J.O., Cacho, I., Frigola, J., Canals, M., 2005. Impact of iceberg melting on Mediterranean thermohaline circulation during Heinrich events. Paleoceanography 20.

Small, J., Martin, J., 2002. The generation of non-linear internal waves in the Gulf of Oman. Continental Shelf Research 22, 1153-1182.

Snoussi, M., Haïda, S., Imassi, S., 2002. Effects of the construction of dams on the water and sediment fluxes of the Moulouya and the Sebou Rivers, Morocco. Regional Environmental Change 3, 5-12.

Stalder, C., El Kateb, A., Vertino, A., Rüggeberg, A., Camozzi, O., Pirkenseer, C.M., Spangenberg, J.E., Hajdas, I., Van Rooij, D., Spezzaferri, S., 2018. Large-scale paleoceanographic variations in the western Mediterranean Sea during the last 34,000 years: From enhanced cold-water coral growth to declining mounds. Marine Micropaleontology 143, 46-62.

Stalder, C., Vertino, A., Rosso, A., Ruggeberg, A., Pirkenseer, C., Spangenberg, J.E., Spezzaferri, S., Camozzi, O., Rappo, S., Hajdas, I., 2015. Microfossils, a key to unravel cold-water carbonate mound evolution through time: Evidence from the eastern Alboran Sea. PLoS One 10, e0140223.

Stalling, D., Westerhoff, M., Hege, H.-C., 2005. 38 - amira: A Highly Interactive System for Visual Data Analysis A2 - Hansen, Charles D, in: Johnson, C.R. (Ed.), Visualization Handbook. Butterworth-Heinemann, Burlington, pp. 749-767.

Stuiver, M., Reimer, P.J., 1993. Extended ^{14}C data base and revised CALIB 3.0 ^{14}C age calibration program. Radiocarbon 35, 215-230.

Stuut, J.-B., Smalley, I., O'Hara-Dhand, K., 2009. Aeolian dust in Europe: African sources and European deposits. Quaternary International 198, 234-245.

Tamborrino, L., Wienberg, C., Titschack, J., Wintersteller, P., Mienis, F., Schröder-Ritzrau, A., Freiwald, A., Orejas, C., Dullo, W.-C., Haberkern, J., Hebbeln, D., 2019. Mid-Holocene extinction of cold-water corals on the Namibian shelf steered by the Benguela oxygen minimum zone. Geology.

Taviani, M., Angeletti, L., Beuck, L., Campiani, E., Canese, S., Foglini, F., Freiwald, A., Montagna, P., Trincardi, F., 2016. Reprint of 'On and off the beaten track: Megafaunal sessile life and Adriatic cascading processes'. Marine Geology 375, 146-160.

Taviani, M., Remia, A., Corselli, C., Freiwald, A., Malinverno, E., Mastrototaro, F., Savini, A., Tursi, A., 2005. First geo-marine survey of living cold-water Lophelia reefs in the Ionian Sea (Mediterranean basin). Facies 50, 409-417.

Taviani, M., Vertino, A., Correa, M.L., Savini, A., De Mol, B., Remia, A., Montagna, P., Angeletti, L., Zibrowius, H., Alves, T., 2011. Pleistocene to recent scleractinian deep-water corals and coral facies in the Eastern Mediterranean. Facies 57, 579-603.

Thiem, Ø., Ravagnan, E., Fosså, J.H., Berntsen, J., 2006. Food supply mechanisms for cold-water corals along a continental shelf edge. Journal of Marine Systems 60, 207-219.

Thierens, M., Browning, E., Pirlet, H., Loutre, M.F., Dorschel, B., Huvenne, V.A.I., Titschack, J., Colin, C., Foubert, A., Wheeler, A.J., 2013. Cold-water coral carbonate mounds as unique palaeo-archives: the Plio-Pleistocene Challenger Mound record (NE Atlantic). Quaternary Science Reviews 73, 14-30.

Titschack, J., Baum, D., De Pol-Holz, R., López Correa, M., Forster, N., Flögel, S., Hebbeln, D., Freiwald, A., Riegl, B., 2015. Aggradation and carbonate accumulation of Holocene Norwegian cold-water coral reefs. Sedimentology 62, 1873-1898.

Titschack, J., Fink, H.G., Baum, D., Wienberg, C., Hebbeln, D., Freiwald, A., 2016. Mediterranean cold-water corals - an important regional carbonate factory? The Depositional Record 2, 74-96.

Titschack, J., Thierens, M., Dorschel, B., Schulbert, C., Freiwald, A., Kano, A., Takashima, C., Kawagoe, N., Li, X., 2009. Carbonate budget of a cold-water coral mound (Challenger Mound, IODP Exp. 307). Marine Geology 259, 36-46.

Toucanne, S., Jouet, G., Ducassou, E., Bassetti, M.-A., Dennielou, B., Angue Minto'o, C.M., Lahmi, M., Touyet, N., Charlier, K., Lericolais, G., Mulder, T., 2012. A 130,000-year record of Levantine Intermediate Water flow variability in the Corsica Trough, western Mediterranean Sea. Quaternary Science Reviews 33, 55-73.

van der Land, C., Eisele, M., Mienis, F., de Haas, H., Hebbeln, D., Reijmer, J.J.G., van Weering, T.C.E., 2014. Carbonate mound development in contrasting settings on the Irish margin. Deep Sea Research Part II: Topical Studies in Oceanography 99, 297-306.

Van Haren, H., 2014. Internal wave–zooplankton interactions in the Alboran Sea (W-Mediterranean). Journal of Plankton Research 36, 1124-1134.

Van Rooij, D., Hebbelin, D., Comas, M., Vandorpe, T., Delivet, S., Nave, S., Michel, E., Lebreiro, S., Terrinha, P., Roque, C., 2013. MD 194/EUROFLEETS à bord du R/V Marion Dufresne. Cadix 10 juin 2013-Lisbonne 20 juin 2013.

van Weering, T.C.E., de Haas, H., de Stigter, H.C., Lykke-Andersen, H., Kouvaev, I., 2003. Structure and development of giant carbonate mounds at the SW and SE Rockall Trough margins, NE Atlantic Ocean. Marine Geology 198, 67-81.

Vandorpe, T., Wienberg, C., Hebbeln, D., Van den Berghe, M., Gaide, S., Wintersteller, P., Van Rooij, D., 2017. Multiple generations of buried cold-water coral mounds since the Early-Middle Pleistocene Transition in the Atlantic Moroccan Coral Province, southern Gulf of Cádiz. Palaeogeography, Palaeoclimatology, Palaeoecology 485, 293-304.

Vargas-Yáñez, M., Plaza, F., Garcıa-Lafuente, J., Sarhan, T., Vargas, J., 2002. About the seasonal variability of the Alboran Sea circulation. Journal of Marine Systems 35, 229-248.

Victorero, L., Blamart, D., Pons-Branchu, E., Mavrogordato, M.N., Huvenne, V.A.I., 2016. Reconstruction of the formation history of the Darwin Mounds, N Rockall Trough: How the dynamics of a sandy contourite affected cold-water coral growth. Marine Geology 378, 186-195.

Waelbroeck, C., Labeyrie, L., Michel, E., Duplessy, J.C., McManus, J., Lambeck, K., Balbon, E., Labracherie, M., 2002. Sea-level and deep water temperature changes derived from benthic foraminifera isotopic records. Quaternary Science Reviews 21, 295-305.

Wagner, H., Purser, A., Thomsen, L., Jesus, C.C., Lundälv, T., 2011. Particulate organic matter fluxes and hydrodynamics at the Tisler cold-water coral reef. Journal of Marine Systems 85, 19-29.

Walker, M.J.C., Berkelhammer, M., Björck, S., Cwynar, L.C., Fisher, D.A., Long, A.J., Lowe, J.J., Newnham, R.M., Rasmussen, S.O., Weiss, H., 2012. Formal subdivision of the Holocene Series/Epoch: a Discussion Paper by a Working Group of INTIMATE (Integration of ice-core, marine and terrestrial records) and the Subcommission on Quaternary Stratigraphy (International Commission on Stratigraphy). Journal of Quaternary Science 27, 649-659.

Wang, H., Lo Iacono, C., Wienberg, C., Titschack, J., Hebbeln, D., 2019. Cold-water coral mounds in the southern Alboran Sea (western Mediterranean Sea): Internal waves as an important driver for mound formation since the last deglaciation. Marine Geology 412, 1-18.

Wefing, A.-M., Arps, J., Blaser, P., Wienberg, C., Hebbeln, D., Frank, N., 2017. High precision U-series dating of scleractinian cold-water corals using an automated chromatographic U and Th extraction. Chemical Geology 475, 140-148.

Wheeler, A.J., Beyer, A., Freiwald, A., de Haas, H., Huvenne, V.A.I., Kozachenko, M., Olu-Le Roy, K., Opderbecke, J., 2007. Morphology and environment of cold-water coral carbonate mounds on the NW European margin. International Journal of Earth Sciences 96, 37-56.

Wheeler, A.J., Kozachenko, M., Beyer, A., Foubert, A., Huvenne, V.A.I., Klages, M., Masson, D.G., Olu-Le Roy, K., Thiede, J., 2005. Sedimentary processes and carbonate mounds in the Belgica Mound province, Porcupine Seabight, NE Atlantic, in: Freiwald, A., Roberts, J.M. (Eds.), Cold-Water Corals and Ecosystems. Springer Berlin Heidelberg, Berlin, Heidelberg, pp. 571-603.

Wheeler, A.J., Kozachenko, M., Henry, L.A., Foubert, A., de Haas, H., Huvenne, V.A.I., Masson, D.G., Olu, K., 2011. The Moira Mounds, small cold-water coral banks in the Porcupine Seabight, NE Atlantic: Part A—an early stage growth phase for future coral carbonate mounds? Marine Geology 282, 53-64.

White, M., Dorschel, B., 2010. The importance of the permanent thermocline to the cold water coral carbonate mound distribution in the NE Atlantic. Earth and Planetary Science Letters 296, 395-402.

White, M., Mohn, C., de Stigter, H., Mottram, G., 2005. Deep-water coral development as a function of hydrodynamics and surface productivity around the submarine banks of the Rockall Trough, NE Atlantic, in: Freiwald, A., Roberts, J.M. (Eds.), Cold-Water Corals and Ecosystems. Springer Berlin Heidelberg, Berlin, Heidelberg, pp. 503-514.

Wienberg, C., 2019. A deglacial cold-water coral boom in the Alborán Sea: from coral mounds and species dominance, in: Orejas, C., Jiménez, C. (Eds.), Mediterranean Cold-Water Corals: Past, Present and Future: Understanding the Deep-Sea Realms of Coral. Springer International Publishing, Cham, pp. 57-60.

Wienberg, C., Frank, N., Mertens, K.N., Stuut, J.-B., Marchant, M., Fietzke, J., Mienis, F., Hebbeln, D., 2010. Glacial cold-water coral growth in the Gulf of Cádiz: Implications of increased palaeo-productivity. Earth and Planetary Science Letters 298, 405-416.

Wienberg, C., Titschack, J., 2017. Framework-forming scleractinian cold-water corals through space and time: A Late Quaternary North Atlantic perspective, in: Rossi, S., Bramanti, L., Gori, A., Orejas Saco del Valle, C. (Eds.), Marine Animal Forests: The Ecology of Benthic Biodiversity Hotspots. Springer International Publishing, Cham, pp. 1-34.

Wienberg, C., Titschack, J., Freiwald, A., Frank, N., Lundälv, T., Taviani, M., Beuck, L., Schröder-Ritzrau, A., Krengel, T., Hebbeln, D., 2018. The giant Mauritanian cold-water coral mound province: Oxygen control on coral mound formation. Quaternary Science Reviews 185, 135-152.